

## Discovery of Branebrutinib (BMS-986195): A Strategy for Identifying a Highly Potent and Selective Covalent Inhibitor Providing Rapid In Vivo Inactivation of Bruton's Tyrosine Kinase (BTK)

Scott H. Watterson, Qingjie Liu, Myra Beaudoin Bertrand, Douglas G. Batt, Ling Li, Mark A. Pattoli, Stacey Skala, Lihong Chen, Mary T. Obermeier, Robin Moore, Zheng Yang, Rodney Vickery, Paul A. Elzinga, Lorell N. Discenza, Celia D'Arienzo, Kathleen M. Gillooly, Tracy L. Taylor, Claudine Pulicicchio, Yifan Zhang, Elizabeth Heimrich, Kim W. McIntyre, Qian Ruan, Richard A Westhouse, Ian M. Catlett, Naiyu Zheng, Charu Chaudhry, Jun Dai, Michael A. Galella, Andrew Joseph Tebben, Matt Pokross, Jianqing Li, Rulin Zhao, Daniel Smith, Richard A. Rampulla, Alban Allentoff, Michael A. Wallace, Arvind Mathur, Luisa Salter-Cid, John E. Macor, Percy H Carter, Abera Fura, James R. Burke, and Joseph A Tino

*J. Med. Chem.*, **Just Accepted Manuscript** • DOI: 10.1021/acs.jmedchem.9b00167 • Publication Date (Web): 20 Mar 2019

Downloaded from <http://pubs.acs.org> on March 20, 2019

### Just Accepted

"Just Accepted" manuscripts have been peer-reviewed and accepted for publication. They are posted online prior to technical editing, formatting for publication and author proofing. The American Chemical Society provides "Just Accepted" as a service to the research community to expedite the dissemination of scientific material as soon as possible after acceptance. "Just Accepted" manuscripts appear in full in PDF format accompanied by an HTML abstract. "Just Accepted" manuscripts have been fully peer reviewed, but should not be considered the official version of record. They are citable by the Digital Object Identifier (DOI®). "Just Accepted" is an optional service offered to authors. Therefore, the "Just Accepted" Web site may not include all articles that will be published in the journal. After a manuscript is technically edited and formatted, it will be removed from the "Just Accepted" Web site and published as an ASAP article. Note that technical editing may introduce minor changes to the manuscript text and/or graphics which could affect content, and all legal disclaimers and ethical guidelines that apply to the journal pertain. ACS cannot be held responsible for errors or consequences arising from the use of information contained in these "Just Accepted" manuscripts.



1  
2  
3  
4  
5  
6  
7  
8  
9  
10  
11  
12  
13  
14  
15  
16  
17  
18  
19  
20  
21  
22  
23  
24  
25  
26  
27  
28  
29  
30  
31  
32  
33  
34  
35  
36  
37  
38  
39  
40  
41  
42  
43  
44  
45  
46  
47  
48  
49  
50  
51  
52  
53  
54  
55  
56  
57  
58  
59  
60

	Macor, John; Bristol-Myers Squibb Research and Development Carter, Percy; Bristol-Myers Squibb Research and Development Fura, Aberra; Bristol-Myers Squibb Research and Development Burke, James; Bristol-Myers Squibb Research and Development Tino, Joseph; Bristol-Myers Squibb Research and Development

SCHOLARONE™  
Manuscripts

# Discovery of Branebrutinib (BMS-986195): A Strategy for Identifying a Highly Potent and Selective Covalent Inhibitor Providing Rapid In Vivo Inactivation of Bruton's Tyrosine Kinase (BTK)

*Scott H. Watterson,\* Qingjie Liu, Myra Beaudoin Bertrand, Douglas G. Batt, Ling Li, Mark A. Pattoli, Stacey Skala, Lihong Cheng, Mary T. Obermeier, Robin Moore, Zheng Yang, Rodney Vickery, Paul A. Elzinga, Lorell Discenza, Celia D'Arienzo, Kathleen M. Gillooly, Tracy L. Taylor, Claudine Pulicicchio, Yifan Zhang, Elizabeth Heimrich, Kim W. McIntyre, Qian Ruan, Richard A. Westhouse, Ian M. Catlett, Naiyu Zheng, Charu Chaudhry, Jun Dai, Michael A. Galella, Andrew J. Tebben, Matt Pokross, Jianqing Li, Rulin Zhao, Daniel Smith, Richard Rampulla, Alban Allentoff, Michael A. Wallace, Arvind Mathur, Luisa Salter-Cid, John E. Macor, Percy H. Carter, Abera Fura, James R. Burke, and Joseph A. Tino*

Bristol-Myers Squibb Research and Development, P.O. Box 4000, Princeton, New Jersey 08543

RECEIVED DATE

1  
2  
3  
4  
5  
6  
7  
8  
9  
10  
11  
12  
13  
14  
15  
16  
17  
18  
19  
20  
21  
22  
23  
24  
25  
26  
27  
28  
29  
30  
31  
32  
33  
34  
35  
36  
37  
38  
39  
40  
41  
42  
43  
44  
45  
46  
47  
48  
49  
50  
51  
52  
53  
54  
55  
56  
57  
58  
59  
60

ABSTRACT: Bruton’s tyrosine kinase (BTK), a non-receptor tyrosine kinase, is a member of the Tec family of kinases and is essential for B cell receptor (BCR)-mediated signaling. BTK also plays a critical role in the downstream signaling pathways for the Fc-gamma receptor in monocytes, the Fc-epsilon receptor in granulocytes, and the RANK receptor in osteoclasts. As a result, pharmacological inhibition of BTK is anticipated to provide an effective strategy for the clinical treatment of autoimmune diseases such as rheumatoid arthritis and lupus. This article will outline the evolution of our strategy to identify a covalent, irreversible inhibitor of BTK that has the intrinsic potency, selectivity, and pharmacokinetic properties necessary to provide a rapid rate of inactivation systemically following a very low dose. With excellent in vivo efficacy and a very desirable tolerability profile, **5a** (branebrutinib, BMS-986195) has advanced into clinical studies.

## Introduction

Bruton's tyrosine kinase (BTK) is a member of the Tec family of non-receptor tyrosine kinases and is expressed in all hematopoietic cells, with the exception of T cells and terminally-differentiated plasma cells. The underlying pathophysiology of autoimmune diseases such as rheumatoid arthritis (RA) and lupus relies on many of the pathways regulated by BTK, including B cell and myeloid cellular functions.<sup>1-3</sup> In B cells, BTK kinase activity is essential in B cell receptor (BCR)-mediated activation, resulting in cell proliferation, antibody and cytokine production, and costimulatory molecule expression (e.g. CD80, CD86, and CD69).<sup>4</sup> In myeloid cells, BTK is a critical component in the signaling pathway of low-affinity activating-Fc $\gamma$  receptors (e.g. Fc $\gamma$ RIIa and Fc $\gamma$ RIIIa) for the immunoglobulin G (IgG)-containing immune complexes in monocytic cells and Fc $\epsilon$  receptor signaling in mast cells and basophils, triggering the expression of pro-inflammatory cytokines, chemokines, and cell adhesion molecules.<sup>5</sup> Of particular interest for the clinical treatment of RA, BTK-dependent signaling is required for RANK-L controlled osteoclastogenesis in monocytic precursors.<sup>6</sup> Overall, with its impact on both BCR signaling and Fc $\gamma$  and Fc $\epsilon$  receptor signaling, inhibition of the kinase activity of BTK<sup>7,8</sup> is expected to provide an effective strategy for the clinical treatment of autoimmune diseases such as lupus and RA, without depleting B cells.

As a result of strong preclinical validation, there has been an intense effort to identify orally active small molecule inhibitors of BTK as clinical therapeutic agents for the treatment of both oncological and autoimmune diseases. With an appropriately positioned non-catalytic cysteine residue (Cys481) in the kinase domain,<sup>9</sup> there has been particular interest in identifying inhibitors that covalently bind to Cys481. Ibrutinib (**1a**), a covalent, irreversible inhibitor of BTK, is approved for the clinical treatment of chronic lymphocytic leukemia, mantle cell lymphoma, Waldenstrom's macroglobulinemia, and chronic graft versus host disease.<sup>10</sup> In spite of significant clinical efficacy in otherwise difficult to treat diseases, administration of **1a** has led to undesirable clinical side effects including rash and diarrhea, attributed to the drug's potent off-target inhibition of the epidermal growth factor receptors (EGFR), as well as

bleeding and atrial fibrillation.<sup>11</sup> Additionally, as a result of high clearance and a slow rate of inactivation, **1a** requires high doses for clinical efficacy (420 – 560 mg QD), which when combined with the side effect profile would likely limit its use to oncological diseases. In an effort to improve upon the overall profile of **1a**, several additional covalent inhibitors,<sup>12,13</sup> as well reversible inhibitors,<sup>14,15</sup> have advanced into clinical trials for the treatment of both oncological and autoimmune disorders. One such drug, acalabrutinib (**1b**) was recently approved for the treatment of mantle cell lymphoma.<sup>13</sup>

We have previously reported on our efforts to identify reversible inhibitors of BTK.<sup>15c-d</sup> This effort led to the discovery of BMS-986142 (**2**, Figure 2), as a single, stable atropisomer, which is currently being evaluated clinically for the treatment of rheumatoid arthritis.<sup>15a-b</sup> Dosing was designed to provide continuous coverage of the IC<sub>50</sub> throughout the dosing interval, as supported by preclinical animal studies.<sup>15</sup> Recognizing that coverage as high as IC<sub>90</sub> might be required for clinical efficacy, we initiated a covalent, irreversible discovery effort. It has been reported in the literature<sup>16</sup> that covalent, irreversible inhibition can provide advantages over traditional reversible inhibition such as increased biochemical efficiency for target disruption and a prolonged pharmacodynamic (PD) effect that outlasts the pharmacokinetics (PK) of the compound, both improving the potential for lower concentrations and subsequent improved therapeutic margins. However, covalent, irreversible inhibition also enhances the risk of off-target reactivity to biomolecules, potentially leading to hepatotoxicity, immunotoxicity, and mutagenicity.<sup>17</sup> As a result of their covalent nature, off-target interaction would be expected to be more significant with the potential for prolonged recovery. Of particular concern with covalent inhibition is the potential for idiosyncratic adverse drug reactions (IADRs), which are characterized as immunogenicity of a protein adduct (haptization) leading to an allergic response or drug hypersensitivity reaction.<sup>17</sup>

In considering this strategy to develop a selective covalent, irreversible inhibitor for the treatment of autoimmune diseases, a low human dose of  $\leq 10$  mg was desired to significantly reduce the potential for off-target reactivity. Drugs with a dose  $\leq 10$  mg are unlikely to cause IADRs, including those that form reactive metabolites.<sup>17a</sup> We reasoned that a low human dose would require that a covalent, irreversible

1 inhibitor have both a rapid rate of enzyme inactivation and PK properties amenable to rapid target  
2 engagement in vivo. As shown in Figure 3, covalent bonding requires a two-step process. The first step  
3 involves non-covalent, reversible binding to the active site of BTK to establish  $[E \bullet I]$ , as measured by  $K_i$ .  
4  
5 The second step involves covalent, irreversible bonding of an electrophilic center on the inhibitor with  
6  
7 the nucleophilic Cys481 residue in the active site, resulting in complete enzyme inactivation  $[EI]$ , as  
8  
9 measured by  $k_{inact}$ . The apparent second order rate of inactivation provided by a covalent, irreversible  
10  
11 inhibitor ( $k_{obs}$ ) is represented by  $k_{inact}/K_i$ . With this in mind, our strategy to attain a rapid rate of  
12  
13 inactivation was to start with a high affinity, highly selective scaffold with reversible binding to the target  
14  
15 in the absence of covalent bonding, where the electrophilic acceptor enhances but does not drive potency  
16  
17 or selectivity. A high affinity compound (optimized  $K_i$ ) would be expected to provide high concentrations  
18  
19 of  $[E \bullet I]$ , which would be essential for a rapid rate of inactivation and enhanced selectivity. Additionally,  
20  
21 a covalent, irreversible inhibitor with an appended acceptor with low intrinsic reactivity would be  
22  
23 desirable to mitigate any off-target interactions. This would require an optimal scaffold, linker, and  
24  
25 acceptor geometry to allow for precise positioning of the acceptor in close proximity to Cys481 to drive  
26  
27 rapid inactivation ( $k_{inact}$ ) while maintaining high affinity binding ( $K_i$ ) to the hinge region of the kinase  
28  
29 domain.  
30  
31  
32  
33  
34  
35  
36

37 To achieve a low human dose, a covalent, irreversible inhibitor would be expected to require PK  
38  
39 properties that provide a balance between clearance and the rate of target engagement and ultimate  
40  
41 enzymatic inactivation. In particular, the rate of target inactivation would need to occur at a rate faster  
42  
43 than that of drug elimination, but remaining compound would need to be cleared rapidly to mitigate any  
44  
45 off-target interactions (Figure 4). We expected that a compact, low molecular weight inhibitor with an  
46  
47 acceptor with low intrinsic reactivity would offer the best chance for success. Overall, this strategy was  
48  
49 anticipated to provide a rapid rate of inactivation of BTK, as well as minimal reactivity to small molecule  
50  
51 thiols, proteins, and DNA to mitigate any off-target interactions.  
52  
53  
54  
55  
56  
57  
58  
59  
60

As we began to focus on a covalent inhibition strategy, our deep understanding of non-covalent, reversible inhibition of BTK played a key role.<sup>15d,18-20</sup> As the X-ray co-crystal structure of our highly potent and selective clinical asset **2**<sup>15d</sup> (Figures 2 and 5; BTK IC<sub>50</sub> = 0.50 nM; hWB IC<sub>50</sub> = 90 nM; 1.5 Å, PDB ID code: 5T18) bound to the kinase domain of BTK revealed, the tetrahydrocarbazole motif provides strong hydrogen bonding interactions with the hinge region. Specifically, the tetrahydrocarbazole NH and the carboxamide carbonyl engaged in hydrogen bonding interactions with Met477 in the hinge region of the active site, while the NH<sub>2</sub> of the carboxamide formed hydrogen bonding interactions with Glu475 and a conserved water, providing a bridging interaction with the gatekeeper Leu408 residue. In addition, a weak hydrogen bonding interaction of the quinazolinedione to the Cys481 residue through a conserved water was observed, highlighting the compound's close proximity. As a result, our initial strategy, as recently reported,<sup>21</sup> involved replacing the quinazolinedione with a simple acrylamide, as shown in Figure 6. Encouragingly, this provided compound **3a** with highly potent, covalent inhibition. As recently disclosed,<sup>21</sup> a truncated dimethyl indole scaffold, as represented by **3b** and **3c**, retained the activity seen with **3a**. Unfortunately, oral dosing of carbazole **3a** in a mouse PK study resulted in low plasma concentrations with an aniline metabolite, resulting from acrylamide hydrolysis, as the predominant drug-related compound in circulation. Alternative acceptors did not resolve the PK issue while sustaining desirable potency, so as a consequence, our revised strategy focused on replacing the aniline linker. Although we explored covalent, irreversibility across the full range of our reversible scaffolds, this article will focus on the SAR development of the dimethylindole carboxamide series since it provided a desirable balance between potency/selectivity and PK properties, as well as overall favorable pharmaceutical properties.<sup>21</sup> This effort ultimately led to our covalent, irreversible clinical compound, branebrutinib (**5a**, BMS-986195).

## Biological Evaluation

The covalent, irreversible compounds presented in this article were evaluated in a human recombinant BTK enzyme assay to determine their intrinsic activity against BTK. It should be noted that the potency of a compound with a BTK IC<sub>50</sub> significantly below 1 nM may be underestimated since this approaches



the lower limit of potency that can be measured in the enzyme assay (limited by enzyme concentration). Given the intrinsic potency of the parent scaffold, significant potency resulting from the addition of an electrophilic acceptor suggests but does not prove covalent, irreversible inhibition. As a result, a dialysis assay was used to determine whether or not a compound was irreversibly bound. In this assay, the compound was incubated with BTK for 90 min. at concentrations approximately 25-fold higher than the  $IC_{50}$ , to ensure saturation of the active site, followed by overnight dialysis against assay buffer with two buffer exchanges. If BTK activity did not return, the compound was regarded as a likely covalent inhibitor (later confirmed by active site occupancy, mass spectrometry, and crystallographic analysis of select compounds). In this assay, a reversible BTK inhibitor showed almost complete recovery of activity. A BCR stimulated calcium flux assay in Ramos B cells was used to establish activity in a cellular environment. In light of the fact that  $IC_{50}$  determinations are dependent on both pre-incubation time and the rate of covalent bonding, the intrinsic potency of a covalent, irreversible inhibitor would need to be evaluated in a time-dependent manner. As a result, the rate of BTK engagement and inactivation of selected analogues was determined in an active site probe-based assay using a biotinylated covalent inactivator<sup>22</sup> to quantify unmodified active sites following incubation with the compound in human whole blood, as well as the kinetics and dose relationships of in vivo inactivation of BTK in mice and cynomolgus monkeys after oral administration. In parallel with the in vitro potency assays, in vitro liability profiling data was assessed to prioritize compounds. Selected compounds were evaluated in multi-species PK studies and ultimately rodent efficacy models of human lupus and RA.

## Results and Discussion

As seen in Table 1, replacing the tolyl or phenyl linker in **3b** and **3c**, respectively, with a 3-amino piperidine ring appended with an acrylamide afforded **4a** (racemic) which resulted in a 20-fold loss in activity. Replacing the acrylamide acceptor with a more reactive vinyl sulfonamide (**4b**) resulted in a ~3-fold increase in activity relative to **4a**. Enantiomerically pure derivatives **4c** and **4d** were subsequently prepared and evaluated, with **4d** providing similar intrinsic potency as both **3b** and **3c** in both the biochemical BTK assay and the Ramos cellular assay. As shown in Table 1, **4d** had substantially

improved stability in human liver microsomes when compared to **1a** (90% remaining;  $T_{1/2}$  of 50 min vs. 1% remaining;  $T_{1/2}$  of 1.5 min., respectively). However, in spite of the increased metabolic stability relative to **1a**, plasma concentrations for **4d** in a mouse coarse PK study were low ( $C_{max}$ : 127 nM; AUC: 0.35  $\mu\text{M}\cdot\text{h}$ ). Unfortunately, metabolite identification studies in human liver microsomes (10  $\mu\text{M}$  incubation, 30 min.) revealed that the primary route of metabolism of **4d** was through direct glutathione addition not mediated through glutathione-S-transferase (GST), which would be undesirable for a covalent, irreversible inhibitor. This suggested that the vinyl sulfonamide acceptor is too reactive and is likely driving the observed potency. Interestingly, in spite of having a highly reactive acceptor, **4d** provided a slower rate of inactivation relative to **1a** in a time-dependent, concentration-dependent BTK inactivation assay in human whole blood, as shown in Figure 7. This clearly suggested that compound **4d** has a less than optimal linker/acceptor geometry to provide both high affinity binding to the hinge region of the kinase domain active site ( $K_i$ ) and optimal positioning of the acceptor for rapid inactivation ( $k_{inact}$ ).

As a result, our strategy evolved into the optimization of the linker and acceptor trajectory. Saturated linkers with varying sizes, points of attachment, and chirality were paired with less reactive acceptors to fine-tune the geometry (Figure 8), with a primary focus on optimizing  $k_{inact}$  while maintaining the intrinsic high affinity ( $K_i$ ) for the target. The SAR representing our effort to improve both potency and pharmacokinetic properties are outlined in Table 2. This effort resulted in two interesting leads, compounds **4k** and **4f**, both providing less than 10 nM cellular potency. Further evaluation showed that **4k** inactivated BTK in the human whole blood assay at a rate similar to **1a** (apparent second order rate =  $1.0 \times 10^{-4} \text{ nM}^{-1}\cdot\text{min}^{-1}$  vs.  $1.2 \times 10^{-4} \text{ nM}^{-1}\cdot\text{min}^{-1}$ , respectively). On a more intriguing note, compound **4f**, with a propiolamide acceptor, provided 1.8 nM activity in the cellular assay and inactivated BTK in the human whole blood assay at a rate >10-fold faster than **1a** ( $>10 \times 10^{-4} \text{ nM}^{-1}\cdot\text{min}^{-1}$  vs.  $1.2 \times 10^{-4} \text{ nM}^{-1}\cdot\text{min}^{-1}$ ). Unfortunately, low plasma concentrations were observed in a mouse PK study. In both human and mouse liver microsomes, the primary metabolic pathway identified corresponded to direct glutathione addition, likely contributing to the poor in vivo exposure, once again suggesting that the acceptor is too

1 reactive. In an effort to mitigate the reactivity, the corresponding but-2-ynamide acceptor **4g** was  
2 investigated. Intriguingly, **4g** was no longer a substrate for direct GSH addition and provided acceptable  
3 plasma concentrations in vivo; however, **4g** was ~20 fold less potent than **4f** in the cellular assay, with an  
4 rate of inactivation similar to that of **1a**.  
5  
6  
7

8  
9 Encouraged by the balance between potency and reactivity as well as PK and stability attained with  
10 the but-2-ynamide acceptor paired with the (*S*)-3-aminopiperadine linker, we directed our attention toward  
11 improving both the intrinsic potency and PK through core modifications. Consistent with our  
12 observations in the reversible effort,<sup>15d</sup> addition of a fluoro substituent at C5 of the indole core, to give  
13 **5a**, provided significant enhancements in potency, with 0.1 nM inhibition of BTK and 7 nM inhibition in  
14 the cellular assay (Table 3). Additionally, **5a** provided significantly higher plasma concentrations in a  
15 mouse PK study relative to **4g** (C<sub>max</sub>: 42 uM; AUC: 52. uM·h vs. C<sub>max</sub>: 0.49 uM; AUC: 1.1 uM·h,  
16 respectively). As shown in Figure 9, **5a** inactivated BTK in the human whole blood assay at a rate 3-fold  
17 faster than **1a**. Adding further support, biochemical kinetic evaluation of **5a** demonstrated a rate of BTK  
18 inactivation 4-fold faster than **1a** ( $3.5 \times 10^{-4} \text{ nM}^{-1} \cdot \text{min}^{-1}$  vs.  $1.2 \times 10^{-4} \text{ nM}^{-1} \cdot \text{min}^{-1}$ , Table 4). This clearly  
19 illustrated that we had optimized the geometry of the compound to allow for both high affinity binding  
20 ( $K_i$ ) and rapid inactivation through covalent bonding with Cys 481 ( $k_{inact}$ ). As expected, the des-methyl  
21 derivative **5b** was shown, when biochemically evaluated, to inactivate BTK at a rate 7-fold faster than **5a**  
22 and consequently would be expected to be too reactive in vivo.  
23  
24  
25  
26  
27  
28  
29  
30  
31  
32  
33  
34  
35  
36  
37  
38  
39  
40

41 An expanded view of the in vitro activity profile of **5a** is outlined in Table 5. In B cells stimulated  
42 through the B cell receptor (BCR), **5a** potently inhibited signaling and functional endpoints, including  
43 calcium flux ( $\text{IC}_{50} = 7 \text{ nM}$ ), production of cytokines, proliferation, and surface expression of the  
44 costimulatory molecule CD86 ( $\text{IC}_{50}$  values < 1 nM). As expected, CD69 expression in peripheral B cells,  
45 when stimulated through CD40, was not impacted by **5a** since this pathway is not dependent on the kinase  
46 activity of BTK to mediate downstream signaling, thus demonstrating the compound's functional  
47 selectivity. When evaluated against IgG-containing immune complex low affinity activating  $\text{Fc}\gamma$  ( $\text{Fc}\gamma\text{RIIa}$   
48 and  $\text{Fc}\gamma\text{RIII}$ ) receptor endpoints in peripheral blood mononuclear cells (PBMC), **5a** was highly effective  
49  
50  
51  
52  
53  
54  
55  
56  
57  
58  
59  
60

at inhibiting TNF $\alpha$  production with equivalent potency to those measured for the BCR-dependent endpoints in B cells. In human whole blood assays, **5a** potently inhibited BCR-stimulated expression of CD69 on B cells with an IC<sub>50</sub> of 11 nM. Measurements of BTK inactivation in these assays showed a similar IC<sub>50</sub> of 5 nM. Since the concentration of BTK in human whole blood is approximately 10 nM, the compound effectively titrated the amount of BTK present in these assays. As previously mentioned, **5a** rapidly inactivated BTK in a time- and concentration-dependent manner when added to human whole blood, providing a second order rate of inactivation of 3.5 x 10<sup>-4</sup> nM<sup>-1</sup>·min<sup>-1</sup>.

In order to gain an understanding of the overall kinase selectivity, **5a** was evaluated against a panel of 245 kinases (Figure 10). A partial list of kinase selectivity data is summarized in Table 6. Dimethylindole **5a** was highly selective, providing >5,000-fold selectivity for BTK over 240 kinases with only the 4 related Tec family kinases demonstrating less than 5000-fold selectivity (9 – 1,000-fold), as shown in Figure 10. Interestingly, 10 kinases have a comparable cysteine residue in the active site, the Tec family, the EGFR family, and JAK3. Out of these 10 kinases, **5a** demonstrated activity of less than 5,000-fold relative to BTK for only the 4 other members of the Tec family. Overall, when compared to reversible inhibitor **2**,<sup>15d</sup> covalent inhibition with **5a** resulted in significant improvement in the overall magnitude of selectivity, with the exception of Tec family kinases TEC, BMX, and TXK. On the other hand, the selectivity of **5a** against Tec family kinase ITK was significantly enhanced relative to **2** (1,000x vs. 30x, respectively). The improved selectivity against ITK observed with **5a** is likely attributed to both the intrinsic structural selectivity of the compound and the impact of the unique cysteine micro-environment of ITK on covalent bonding, compared to the other four Tec family kinases, BTK, TEC, BMX and TXK, which all share a similar micro-environment.<sup>13c</sup> Of particular note, **5a** was >10,000-fold selective for BTK over members of the EGFR family (HER1 and HER4). Since a kinase assay does not fully capture the time-dependent nature of a covalent inhibitor, compound **5a** was evaluated against an EGFR-dependent AU565 breast cancer cell line to assess functional EGFR kinase activity over a three day period. Compound **5a** failed to show inhibition at concentrations up to 25,000 nM in this assay. Compound **1a**, on the other hand, inhibited this assay with an IC<sub>50</sub> of 30 nM.

The X-ray co-crystal structure of **5a** bound to the kinase domain of BTK (Figure 11, PDB ID code: 608I) clearly highlighted that the compact nature of **5a** binds tightly in the active site to facilitate the rapid rate of BTK inactivation that is observed. Consistent with our reversible clinical inhibitor **2**,<sup>15d</sup> the co-crystal structure revealed that the tetrahydrocarbazole NH and the carboxamide carbonyl are engaged in a hydrogen bonding interaction with Met477 in the hinge region of the active site. The NH<sub>2</sub> of the carboxamide is not only forming a hydrogen bonding interaction with Glu475, but also with a conserved water, providing a bridging interaction with the gatekeeper Leu408 residue. Most importantly, the structure confirmed the covalent nature of the inhibitor through a clearly defined, albeit stereochemically non-selective, covalent bond with the sulfur of Cys481. As shown in Figure 12, the overlay of the single crystal X-ray structure with the co-crystal structure of **5a** bound with BTK clearly illustrates that we have designed a covalent, irreversible inhibitor that maintains both the high affinity binding of our reversible compounds while orienting the acceptor in close proximity to the cysteine nucleophile for rapid inactivation.

With a highly desirable activity and selectivity profile, a rapid rate of BTK inactivation, a favorable liability profile (Table 7) particularly for a covalent inhibitor, and desirable compound plasma concentrations in mice, **5a** was further evaluated in vivo.<sup>23</sup> In multi-species pharmacokinetic studies (Table 8), the absolute oral bioavailability of **5a** was 100% in mice, 74% in rats, 46% in cynomolgus monkeys, and 81% in dogs. The total body plasma clearance of **5a** was low in all species. The steady-state volume of distribution observed was greater than the plasma volume but less than the total body water, indicative of extravascular distribution, in spite of the high protein binding (free fraction: 0.2 – 1.2%, Table 7). However, brain penetration was very low in mice, rats, and dogs (<5% of plasma concentration). Of particular interest, both the plasma  $T_{1/2}$  (i.v.) and  $T_{max}$  (p.o.) values were short across species (0.46 – 4.3 h and 0.58 – 1.0 h, respectively, Table 8). We viewed this as important for a covalent inhibitor since the compound would need to have adequate intrinsic stability to facilitate rapid enzymatic inactivation in vivo, but remaining inhibitor would need to be cleared quickly to mitigate any off-target interaction.

When administered orally to BALB/c mice, **5a** dose-dependently inactivated BTK in peripheral blood with a single dose of 0.5 mg/kg, providing 90% inactivation 4 hours after dosing (Figure 13A). Consistent with a slow rate of BTK resynthesis, inactivation was sustained at this dose with 86% inactivation remaining at 24 h post-dose. Evaluation of **5a** in BALB/C mice (0.5 – 2.5 mg/kg p.o.) for 48 h indicated that approximately 25% of BTK active sites were resynthesized over 24 h. In cynomolgus monkeys, when administered orally with a single 0.5 mg/kg dose, 100% inactivation was achieved at the 4 hour time point with 74% inactivation remaining at 72 hours (Figure 13B). The drop in inactivation over 72 hours is reflective of the slow resynthesis rate of BTK. Interestingly, the compound was largely cleared within 4 - 6 hours after dosing in both studies, clearly highlighting one of the key advantages of covalent inhibition. When compared with **1a**, **5a** was ~30 fold more potent at inactivating BTK in mice after a single dose (Figure 13C).

Dimethylindole **5a** was evaluated in vivo in a mouse collagen-induced arthritis (CIA) model of human RA, which is both B cell- and Fc $\gamma$ R-dependent. Once daily oral dosing of **5a**, started at the time of the initial collagen immunization and continued throughout the duration of the study (38 days), resulted in dose-dependent inhibition of clinically evident disease with 21%, 83%, and 92% inhibition observed at the end of the study at doses of 0.1, 0.5, and 2.5 mg/kg p.o., q.d., respectively (Figure 14). Of particular note, the 0.5 mg/kg and 2.5 mg/kg dose levels provided robust protection from clinically evident disease (Figure 14A and 14B). Measurements of BTK inactivation in blood samples collected 24 hours after the last dose showed high levels of inactivation (0.1 mg/kg – 64%; 0.5 mg/kg – 97%, and 2.5 mg/kg – 99%, Figure 14B). Histological evaluation of the right hind paws, evaluating bone resorption and inflammation, was consistent with the clinical scores (*data not shown*). Micro-computed tomography of the hind limbs (Figure 14C) illustrated that **5a** provided a dose-dependent protection against pitting, loss of bone mass, woven porous bone, and fusion of the small bones evident in the mice receiving only vehicle. The animals receiving 0.5 mg/kg showed essentially complete protection, as illustrated by the presence of a smooth bone surface and easily recognizable small individual bones of the foot and ankle. The compound was

also effective at 0.5 mg/kg p.o, q.d. in blocking disease progression when dosed in a pseudo-established dosing mode (data not shown).<sup>23</sup>

Additionally, **5a** was evaluated in vivo in a NZB/W lupus-prone mouse model, in which the mice develop a disease closely resembling human systemic lupus erythematosus and lupus nephritis (Figure 15). Mice were dosed by once daily oral gavage for 14 weeks with either **5a** (0.2, 0.5, and 1.5 mg/kg), prednisolone (10 mg/kg), or vehicle (80:20 PEG400:water). In this study, treatment with **5a** provided complete protection from disease-related death over the course of treatment (Figure 15A). Additionally, compound **5a** was shown to dose-dependently inhibit the increase in severe proteinuria (Figure 15B), a measure of the underlying nephritis. Serum anti-double stranded deoxyribonucleic acid (anti-dsDNA) titers, which progressively increased over the course of the study in vehicle control mice, were also inhibited in a dose-dependent manner (Figure 15C) with 40%, 51%, and 61% reductions at the end of the study at the 0.2, 0.5, and 1.5 mg/kg doses, respectively. Histological evaluation of the kidneys confirmed that treatment with **5a** at all doses provided robust protection against tubulo-interstitial and glomerular nephritis, as well as inflammatory infiltration, at levels equivalent to those seen with prednisolone (Figure 15D). IgG immune complex deposition, critical in driving disease pathobiology in both this murine model and human lupus nephritis, was prominent in the capillaries of the glomeruli of vehicle control mice. As seen in Figure 15E, histological evaluation revealed that **5a** reduced the level of immune complex deposits as effectively as prednisolone. Measurements of BTK inactivation in blood samples collected 24 hours after the last dose showed high levels of inactivation at all three doses (0.2 mg/kg – 92%; 0.5 mg/kg – 99%, and 1.5 mg/kg – 100%, Figure 15F).

In evaluating the in vivo efficacy results, achieving > 90% inactivation was associated with a very robust response, with near complete protection from disease. On the basis of these results, we felt that a projected human dose targeting BTK inactivation of  $\geq 95\%$  was desirable. Considering the rapid rate of inactivation in human whole blood, the hepatocyte metabolism in human and other species, and the in vivo PK results in multiple species, the human dose to achieve  $\geq 95\%$  inactivation was projected to be < 10 mg, p.o., q.d.

With highly desirable pharmacology favoring a low projected human dose, we concentrated our efforts on assessing the off-target reactivity and overall toxicity. As previously mentioned, the concern with covalent, irreversible inhibition is the potential for off-target reactivity to biomolecules. To assess the risk for **5a**, several studies were undertaken to evaluate intrinsic reactivity to thiols, proteins, and DNA and to evaluate non-specific protein covalent binding both in vitro and in vivo. Evaluation of covalent binding in vitro in human hepatocytes incubated for 2 h at a concentration of 10  $\mu$ M using  $^{14}$ C-labeled **5a**, incorporated in the carbonyl of the acetylene acceptor (see experimental section), revealed very low levels of protein covalent binding (1.0 %,  $131 \pm 2$  pmol/mg of protein). In addition, no covalent binding was observed with off-target cysteine residues in protein mixtures containing BTK (10 cysteine residues), human hemoglobin, or human serum albumin, up to 10  $\mu$ M concentrations of **5a**. In fact, only <10% protein binding in human hemoglobin was observed at a concentration of 100  $\mu$ M. When incubated with GSH in enzyme free phosphate buffer, no GSH addition was observed, indicating a low intrinsic chemical reactivity to thiol containing nucleophiles. This is consistent with the previously reported GSH reactivity data for acalabrutinib, which benefits from the same but-2-ynamide acceptor.<sup>13c</sup>

In a rat quantitative whole body autoradiography study (10 mg/kg, p.o.) evaluating tissue distribution and retention, the majority of the compound was cleared within 24 h with only minor radioactivity remaining in the liver, kidneys, and skin after 48 to 96 h, indicating low tissue binding. Consistent with this finding, a mass balance study with  $^{14}$ C-labeled **5a** (10 mg/kg, PO) in intact rats ( $n = 3$ ) showed complete recovery of the total radioactivity in urine and feces over 72 h with only 0.7% ( $\pm 0.2$ ) of the radioactivity remaining in the carcass. Furthermore, very low covalent binding was observed in the organs studied, including liver ( $\leq 0.03\%$  of dose), spleen ( $\leq 0.007\%$  of dose), and pancreas ( $\leq 0.002\%$  of dose) in rats over a 7-24 h time point with a single, oral dose of **5a** (1 and 10 mg/kg). Additionally, no significant increase in covalent binding was observed in these tissues after 5 days of daily, oral dosing (1 and 10 mg/kg) in rats.

A recent report outlined a strategy to predict the in vivo daily covalent binding burden (DCBB) for covalent, irreversible inhibitors derived from an analysis of several marketed covalent drugs that have



established safe clinical profiles, as well as compounds that did not.<sup>24</sup> The authors concluded that if a compound has an estimated DCBB of  $\leq 10$  mg/day, it is more likely to be clinically safe. When applying this strategy to **5a** considering the low projected human dose of  $< 10$  mg q.d., p.o. and the assessment of both in vitro protein covalent binding ( $< 1\%$ ) in human hepatocytes and in vivo rat studies, **5a** was determined to have a DCBB of  $< 0.10$  mg/day. This value is significantly lower than the literature reported upper limit of 10 mg/day for clinically safe drugs. While this does not guarantee that **5a** will be safe in humans, it does instill a sense of confidence as the compound proceeds clinically. In evaluating genotoxicity, **5a** was negative in both Ames and in vitro micronucleus (CHO cells) assessments (Table 7). With an extremely low DCBB and a very desirable tolerability in toxicity studies in both rat and dog, compound **5a** was advanced into clinical development.<sup>25</sup>

## Chemistry

The synthetic pathways utilized in the preparation of the compounds presented in this article are provided in Schemes 1 – 2.<sup>26</sup> Analogues **4** were prepared as outlined in Scheme 1. The desired commercially available primary and secondary amines were coupled with **6** under Buchwald-Hartwig amination conditions<sup>27</sup> to provide intermediates **7a** and **7b**. Attempts to perform the amination step on carboxamide intermediate **13** failed to provide any appreciable product. Heating a mixture of either **7a** or **7b** in sulfuric acid at 60 °C for 1 h resulted in concurrent hydrolysis of the carbonitrile to the carboxamide and deprotection of the protecting group. The final covalent, irreversible analogues **4a** – **4q** were prepared by an acylation step using chloromethanesulfonyl chloride, acryloyl chloride, propiolic acid, or but-2-ynoic acid, as indicated in Scheme 1. C5 Fluoro substituted derivatives **5a** and **5b** were prepared in a similar fashion as analogues **4** starting from compound **9**, as outlined in Scheme 2. The absolute structure of **5a** was determined by single crystal X-ray structure analysis (CCDC # 1901788) (see experimental for more detail). As previously reported,<sup>21</sup> dimethylindoles **3b** and **3c** were prepared as depicted in Scheme 3.

The dimethylindole core intermediates **6** and **9** in Schemes 1 and 2, respectively, were prepared as outlined in Scheme 4. Both the C5 hydrogen and the C5 fluoro substituted cores, utilized in the

preparation of analogues **4** and **5**, were prepared through a Fischer indole cyclization between hydrazines **12**<sup>15d,19-21</sup> and 2-butanone in the presence of acetic acid to afford dimethylindoles **13** in good yield. The acids (**13**) were then activated with EDCI and HOBt and treated with ammonium hydroxide to afford dimethylindole amides **14**. The carbonitrile intermediates **6** (R = H) and **9** (R = F) utilized in Schemes 1 and 2 were prepared in high yield when the corresponding amines were stirred with POCl<sub>3</sub> in tetrahydrofuran at room temperature overnight.

## Conclusions

In summary, we have outlined a strategy to identify a covalent, irreversible inhibitor of BTK which provides both a rapid in vivo enzymatic inactivation and a low projected human dose. The strategy involved starting with a scaffold with high intrinsic affinity ( $K_i$ ) for both binding and selectivity, in the absence of covalent inhibition, where the acceptor only enhances but does not drive potency and selectivity. Electrophilic acceptors were explored to bond with Cys481 with low intrinsic reactivity to mitigate off-target interactions. This required optimizing the linker and acceptor geometry to enhance  $k_{inact}$  while maintaining the overall binding affinity ( $K_i$ ). In addition, this strategy focused on identifying a compound with PK/ADME properties amenable for rapid target engagement but would allow for excess compound to be rapidly cleared. This effort resulted in the identification of branebrutinib, **5a**, (S)-4-(3-(but-2-ynamido)piperidin-1-yl)-5-fluoro-2,3-dimethyl-1H-indole-7-carboxamide, as a highly selective covalent, irreversible inhibitor of BTK with rapid target inactivation in vivo, supporting a low projected oral human dose of < 10 mg p.o., q.d. With a very low off-target/non-specific daily covalent binding burden of < 0.10 mg/day and a desirable safety and tolerability profile, **5a** was advanced for clinical evaluation. In Phase I randomized, placebo-controlled multiple-ascending dose studies in healthy participants, **5a** was well tolerated providing >99% BTK occupancy (inactivation) at doses of  $\geq 3$  mg dosed orally, once daily.<sup>25</sup> This data is consistent with our preclinical dose projection and highly supports the continued clinical investigation of this novel agent.

## Experimental Section

Proton magnetic resonance ( $^1\text{H}$ ) spectra were recorded on either a Bruker Avance 400 (400 MHz), a Bruker Avance III 500 (500 MHz), or a JEOL Eclipse 500 (500 MHz) spectrometer and are reported in *ppm* relative to the reference solvent of the sample in which they were run. LCMS analyses were conducted using a Shimadzu SCL-10A liquid chromatograph and a SPD UV-vis detector at 220 or 254 nm with the MS detection performed on a Waters Micromass ZQ spectrometer or a Waters Acquity UPLC with a MS detection performed on a Waters SQ spectrometer. Preparative, reverse-phase HPLC purifications were performed using one of the following conditions: (1) Analogues **4a-d,g-j,m-q** were purified via preparative LC/MS with the following conditions: Column: Waters XBridge C18, 19 x 250 mm, 5- $\mu\text{m}$  particles; Mobile Phase A: 5:95 acetonitrile: water with 10 mM ammonium acetate; Mobile Phase B: 95:5 acetonitrile: water with 10 mM ammonium acetate; Gradient: 5-100% *or* 15-55% B over 25 minutes, then a 5-minute hold at 100% B; Flow: 20 mL/min. Fractions containing the desired product were combined and dried via centrifugal evaporation; (2) Analogue **4e** was purified via preparative LC/MS with the following conditions: Column: Waters XBridge C18, 19 x 250 mm, 5- $\mu\text{m}$  particles; Mobile Phase A: 5:95 acetonitrile:water with 0.05% TFA; Mobile Phase B: 95:5 acetonitrile:water with 0.05% TFA; Gradient: 0-100% B over 25 minutes, then a 5-minute hold at 100% B; Flow: 20 mL/min. Fractions containing the desired product were combined and dried via centrifugal evaporation; or (3) Analogue **4l** was purified via preparative HPLC with the following conditions: Columns: Phenomenex Axia C<sub>18</sub> column with a binary solvent system where solvent A = 5% acetonitrile, 95% water, 0.05% trifluoroacetic acid and solvent B = 95% acetonitrile, 5% water, and 0.05% trifluoroacetic acid and eluting with a gradient of increasing concentration of acetonitrile suitable to the column size and separation to be achieved. Fractions containing the product were neutralized with an aqueous solution of sodium bicarbonate and concentrated under reduced pressure. The residue was dissolved in an organic solvent, washed with water, dried over anhydrous sodium sulfate or magnesium sulfate, and concentrated under reduced pressure. All flash column chromatography was performed on EM Science silica gel 60 (particle size of 40 – 60  $\mu\text{m}$ ) or with an ISCO column. All reagents were purchased from commercial sources and

used without further purification unless otherwise noted. All reactions were performed under an inert atmosphere.

Research involving animals was performed in accordance with institutional guidelines as defined in the U.S. by the Institutional Animal Care and Use Committee.

HPLC analyses were performed using the following conditions. All final compounds had an HPLC purity of  $\geq 95\%$ .

**Method A:** A linear gradient using 5% acetonitrile, 95% water, and 0.05% trifluoroacetic acid (Solvent A) and 95% acetonitrile, 5% water, and 0.05% trifluoroacetic acid (Solvent B);  $t = 0$  min., 10% B,  $t = 12$  min., 100% B (15 min.) was employed on a SunFire C18 3.5 $\mu$ m, 3.0 x 150 mm column. Flow rate was 1.0 mL/min and UV detection was set to 220/254 nm. The LC column was maintained at ambient temperature.

**Method B:** A linear gradient using 5% acetonitrile, 95% water, and 0.05% trifluoroacetic (Solvent A) and 95% acetonitrile, 5% water, and 0.05% trifluoroacetic (Solvent B);  $t = 0$  min., 10% B,  $t = 12$  min., 100% B (15 min.) was employed on a XBridge Ph 3.5 $\mu$ m, 3.5 x 150 mm column. Flow rate was 1.0 mL/min and UV detection was set to 220/254 nm. The LC column was maintained at ambient temperature.

**Method C.** Column: Waters Acquity UPLC BEH C18, 2.1 x 50 mm, 1.7- $\mu$ m particles; Mobile Phase A: 5:95 acetonitrile:water with 10 mM ammonium acetate; Mobile Phase B: 95:5 acetonitrile:water with 10 mM ammonium acetate; Temperature: 50 °C; Gradient: 0-100% B over 3 minutes, then a 0.75-minute hold at 100% B; Flow: 1.11 mL/min; Detection: UV at 220 nm.

**Method D.** Column: Waters Acquity UPLC BEH C18, 2.1 x 50 mm, 1.7- $\mu$ m particles; Mobile Phase A: 5:95 acetonitrile:water with 0.1% trifluoroacetic acid; Mobile Phase B: 95:5 acetonitrile:water with 0.1% trifluoroacetic acid; Temperature: 50 °C; Gradient: 0-100% B over 3 minutes, then a 0.75-minute hold at 100% B; Flow: 1.11 mL/min; Detection: UV at 220 nm.

**Method E.** A linear gradient using 10% methanol, 90% water, and 0.2% phosphoric acid (Solvent A) and 90% methanol, 10% water, and 0.2% phosphoric acid (Solvent B);  $t = 0$  min., 0% B,  $t = 9$  min., 100% B (8 min.) was employed on a YMC ProC18 S5 ODS 4.6 x 50 mm column (oven temperature: 40 °C). Flow

rate was 2.5 mL/min and UV detection was set to 220 nm. The LC column was maintained at ambient temperature.

**Method F.** Waters UPLC; Column: Waters Acquity BEH C18 1.7 $\mu$ m 2.1 x 150 mm at 40 °C; Flow rate: 0.4 mL/min.; Mobile Phase: A: 0.05% trifluoroacetic acid in water and B: acetonitrile; Gradient: 0 min. (10% B), 15 min. (95% B), 17 min. (95% B), and 17.1 min. (10% B); Detection: UV 220 – 400 nm.

#### 4-(3-Acrylamido-2-methylphenyl)-7-(2-hydroxypropan-2-yl)-9H-carbazole-1-carboxamide

**(3a).** A mixture of 3-bromo-2-methylaniline (6.20 g, 33.3 mmol), 4,4,4',4',5,5,5',5'-octamethyl-2,2'-bi(1,3,2-dioxaborolane) (9.31 g, 36.7 mmol) and potassium acetate (6.54 g, 66.6 mmol) in 1,4-dioxane (83 mL) was purged with nitrogen for 10 min. The PdCl<sub>2</sub>(dppf)-CH<sub>2</sub>Cl<sub>2</sub> adduct catalyst (0.653 g, 0.800 mmol) was added, and the mixture was purged for another 5 min. and then heated at reflux (110 °C) for 2.75 h. The reaction mixture was cooled and filtered through Celite®, and the pad was washed with ethyl acetate. The filtrate was washed with water, washed with brine, and dried over anhydrous sodium sulfate. Concentration under reduced pressure followed by purification by silica gel chromatography (ISCO 120 g column, 10-20% ethyl acetate in hexane) afforded 2-methyl-3-(4,4,5,5-tetramethyl-1,3,2-dioxaborolan-2-yl)aniline (7.09 g, 30.4 mmol, 91% yield) as a light yellow solid. LCMS (ESI) *m/z* Calcd for C<sub>13</sub>H<sub>20</sub>BNO<sub>2</sub> [M + H]<sup>+</sup> 234.2. Found: 234.1. <sup>1</sup>H-NMR (400 MHz, CDCl<sub>3</sub>)  $\delta$  7.23 (dd, *J*=7.3, 1.1 Hz, 1H), 7.04 (t, *J*=7.6 Hz, 1H), 6.77 (dd, *J*=7.9, 1.1 Hz, 1H), 3.61 (br. s., 2H), 2.39 (s, 3H), and 1.35 (s, 12H).

To a solution of 2-methyl-3-(4,4,5,5-tetramethyl-1,3,2-dioxaborolan-2-yl)aniline (0.525 g, 2.25 mmol) and Hunig's base (0.433 mL, 2.48 mmol) in dichloromethane (11.3 mL) was added acryloyl chloride (0.192 mL, 2.37 mmol). The reaction mixture was stirred at room temperature for 2h, partitioned between brine and dichloromethane, and the organic phase was collected and dried over sodium sulfate. Concentration under reduced pressure followed by purification by silica gel chromatography (ISCO 40 g column; 5-20% ethyl acetate in hexane) gave N-(2-methyl-3-(4,4,5,5-tetramethyl-1,3,2-dioxaborolan-2-yl)phenyl)acrylamide as a pale yellow solid. LCMS (ESI) *m/z* Calcd for C<sub>16</sub>H<sub>22</sub>BNO<sub>3</sub> [M + H]<sup>+</sup> 288.2. Found: 288.3. <sup>1</sup>H-NMR (400 MHz, CDCl<sub>3</sub>)  $\delta$  8.01 (br. s., 1H), 7.64 (d, *J*=5.9 Hz, 1H), 7.23 (t, *J*=7.7 Hz,

1H), 7.07 (br. s., 1H), 6.48 - 6.40 (m, 1H), 6.32 (br. s., 1H), 5.78 (d,  $J=9.5$  Hz, 1H), 2.49 (s, 3H), and 1.36 (s, 12H).

A mixture of 4-bromo-7-(2-hydroxypropan-2-yl)-9H-carbazole-1-carboxamide<sup>15d,19b</sup> (40 mg, 0.115 mmol), N-(2-methyl-3-(4,4,5,5-tetramethyl-1,3,2-dioxaborolan-2-yl)phenyl)acrylamide (36.4 mg, 0.127 mmol), and tetrakis(triphenylphosphine)palladium (6.66 mg, 5.76  $\mu$ mol) in toluene (2.2 mL) and ethanol (720 mL) was degassed with argon for 2-5 min. To the mixture was added 2 M aqueous sodium carbonate (146  $\mu$ L, 0.291 mmol), followed by purging with argon. The reaction mixture was heated at 90 °C overnight, concentrated under reduced pressure, and purified by reverse-phase, preparative HPLC to give **3a** (12 mg, 0.028 mmol, 24%) as a pale yellow solid. HPLC purity: 99% ( $t_r$  = 1.29 min. – Method C;  $t_r$  = 1.28 min. - Method D); LCMS (ESI)  $m/z$  Calcd for  $C_{26}H_{25}N_3O_3$  [ $M + H$ ]<sup>+</sup> 428.2. Found: 428.2. <sup>1</sup>H-NMR (500 MHz, DMSO- $d_6$ )  $\delta$  11.42 (s, 1H), 9.69 (s, 1H), 8.16 (br. s., 1H), 7.95 (s, 1H), 7.86 (d,  $J=1.0$  Hz, 1H), 7.64 (d,  $J=7.9$  Hz, 1H), 7.47 (br. s., 1H), 7.36 (t,  $J=7.7$  Hz, 1H), 7.12 (d,  $J=7.4$  Hz, 1H), 6.99 (dd,  $J=8.4$ , 1.5 Hz, 1H), 6.94 (d,  $J=7.4$  Hz, 1H), 6.73 (d,  $J=8.4$  Hz, 1H), 6.56 (dd,  $J=17.1$ , 10.2 Hz, 1H), 6.27 (dd,  $J=16.8$ , 2.0 Hz, 1H), 5.78 - 5.74 (m, 1H), 4.98 (s, 1H), 1.88 (s, 3H), and 1.44 (s, 6H).

**4-(3-Acrylamido-2-methylphenyl)-2,3-dimethyl-1H-indole-7-carboxamide (3b).**<sup>26</sup> Following the procedure used to prepare **3a**, 2-methyl-3-(4,4,5,5-tetramethyl-1,3,2-dioxaborolan-2-yl)aniline (*see procedure for 3a*) was converted into N-(2-methyl-3-(4,4,5,5-tetramethyl-1,3,2-dioxaborolan-2-yl)phenyl)acrylamide in 80% yield. <sup>1</sup>H-NMR (400 MHz, CDCl<sub>3</sub>)  $\delta$  8.01 (br. s., 1H), 7.64 (d,  $J=5.9$  Hz, 1H), 7.23 (t,  $J=7.7$  Hz, 1H), 7.07 (br. s., 1H), 6.48-6.40 (m, 1H), 6.32 (br. s., 1H), 5.78 (d,  $J=9.5$  Hz, 1H), 2.49 (s, 3H), and 1.36 (s, 12H).

A mixture of 4-bromo-2,3-dimethyl-1H-indole-7-carboxamide (50 mg, 0.112 mmol), N-(2-methyl-3-(4,4,5,5-tetramethyl-1,3,2-dioxaborolan-2-yl)phenyl)acrylamide (35.5 mg, 0.124 mmol), and tetrakis(triphenylphosphine)palladium (6.49 mg, 5.62  $\mu$ mol) in a mixture of toluene (2.1 mL) and ethanol (0.70 mL) was degassed under argon for 2-5 min. To the mixture was added 2 M aqueous sodium carbonate (140  $\mu$ L, 0.281 mmol), followed by purging with argon. The reaction mixture was heated at 90 °C overnight, concentrated under reduced pressure, and purified by reverse-phase, preparative HPLC to

provide **3b** (10.8 mg, 0.031 mmol, 28%). HPLC purity: 97%;  $t_r$  = 1.41 min. (Method C); LCMS (ESI)  $m/z$  Calcd for  $C_{21}H_{21}N_3O_2$   $[M + H]^+$  348.2. Found: 348.2.  $^1H$ -NMR (500 MHz, DMSO- $d_6$ )  $\delta$  10.74 (s, 1H), 9.60 (s, 1H), 8.00 (br. s., 1H), 7.58 (d,  $J$ =7.9 Hz, 1H), 7.48 (d,  $J$ =7.9 Hz, 1H), 7.32 (br. s., 1H), 7.23 (t,  $J$ =7.7 Hz, 1H), 7.01 (d,  $J$ =7.4 Hz, 1H), 6.69 (d,  $J$ =7.4 Hz, 1H), 6.53 (dd,  $J$ =17.1, 10.2 Hz, 1H), 6.24 (dd,  $J$ =17.3, 2.0 Hz, 1H), 5.74 (dd,  $J$ =10.4, 2.0 Hz, 1H), 2.29 (s, 3H), 1.83 (s, 3H), and 1.50 (s, 3H).

**4-(3-Acrylamidophenyl)-2,3-dimethyl-1H-indole-7-carboxamide (3c).**<sup>26</sup> A mixture of 3-bromoaniline (1.00 g, 5.81 mmol), 4,4,4',4',5,5,5',5'-octamethyl-2,2'-bi(1,3,2-dioxaborolane) (1.55 g, 6.10 mmol), and potassium acetate (1.14 g, 11.6 mmol) in 1,4-dioxane (14.5 mL) was purged with nitrogen for 10 min. The mixture was treated with  $PdCl_2(dppf)$  dichloromethane adduct (0.114 g, 0.140 mmol) and bubbled with nitrogen for an additional 5 min. The mixture was heated at reflux for 2.75 h and then cooled to room temperature and filtered through Celite®. The pad was washed with ethyl acetate and tetrahydrofuran, and the filtrate was concentrated under reduced pressure and purified by silica gel chromatography (ISCO 40 g, 10-25% ethyl acetate in hexanes) to provide 3-(4,4,5,5-tetramethyl-1,3,2-dioxaborolan-2-yl)aniline as an off-white solid (1.27 g, >99%). LCMS (ESI)  $m/z$  Calcd for  $C_{12}H_{18}BNO_2$   $[M + H]^+$  220.2. Found: 220.  $^1H$ -NMR (400 MHz,  $CDCl_3$ )  $\delta$  7.24-7.13 (m, 3H), 6.82-6.77 (m, 1H), 3.64 (br. s., 2H), and 1.35 (s, 12H).

A solution of 3-(4,4,5,5-tetramethyl-1,3,2-dioxaborolan-2-yl)aniline (0.300 g, 1.37 mmol) and Hunig's base (0.311 mL, 1.78 mmol) in dichloromethane (9.1 mL) was cooled in an ice-bath and treated with acryloyl chloride (0.117 mL, 1.44 mmol). The mixture was stirred at room temperature for 40 min, concentrated under reduced pressure, and purified by silica gel chromatography (ISCO 24 g, 15-40% ethyl acetate in hexanes) to provide *N*-(3-(4,4,5,5-tetramethyl-1,3,2-dioxaborolan-2-yl)phenyl) acrylamide as a white solid (0.292 g, 78% yield). LCMS (ESI)  $m/z$  Calcd for  $C_{15}H_{20}BNO_3$   $[M + H]^+$  274.2. Found: 274.0.

A mixture of 4-bromo-2,3-dimethyl-1H-indole-7-carboxamide (30 mg, 0.112 mmol), *N*-(3-(4,4,5,5-tetramethyl-1,3,2-dioxaborolan-2-yl)phenyl)acrylamide (32.2 mg, 0.118 mmol), and tetrakis(triphenylphosphine)palladium (6.49 mg, 5.62  $\mu$ mol) in toluene (2.1 mL) and ethanol (0.7 mL) was degassed for 2-5 min. The mixture was treated with a 2 M aqueous sodium carbonate (142  $\mu$ L, 0.284

mmol), degassed again, and the reaction mixture was heated at 90 °C overnight, concentrated under reduced pressure, and purified by reverse-phase, preparative HPLC to give **3c** (10.2 mg, 0.030 mmol, 27% yield). HPLC purity: 98% ( $t_r$  = 1.41 min. – Method C;  $t_r$  = 1.40 min. - Method D); LCMS (ESI)  $m/z$  Calcd for  $C_{20}H_{19}N_3O_2$   $[M + H]^+$  334.2. Found: 334.1.  $^1H$ -NMR (500 MHz, DMSO- $d_6$ )  $\delta$  10.82 (br. s., 1H), 10.23 (br. s., 1H), 8.02 (br. s., 1H), 7.73 (br. s., 1H), 7.68 (d,  $J$ =7.9 Hz, 1H), 7.59 (dd,  $J$ =7.4, 4.0 Hz, 1H), 7.42 - 7.31 (m, 2H), 7.11 - 7.05 (m, 1H), 6.80 (dd,  $J$ =7.7, 4.2 Hz, 1H), 6.49 - 6.39 (m, 1H), 6.25 (d,  $J$ =17.3 Hz, 1H), 5.76 (d,  $J$ =9.9 Hz, 1H), 2.33 (d,  $J$ =4.0 Hz, 3H), and 1.71 (d,  $J$ =3.5 Hz, 3H).

**(*RS*)-4-(3-Acrylamidopiperidin-1-yl)-2,3-dimethyl-1H-indole-7-carboxamide (4a).**<sup>26</sup> Following the procedures used for the preparation of **4d** but substituting (*RS*)-benzyl piperidin-3-ylcarbamate for (*S*)-benzyl piperidin-3-ylcarbamate, 4-bromo-2,3-dimethyl-1H-indole-7-carbonitrile (**6**) was converted into (*RS*)-4-(3-aminopiperidin-1-yl)-2,3-dimethyl-1H-indole-7-carboxamide. LCMS (ESI)  $m/z$  Calcd for  $C_{16}H_{22}N_4O$   $[M + H]^+$  287.2. Found: 287<sup>+</sup>.

To a solution of 4-(3-aminopiperidin-1-yl)-2,3-dimethyl-1H-indole-7-carboxamide (35 mg, 0.092 mmol) and Hunig's base (21  $\mu$ L, 0.119 mmol) in a 1:1 mixture of dichloromethane and tetrahydrofuran (1.8 mL), cooled in an ice-bath, was added acryloyl chloride (8.19  $\mu$ L, 0.101 mmol). The resulting reaction mixture was stirred at room temperature for 1h. Concentrated under reduce pressure followed by purification by reverse-phase, preparative HPLC gave **4a** (10 mg, 0.029 mmol, 32% yield). HPLC purity: 99% ( $t_r$  = 1.29 min. – Method C;  $t_r$  = 1.21 min. - Method D); LCMS (ESI)  $m/z$  Calcd for  $C_{19}H_{24}N_4O_2$   $[M + H]^+$  341.2. Found: 341.1.  $^1H$ -NMR (500 MHz, DMSO- $d_6$ )  $\delta$  10.60 (br. s., 1H), 8.13 - 8.01 (m, 1H), 7.82 (br. s., 1H), 7.46 (dd,  $J$ =7.9, 4.0 Hz, 1H), 7.12 (br. s., 1H), 6.53 (dd,  $J$ =8.2, 3.7 Hz, 1H), 6.28 - 6.16 (m, 1H), 6.13 - 6.02 (m, 1H), 5.58 (dd,  $J$ =10.2, 2.2 Hz, 1H), 4.02 (br. s., 1H), 3.39 (br. s., 1H), 3.17 (br. s., 1H), 2.63 (br. s., 1H), 2.43 - 2.26 (m, 7H), 1.99 - 1.67 (m, 3H), and 1.36 (d,  $J$ =11.4 Hz, 1H).

**(*RS*)-2,3-Dimethyl-4-(3-(vinylsulfonamido)piperidin-1-yl)-1H-indole-7-carboxamide (4b).**<sup>26</sup> To a solution of 4-(3-aminopiperidin-1-yl)-2,3-dimethyl-1H-indole-7-carboxamide (30 mg, 0.105 mmol) (*see procedure for 4a*) and Hunig's base (46  $\mu$ L, 0.262 mmol) in dichloromethane (1.3 mL), cooled at



0°C, was added 2-chloroethanesulfonyl chloride (22  $\mu$ L, 0.210 mmol) dropwise. The resulting reaction mixture was stirred at room temperature for 3h. Concentration under reduce pressure followed by purification by reverse-phase, preparative HPLC provided **4b** (7.2 mg, 0.105 mmol, 18% yield). HPLC purity: 97% ( $t_r$  = 1.43 min. – Method C;  $t_r$  = 1.43 min. - Method D); LCMS (ESI)  $m/z$  Calcd for  $C_{18}H_{24}N_4O_3S [M + H]^+$  377.2. Found: 377.1.  $^1H$ -NMR (500 MHz, Methanol- $d_4$ )  $\delta$  7.40 (d,  $J$ =7.9 Hz, 1H), 6.63 - 6.54 (m, 2H), 6.20 (d,  $J$ =16.8 Hz, 1H), 5.90 (d,  $J$ =9.9 Hz, 1H), 3.52 (br. s., 2H), 3.21 (br. s., 1H), 2.75 - 2.50 (m, 2H), 2.41 (s, 3H), 2.34 (s, 3H), 2.09 - 2.00 (m, 1H), 1.90 - 1.77 (m, 2H), and 1.43 (br. s., 1H).

**(*R*)-2,3-Dimethyl-4-(3-(vinylsulfonamido)piperidin-1-yl)-1H-indole-7-carboxamide (4c).<sup>26</sup>**

Following the procedures used to prepare **4d** but substituting (*R*)-benzyl piperidin-3-ylcarbamate for (*S*)-benzyl piperidin-3-ylcarbamate, 4-bromo-2,3-dimethyl-1*H*-indole-7-carbonitrile (**6**) was converted into (*R*)-4-(3-aminopiperidin-1-yl)-2,3-dimethyl-1*H*-indole-7-carboxamide. LCMS (ESI)  $m/z$  Calcd for  $C_{18}H_{24}N_4O_3S [M + H]^+$  287.2. Found: 287<sup>+</sup>.

To a solution of (*R*)-4-(3-aminopiperidin-1-yl)-2,3-dimethyl-1*H*-indole-7-carboxamide (50 mg, 0.105 mmol) and Hunig's base (37  $\mu$ L, 0.210 mmol) in a 1:1 mixture of dichloromethane and tetrahydrofuran (1.9 mL), cooled in an ice-acetone-dry ice bath, was added a solution of 2-chloroethanesulfonyl chloride (20  $\mu$ L, 0.189 mmol) in dichloromethane (273  $\mu$ L). The resulting reaction mixture was stirred at 0°C for 1h. Concentration under reduced pressure followed by purification by reverse-phase, preparative HPLC afforded **4c** (5.8 mg, 0.015 mmol, 15% yield). HPLC purity: 99% ( $t_r$  = 1.32 min. – Method C;  $t_r$  = 1.29 min. - Method D); LCMS (ESI)  $m/z$  Calcd for  $C_{18}H_{24}N_4O_3S [M + H]^+$  377.2. Found: 377.2.  $^1H$ -NMR (500 MHz, DMSO- $d_6$ )  $\delta$  10.61 (s, 1H), 7.82 (br. s., 1H), 7.47 (d,  $J$ =7.9 Hz, 2H), 7.13 (br. s., 1H), 6.76 (dd,  $J$ =16.5, 9.8 Hz, 1H), 6.52 (d,  $J$ =7.9 Hz, 1H), 6.05 (d,  $J$ =16.5 Hz, 1H), 5.94 (d,  $J$ =9.8 Hz, 1H), 3.39 (br. s., 2H), 3.13 (br. s., 1H), 2.56 (br. s., 1H), 2.42 (d,  $J$ =11.0 Hz, 1H), 2.32 (d,  $J$ =10.4 Hz, 6H), 1.97 (d,  $J$ =11.0 Hz, 1H), 1.78 (br. s., 1H), 1.68 (d,  $J$ =13.4 Hz, 1H), and 1.32 (d,  $J$ =13.4 Hz, 1H).

**(*S*)-2,3-Dimethyl-4-(3-(vinylsulfonamido)piperidin-1-yl)-1H-indole-7-carboxamide (4d).<sup>26</sup>** A

mixture of 4-bromo-2,3-dimethyl-1*H*-indole-7-carbonitrile (**6**) (2.50 g, 10.0 mmol), (*S*)-benzyl piperidin-

3-ylcarbamate (2.47 g, 10.5 mmol), 2,2'-bis(diphenylphosphino)-1,1'-binaphthalene (0.312 g, 0.502 mmol), tris(dibenzylideneacetone)dipalladium (0.460 g, 0.502 mmol) and cesium carbonate (4.58 g, 14.1 mmol) in 1,4-dioxane (143 mL) was purged with nitrogen and then heated at 100 °C for 16 h. The reaction mixture was cooled to room temperature, diluted with tetrahydrofuran, filtered through Celite®, and the solids were washed with tetrahydrofuran. The filtrate was concentrated under reduced pressure and purified by silica gel chromatography (ISCO 80 g column, 15-30% ethyl acetate in hexanes) to provide (*S*)-benzyl (1-(7-cyano-2,3-dimethyl-1*H*-indol-4-yl)piperidin-3-yl)carbamate as a light yellow solid (2.13 g, 53% yield). LCMS (ESI) *m/z* Calcd for C<sub>24</sub>H<sub>26</sub>N<sub>4</sub>O<sub>2</sub> [M + H]<sup>+</sup> 403.2. Found: 403<sup>+</sup>. <sup>1</sup>H-NMR (400 MHz, DMSO-*d*<sub>6</sub>) δ 11.43 (s, 1H), 7.40-7.26 (m, 7H), 6.62 (d, *J*=8.1 Hz, 1H), 5.08-4.94 (m, 2H), 3.79-3.65 (m, 1H), 3.41 (d, *J*=10.1 Hz, 1H), 3.20 (d, *J*=11.0 Hz, 1H), 2.60 (t, *J*=10.7 Hz, 1H), 2.43-2.16 (m, 7H), 1.92 (d, *J*=9.5 Hz, 1H), 1.86-1.78 (m, 1H), 1.71 (d, *J*=11.2 Hz, 1H), and 1.40-1.26 (m, 1H).

A suspension of (*S*)-benzyl (1-(7-cyano-2,3-dimethyl-1*H*-indol-4-yl)piperidin-3-yl)carbamate (1.69 g, 3.44 mmol) in 80% aqueous sulfuric acid (11 mL, 172 mmol) was heated at 60 °C for 2.5 h. The mixture was cooled to room temperature and then poured over ice. The pH of the mixture was adjusted to about 9-10 with concentrated aqueous potassium hydroxide, and the resulting mixture was extracted with a 3:1 mixture of chloroform and isopropanol. The organic phase was dried over anhydrous sodium sulfate and concentrated to provide (*S*)-4-(3-aminopiperidin-1-yl)-2,3-dimethyl-1*H*-indole-7-carboxamide as a brown solid (1.66 g, 99% yield), which was used without further purification. LCMS (ESI) *m/z* Calcd for C<sub>16</sub>H<sub>22</sub>N<sub>4</sub>O [M + H]<sup>+</sup> 287.2. Found: 287<sup>+</sup>.

To a solution of (*S*)-4-(3-aminopiperidin-1-yl)-2,3-dimethyl-1*H*-indole-7-carboxamide (40 mg, 0.095 mmol) and Hunig's base (58 μL, 0.332 mmol) in dichloromethane (1.9 mL), cooled at 0 °C, was slowly added 2-chloroethanesulfonyl chloride (30 μL, 0.285 mmol) dropwise. The resulting reaction mixture was stirred at room temperature for 3 h, concentrated under reduced pressure, and purified by reverse-phase, preparative HPLC to give **4d** (13 mg, 0.033 mmol, 35%). HPLC purity: 99% (*t*<sub>r</sub> = 1.36 min. - Method C; *t*<sub>r</sub> = 1.31 min. - Method D); LCMS (ESI) *m/z* Calcd for C<sub>18</sub>H<sub>24</sub>N<sub>4</sub>O<sub>3</sub>S [M + H]<sup>+</sup> 377.2. Found: 376.9. <sup>1</sup>H-NMR (500 MHz, DMSO-*d*<sub>6</sub>) δ 10.62 (s, 1H), 7.83 (br. s., 1H), 7.52 - 7.40 (m, 2H), 7.14 (br. s., 1H), 6.76

(dd,  $J=16.3, 9.9$  Hz, 1H), 6.58 - 6.46 (m, 1H), 6.06 (d,  $J=16.8$  Hz, 1H), 5.94 (d,  $J=9.9$  Hz, 1H), 3.42 - 3.36 (m, 2H), 3.14 (d,  $J=9.9$  Hz, 1H), 2.61 - 2.53 (m, 1H), 2.42 (d,  $J=10.9$  Hz, 1H), 2.32 (d,  $J=10.9$  Hz, 6H), 1.97 (d,  $J=10.9$  Hz, 1H), 1.83 - 1.76 (m, 1H), 1.74 - 1.60 (m, 1H), and 1.40 - 1.26 (m, 1H).

**Alternative Procedure:** To a solution of (*S*)-4-(3-aminopiperidin-1-yl)-2,3-dimethyl-1H-indole-7-carboxamide (2.2 g, 4.23 mmol) and Hunig's base (1.26 mL, 7.18 mmol) in a 2:1 mixture of dichloromethane and tetrahydrofuran (63 mL), cooled in ice-acetone-dry ice at -20 °C, was slowly added a solution of 2-chloroethaneulfonyl chloride (0.71 mL, 6.76 mmol) in dichloromethane (9.0 mL). The resulting brown suspension was stirred at 0 °C for 1h. The reaction was filtered under reduce pressure, and the brown solid was washed with tetrahydrofuran and ethyl acetate. The filtrates were concentrated under reduced pressure and purified by silica gel chromatography (ISCO 80g column, 50-70%/15min, 70-80%/13min, 70-80%/12min, 80%/8 min, 80-90/5min, 90%/15min - ethyl acetate in hexane) to afford **4d** (0.519, 1.34 mmol, 32% yield) as a pale yellow solid. HPLC purity: 97.1%;  $t_r = 7.73$  min. (Method A); 96.1%;  $t_r = 7.36$  min. (Method B); LCMS (ESI)  $m/z$  Calcd for  $C_{18}H_{24}N_4O_3S$   $[M + H]^+$  377.2. Found: 377.2.  $^1H$ -NMR (400 MHz, DMSO- $d_6$ )  $\delta$  10.60 (s, 1H), 7.80 (br. s., 1H), 7.51 - 7.39 (m, 2H), 7.11 (br. s., 1H), 6.76 (dd,  $J=16.5, 9.9$  Hz, 1H), 6.53 (d,  $J=8.1$  Hz, 1H), 6.06 (d,  $J=16.5$  Hz, 1H), 5.94 (d,  $J=9.9$  Hz, 1H), 3.39 (d,  $J=9.9$  Hz, 2H), 3.14 (d,  $J=11.0$  Hz, 1H), 2.62 - 2.55 (m, 1H), 2.46 - 2.38 (m, 1H), 2.32 (d,  $J=8.6$  Hz, 6H), 1.97 (d,  $J=12.1$  Hz, 1H), 1.85 - 1.76 (m, 1H), 1.75 - 1.63 (m, 1H), and 1.39 - 1.27 (m, 1H).

**(*R*)-2,3-Dimethyl-4-(3-propiolamidopiperidin-1-yl)-1H-indole-7-carboxamide (4e).**<sup>26</sup> A solution of (*R*)-4-(3-aminopiperidin-1-yl)-2,3-dimethyl-1H-indole-7-carboxamide (50 mg, 0.105 mmol) (*see procedure for 4c*), HATU (80 mg, 0.210 mmol), Hunig's base (55  $\mu$ L, 0.314 mmol), and propiolic acid (8.07 mg, 0.115 mmol) in N,N-dimethylformamide (1.7 mL) was stirred at room temperature for 2.5 h. The reaction mixture was filtered, and the filtrate was concentrated and purified by reverse-phase, preparative HPLC to provide **4e** (21 mg, 0.062 mmol, 59% yield). HPLC purity: 96% ( $t_r = 1.34$  min. - Method C;  $t_r = 1.30$  min. - Method D); LCMS (ESI)  $m/z$  Calcd for  $C_{19}H_{22}N_4O_2$   $[M + H]^+$  339.2. Found: 339.2.  $^1H$ -NMR (500 MHz, DMSO- $d_6$ )  $\delta$  10.62 (s, 1H), 8.83 - 8.72 (m, 1H), 7.48 (d,  $J=8.1$  Hz, 1H), 6.54 (d,  $J=8.4$  Hz, 1H), 3.99 (br. s., 1H), 2.65 - 2.55 (m, 1H), 2.36 (s, 3H), 2.30 (s, 3H), 1.93 - 1.65 (m, 3H),

and 1.37 (br. s., 1H) (Some alkyl and exchangeable carboxamide protons were not observed due to water suppression).

**(S)-2,3-Dimethyl-4-(3-propiolamidopiperidin-1-yl)-1H-indole-7-carboxamide (4f).**<sup>26</sup> A mixture of (S)-4-(3-aminopiperidin-1-yl)-2,3-dimethyl-1H-indole-7-carboxamide (0.077 g, 0.269 mmol) (*see procedure for 4d*), propiolic acid (0.020 mL, 0.323 mmol), HATU (0.143 g, 0.376 mmol), and Hunig's base (0.164 mL, 0.941 mmol) in N,N-dimethylformamide (2.0 mL) was stirred at room temperature for 40 min. The mixture was diluted with ethyl acetate, washed with 10% aqueous lithium chloride (2x), and washed with brine. The organic layer was collected, and the aqueous layers were sequentially extracted with ethyl acetate (2x). The combined organic layers were dried over anhydrous sodium sulfate and concentrated. Purification by silica gel chromatography (ISCO 12 g column, 0% - 5% methanol in dichloromethane) afforded (S)-2,3-dimethyl-4-(3-propiolamidopiperidin-1-yl)-1H-indole-7-carboxamide (0.061 g, 0.177 mmol, 66 % yield) as a pale yellow solid. HPLC purity: 98.1%;  $t_r$  = 7.82 min. (Method A); 98.4%;  $t_r$  = 7.43 min. (Method B); LCMS (ESI)  $m/z$  Calcd for  $C_{19}H_{22}N_4O_2$   $[M + H]^+$  339.2. Found: 339.2. <sup>1</sup>H-NMR (500 MHz, DMSO- $d_6$ )  $\delta$  10.61 (s, 1H), 8.74 (d,  $J$ =7.8 Hz, 1H), 7.91 - 7.73 (m, 1H), 7.48 (d,  $J$ =8.1 Hz, 1H), 7.19 - 7.04 (m, 1H), 6.54 (d,  $J$ =8.1 Hz, 1H), 4.05 - 3.93 (m, 1H), 3.36 - 3.33 (m, 1H), 3.30 - 3.28 (m, 1H), 3.25 - 3.14 (m, 1H), 2.67 - 2.55 (m, 1H), 2.44 - 2.39 (m, 1H), 2.38 - 2.36 (m, 3H), 2.34 - 2.30 (m, 3H), 1.95 - 1.67 (m, 3H), and 1.45 - 1.31 (m, 1H).

**(S)-4-(3-(But-2-ynamido)piperidin-1-yl)-2,3-dimethyl-1H-indole-7-carboxamide (4g).**<sup>26</sup> To a mixture of (S)-4-(3-aminopiperidin-1-yl)-2,3-dimethyl-1H-indole-7-carboxamide (60 mg, 0.210 mmol) (*see procedure for 4d*), HATU (159 mg, 0.419 mmol), and Hunig's base (110  $\mu$ L, 0.629 mmol) in N,N-dimethylformamide (3.1 mL) at room temperature was added but-2-ynoic acid (18.5 mg, 0.220 mmol). The reaction mixture was stirred at room temperature for 2 h. Concentration under reduce pressure followed by purification by silica gel flash chromatography (ISCO 12g column, 30-65% ethyl acetate in hexane) afforded **4g** (37 mg, 0.102 mmol, 49% yield) as a pale yellow solid. HPLC purity: 97.0%;  $t_r$  = 8.74 min. (Method A); LCMS (ESI)  $m/z$  Calcd for  $C_{20}H_{24}N_4O_2$   $[M + H]^+$  353.2. Found: 353.2. <sup>1</sup>H-NMR (400 MHz, DMSO- $d_6$ )  $\delta$  10.58 (s, 1H), 8.46 (d,  $J$ =7.9 Hz, 1H), 7.79 (br. s., 1H), 7.46 (d,  $J$ =7.9 Hz, 1H),

7.09 (br. s., 1H), 6.51 (d,  $J=8.1$  Hz, 1H), 3.97 (br. s., 1H), 3.60 (t,  $J=6.4$  Hz, 2H), 3.17 (d,  $J=11.9$  Hz, 1H), 2.57 (d,  $J=10.6$  Hz, 1H), 2.37 - 2.29 (m, 6H), 1.94 (s, 3H), 1.91 - 1.77 (m, 3H), and 1.34 - 1.28 (m, 1H).

**(*RS*)-4-(3-Acrylamidopyrrolidin-1-yl)-2,3-dimethyl-1H-indole-7-carboxamide (4h).**<sup>26</sup> Following the procedures used to prepare **4d** but substituting (*RS*)-benzyl pyrrolidin-3-ylcarbamate for (*S*)-benzyl piperidin-3-ylcarbamate, 4-bromo-2,3-dimethyl-1H-indole-7-carbonitrile (**6**) was converted into (*RS*)-4-(3-aminopyrrolidin-1-yl)-2,3-dimethyl-1H-indole-7-carboxamide. LCMS (ESI)  $m/z$  Calcd for  $C_{15}H_{20}N_4O$   $[M + H]^+$  273.2. Found: 273<sup>+</sup>. <sup>1</sup>H-NMR (400 MHz, DMSO- $d_6$ )  $\delta$  10.60 (s, 1H), 7.73 (dd,  $J=8.7, 5.6$  Hz, 1H), 7.44 (d,  $J=8.1$  Hz, 1H), 6.96 (br. s., 3H), 6.44 (d,  $J=8.1$  Hz, 1H), 3.56-3.46 (m, 1H), 3.26-3.08 (m, 3H), 2.82 (dd,  $J=9.5, 5.3$  Hz, 1H), 2.33 (s, 3H), 2.30 (s, 3H), 2.19-2.11 (m, 1H), 1.61-1.50 (m, 1H).

To a solution of 4-(3-aminopyrrolidin-1-yl)-2,3-dimethyl-1H-indole-7-carboxamide (35 mg, 0.129 mmol) and Hunig's base (29  $\mu$ L, 0.167 mmol) in a 1:1 mixture of dichloromethane and tetrahydrofuran (2.6 mL), cooled in an ice-bath, was added acryloyl chloride (12  $\mu$ L, 0.141 mmol). The reaction mixture was stirred at room temperature for 3h, concentrated under reduced pressure, and purified by reverse-phase, preparative HPLC to give **4h** (12 mg, 0.037 mmol, 29% yield). HPLC purity: 99% ( $t_r$  = 1.15 min. – Method C); LCMS (ESI)  $m/z$  Calcd for  $C_{18}H_{22}N_4O_2$   $[M + H]^+$  327.2. Found: 327.1. <sup>1</sup>H-NMR (500 MHz, DMSO- $d_6$ )  $\delta$  10.63 (s, 1H), 8.39 (d,  $J=6.4$  Hz, 1H), 7.78 (br. s., 1H), 7.45 (d,  $J=7.9$  Hz, 1H), 7.07 (br. s., 1H), 6.48 (d,  $J=8.4$  Hz, 1H), 6.33 - 6.20 (m, 1H), 6.14 - 6.04 (m, 1H), 5.59 (dd,  $J=9.9, 2.0$  Hz, 1H), 4.45 - 4.30 (m, 1H), 3.30 - 3.23 (m, 2H), 3.14 - 2.98 (m, 2H), 2.38 - 2.22 (m, 7H), and 1.85 - 1.77 (m, 1H).

**(*RS*)-2,3-Dimethyl-4-(3-(vinylsulfonamido)pyrrolidin-1-yl)-1H-indole-7-carboxamide (4i).**<sup>26</sup> To a solution of 4-(3-aminopyrrolidin-1-yl)-2,3-dimethyl-1H-indole-7-carboxamide (30 mg, 0.088 mmol) (*see procedure for 4h*) and Hunig's base (39  $\mu$ L, 0.220 mmol) in dichloromethane (1.1 mL), cooled at 0 °C, was added 2-chloroethanesulfonyl chloride (18  $\mu$ L, 0.176 mmol) dropwise. The reaction mixture was stirred at room temperature for 3 h, concentrated under reduce pressure, and purified by reverse-phase, preparative HPLC to give **4i** (9.8 mg, 0.029 mmol, 36% yield). HPLC purity: 99% ( $t_r$  = 1.30 min. –

Method C;  $t_r$  = 1.22 min. – Method D); LCMS (ESI)  $m/z$  Calcd for  $C_{17}H_{22}N_4O_3S$   $[M + H]^+$  363.2. Found: 363.1.  $^1H$ -NMR (500 MHz, DMSO- $d_6$ )  $\delta$  10.64 (s, 1H), 7.77 (d,  $J$ =14.9 Hz, 1H), 7.69 (br. s., 1H), 7.45 (d,  $J$ =7.9 Hz, 1H), 7.08 (br. s., 1H), 6.78 (dd,  $J$ =16.3, 9.9 Hz, 1H), 6.46 (d,  $J$ =7.9 Hz, 1H), 6.08 (d,  $J$ =16.3 Hz, 1H), 5.99 (d,  $J$ =9.9 Hz, 1H), 3.83 (br. s., 1H), 3.42 - 3.38 (m, 1H), 3.21 - 3.09 (m, 2H), 3.00 (dd,  $J$ =9.7, 6.2 Hz, 1H), 2.35 - 2.21 (m, 7H), and 1.88 - 1.78 (m, 1H).

**(*R*)-2,3-Dimethyl-4-(3-propiolamidopyrrolidin-1-yl)-1H-indole-7-carboxamide (4j).**<sup>26</sup> Following the procedures used to prepare **4d** but substituting (*R*)-benzyl pyrrolidin-3-ylcarbamate for (*S*)-benzyl piperidin-3-ylcarbamate, 4-bromo-2,3-dimethyl-1*H*-indole-7-carbonitrile (**6**) was converted into (*R*)-4-(3-aminopyrrolidin-1-yl)-2,3-dimethyl-1*H*-indole-7-carboxamide. LCMS (ESI)  $m/z$  Calcd for  $C_{15}H_{20}N_4O$   $[M + H]^+$  373.2. Found: 273<sup>+</sup>.

A solution of (*R*)-4-(3-aminopyrrolidin-1-yl)-2,3-dimethyl-1*H*-indole-7-carboxamide (30 mg, 0.094 mmol), HATU (71 mg, 0.187 mmol), Hunig's base (49  $\mu$ L, 0.281 mmol) and propiolic acid (7.2 mg, 0.103 mmol) in *N,N*-dimethylformamide (1.3 mL) was stirred at room temperature for 4 h, concentrated under reduced pressure, and purified by reverse-phase, preparative HPLC to provide **4j** (4.0 mg, 0.024 mmol, 13% yield). HPLC purity: 96% ( $t_r$  = 1.20 min. – Method C;  $t_r$  = 1.08 min. - Method D); LCMS (ESI)  $m/z$  Calcd for  $C_{18}H_{20}N_4O_2$   $[M + H]^+$  325.2. Found: 325.2.  $^1H$ -NMR (500 MHz, DMSO- $d_6$ )  $\delta$  10.63 (s, 1H), 9.08 (d,  $J$ =6.1 Hz, 1H), 7.79 (br. s., 1H), 7.45 (d,  $J$ =7.9 Hz, 1H), 7.07 (br. s., 1H), 6.47 (d,  $J$ =7.9 Hz, 1H), 4.32 (br. s., 1H), 4.14 (s, 1H), 3.26 - 3.13 (m, 2H), 3.12 - 2.98 (m, 2H), 2.31 (d,  $J$ =13.4 Hz, 6H), 2.24 (dd,  $J$ =13.7, 5.8 Hz, 1H), and 1.85 (dd,  $J$ =12.8, 6.1 Hz, 1H).

**(*S*)-4-((1-Acryloylpyrrolidin-3-yl)amino)-2,3-dimethyl-1H-indole-7-carboxamide (4k).**<sup>26</sup> A mixture of 4-bromo-2,3-dimethyl-1*H*-indole-7-carbonitrile (**6**) (0.400 g, 1.61 mmol) and (*S*)-*tert*-butyl 3-aminopyrrolidine-1-carboxylate (0.336 g, 1.80 mmol) in 1,4-dioxane (15 mL) was purged with nitrogen for 5 min. To the mixture was added 2,2'-bis(diphenylphosphino)-1,1'-binaphthalene (0.050 g, 0.080 mmol), tris(dibenzylideneacetone)dipalladium (0.074 g, 0.080 mmol), and cesium carbonate (0.732 g, 2.25 mmol), and the reaction mixture was sealed under nitrogen and heated at 100 °C for 19 h. After cooling to room temperature, the mixture was diluted with ethyl acetate (50 mL), washed with water (50

mL), and washed with brine. The organic layer was collected, and the aqueous layers were sequentially washed with ethyl acetate (3 x 50 mL). The combined organic layers were dried over anhydrous sodium sulfate and concentrated under reduced pressure. The residue was purified by silica gel chromatography, eluting with ethyl acetate and hexanes, to provide (*S*)-*tert*-butyl 3-((7-cyano-2,3-dimethyl-1*H*-indol-4-yl)amino) pyrrolidine-1-carboxylate as a pale yellow solid (0.47 g, 79% yield). LCMS (ESI) *m/z* Calcd for C<sub>20</sub>H<sub>26</sub>N<sub>4</sub>O<sub>2</sub> [M + H]<sup>+</sup> 355.2. Found: 355<sup>+</sup>. <sup>1</sup>H-NMR (400 MHz, DMSO-*d*<sub>6</sub>) δ 11.16 (s, 1H), 7.24 (d, *J*=8.1 Hz, 1H), 6.23 (d, *J*=8.4 Hz, 1H), 5.36 (br. s., 1H), 4.25-4.08 (m, 1H), 3.69-3.57 (m, 1H), 3.48-3.37 (m, 1H), 3.38-3.31 (m, 1H), 3.27-3.16 (m, 1H), 2.34 (s, 3H), 2.24 (s, 3H), 2.22-2.13 (m, 1H), 1.97-1.86 (m, 1H), and 1.49-1.31 (m, 9H).

A mixture of (*S*)-*tert*-butyl 3-((7-cyano-2,3-dimethyl-1*H*-indol-4-yl)amino) pyrrolidine-1-carboxylate (0.470 g, 1.33 mmol) and dichloromethane (5 mL) was cooled to 0 °C, treated with trifluoroacetic acid (5 mL), and stirred for 1 h. The mixture was concentrated under reduced pressure to provide (*S*)-2,3-dimethyl-4-(pyrrolidin-3-ylamino)-1*H*-indole-7-carbonitrile as a trifluoroacetic acid salt. LCMS (ESI) *m/z* Calcd for C<sub>15</sub>H<sub>18</sub>N<sub>4</sub> [M + H]<sup>+</sup> 255.2. Found: 255<sup>+</sup>. <sup>1</sup>H-NMR (400 MHz, DMSO-*d*<sub>6</sub>) δ 11.23 (s, 1H), 8.93-8.72 (m, 1H), 7.27 (d, *J*=8.1 Hz, 1H), 6.21 (d, *J*=8.6 Hz, 1H), 5.48 (br. s., 1H), 4.27 (br. s., 1H), 3.54-3.44 (m, 1H), 3.42-3.33 (m, 1H), 3.31-3.17 (m, 2H), 2.38 (s, 3H), 2.36-2.28 (m, 1H), 2.26 (s, 3H), and 2.09-2.00 (m, 1H).

A mixture of (*S*)-2,3-dimethyl-4-(pyrrolidin-3-ylamino)-1*H*-indole-7-carbonitrile, TFA salt (488 mg, 1.33 mmol) and 80% aqueous sulfuric acid (3 mL) was heated at 60 °C for 2 h. The mixture was cooled to room temperature and was then slowly added to a 10 M aqueous solution of sodium hydroxide at 0 °C. The aqueous layer was removed from the resulting sticky brown solid by decantation. Water was added to the solid, and the mixture was extracted with ethyl acetate (4 x 50 mL). The combined organic layers were washed with brine, dried over anhydrous sodium sulfate, and concentrated to provide (*S*)-2,3-dimethyl-4-(pyrrolidin-3-ylamino)-1*H*-indole-7-carboxamide (270 mg, 75% yield) as an orange solid. LCMS (ESI) *m/z* Calcd for C<sub>15</sub>H<sub>20</sub>N<sub>4</sub>O [M + H]<sup>+</sup> 273.2. Found: 273<sup>+</sup>. <sup>1</sup>H-NMR (400 MHz, DMSO-*d*<sub>6</sub>) δ 10.40 (s, 1H), 7.59 (br. s., 1H), 7.42 (d, *J*=8.4 Hz, 1H), 6.85 (br. s., 1H), 6.05 (d, *J*=8.4 Hz, 1H), 5.07 (d,

$J=6.8$  Hz, 1H), 3.99-3.89 (m, 1H), 3.30 (br. s., 1H), 3.04 (dd,  $J=11.1$ , 6.1 Hz, 1H), 2.98-2.88 (m, 1H), 2.82-2.67 (m, 2H), 2.36 (s, 3H), 2.26 (s, 3H), 2.10 (td,  $J=13.4$ , 7.5 Hz, 1H), and 1.68-1.53 (m, 1H).

To a mixture of (*S*)-2,3-dimethyl-4-(pyrrolidin-3-ylamino)-1*H*-indole-7-carboxamide (80 mg, 0.294 mmol) and Hunig's base (0.154 mL, 0.881 mmol) in a mixture of tetrahydrofuran (7 mL) and dichloromethane (1 mL), cooled to 0 °C, was added a solution of acryloyl chloride (0.14 mL, 1.76 mmol) in 1.3 mL of tetrahydrofuran dropwise over 3 min. The reaction mixture was stirred at 0°C for 1.5 h and then concentrated and purified by silica gel chromatography (ISCO, 0-10% methanol in dichloromethane) to provide **4k** (78 mg, 0.234 mmol, 80% yield) as a pale yellow solid. HPLC purity: 98.2%;  $t_r$  = 6.10 min. (Method A); 98.6%;  $t_r$  = 9.07 min. (Method B); LCMS (ESI)  $m/z$  Calcd for  $C_{18}H_{22}N_4O_2$   $[M + H]^+$  327.2. Found: 327.1.  $^1H$ -NMR (400 MHz, DMSO- $d_6$ )  $\delta$  10.43 (s, 1H), 7.59 (br. s., 1H), 7.45 (d,  $J=7.0$  Hz, 1H), 6.88 (br. s., 1H), 6.68 - 6.45 (m, 1H), 6.24 - 6.05 (m, 2H), 5.73 - 5.59 (m, 1H), 5.16 (dd,  $J=9.7$ , 6.6 Hz, 1H), 4.34 - 4.22 (m, 0.5H), 4.20 - 4.10 (m, 0.5H), 3.99 (dd,  $J=10.1$ , 6.2 Hz, 0.5H), 3.84 - 3.71 (m, 1H), 3.67- 3.64 (m, 0.5H), 3.62 - 3.55 (m, 0.5H), 3.53 - 3.40 (m, 1.5H), 2.34 (s, 3H), 2.33 - 2.31 (m, 0.5H), 2.26 (s, 3H), 2.24 - 2.18 (m, 0.5H), 2.14 - 2.03 (m, 0.5H), and 2.02 - 1.94 (m, 0.5H).

**(*R*)-4-((1-Acryloylpyrrolidin-3-yl)amino)-2,3-dimethyl-1*H*-indole-7-carboxamide (**4l**).<sup>26</sup>**

Following the procedures used to prepare **4k** but substituting (*R*)-*tert*-butyl 3-aminopyrrolidine-1-carboxylate for (*S*)-*tert*-butyl 3-aminopyrrolidine-1-carboxylate, 4-bromo-2,3-dimethyl-1*H*-indole-7-carbonitrile (**6**) was converted into (*R*)-2,3-dimethyl-4-(pyrrolidin-3-ylamino)-1*H*-indole-7-carboxamide. LCMS (ESI)  $m/z$  Calcd for  $C_{15}H_{20}N_4O$   $[M + H]^+$  273.2. Found: 273<sup>+</sup>.  $^1H$ -NMR (400 MHz, DMSO- $d_6$ )  $\delta$  10.40 (s, 1H), 7.59 (br. s., 1H), 7.42 (d,  $J=8.4$  Hz, 1H), 6.85 (br. s., 1H), 6.05 (d,  $J=8.4$  Hz, 1H), 5.07 (d,  $J=6.8$  Hz, 1H), 3.99-3.89 (m, 1H), 3.30 (br. s., 1H), 3.04 (dd,  $J=11.1$ , 6.1 Hz, 1H), 2.98-2.88 (m, 1H), 2.82-2.67 (m, 2H), 2.36 (s, 3H), 2.26 (s, 3H), 2.10 (td,  $J=13.4$ , 7.5 Hz, 1H), and 1.68-1.53 (m, 1H).

To a mixture of (*R*)-2,3-dimethyl-4-(pyrrolidin-3-ylamino)-1*H*-indole-7-carboxamide (50mg, 0.184 mmol) and Hunig's base (0.096 mL, 0.551 mmol) in a mixture of tetrahydrofuran (6 mL) and dichloromethane (1 mL), cooled to 0 °C, was added a solution of acryloyl chloride (0.012 mL, 0.147 mmol) in tetrahydrofuran (0.5 mL) slowly over 3 minutes. The reaction mixture was stirred at 0°C for 1



h, concentrated under reduced pressure, and purified by reverse-phase, preparative HPLC to afford **4l** (8.0 mg, 0.024 mmol, 13% yield) as an off-white solid. HPLC purity: 99% ( $t_r$  = 4.19 min. – Method E); LCMS (ESI)  $m/z$  Calcd for  $C_{18}H_{22}N_4O_2$   $[M + H]^+$  327.2. Found: 327.3.  $^1H$ -NMR (400 MHz, methanol- $d_4$ )  $\delta$  7.44 (d,  $J$ =8.3 Hz, 1H), 6.70 - 6.53 (m, 1H), 6.33 - 6.22 (m, 2H), 5.74 (ddd,  $J$ =15.2, 10.5, 2.0 Hz, 1H), 4.40 - 4.32 (m, 1H), 4.32 - 4.23 (m, 1H), 3.90 (dd,  $J$ =12.8, 5.9 Hz, 1H), 3.86 - 3.58 (m, 3H), 2.47 - 2.33 (s, 3H), 2.30 (s, 3H), 2.24 - 2.14 (m, 1H), and 2.14 - 2.02 (m, 1H).

**(S)-2,3-Dimethyl-4-((1-propioloylpyrrolidin-3-yl)amino)-1H-indole-7-carboxamide (4m).**<sup>26</sup> A solution of 2,3-dimethyl-4-(pyrrolidin-3-ylamino)-1H-indole-7-carboxamide (35 mg, 0.096 mmol) (*see procedure for 4k*), HATU (73 mg, 0.193 mmol), Hunig's base (51  $\mu$ L, 0.289 mmol) and propiolic acid (7.4 mg, 0.106 mmol) in N,N-dimethylformamide (1.4 mL) was stirred at room temperature for 4 h, concentrated under reduced pressure, and purified by reverse-phase, preparative HPLC to provide **4m** (7.1 mg, 0.022 mmol, 28% yield). HPLC purity: 95% ( $t_r$  = 1.03 min. – Method C;  $t_r$  = 1.02 min. - Method D); LCMS (ESI)  $m/z$  Calcd for  $C_{18}H_{20}N_4O_2$   $[M + H]^+$  325.2. Found: 325.2.  $^1H$ -NMR (500 MHz, DMSO- $d_6$ )  $\delta$  10.44 (s, 1H), 7.64 (br. s., 1H), 7.44 (d,  $J$ =8.5 Hz, 1H), 6.88 (br. s., 1H), 6.15 (dd,  $J$ =18.9, 7.9 Hz, 1H), 5.20 (br. s., 1H), 4.52 - 4.40 (m, 1H), 4.29 - 4.17 (m, 1H), 4.11 (br. s., 1H), 3.83 - 3.51 (m, 3H), 2.38 - 2.19 (m, 7H), and 2.12 - 1.98 (m, 1H).

**4-((1-Acryloylpiperidin-4-yl)amino)-2,3-dimethyl-1H-indole-7-carboxamide (4n).**<sup>26</sup> Following the procedures used to prepare **4d** but substituting benzyl 4-aminopiperidine-1-carboxylate for (*S*)-benzyl piperidin-3-ylcarbamate, 4-bromo-2,3-dimethyl-1H-indole-7-carbonitrile (**6**) was converted into 2,3-dimethyl-4-(piperidin-4-ylamino)-1H-indole-7-carboxamide. LCMS (ESI)  $m/z$  Calcd for  $C_{16}H_{22}N_4O$   $[M + H]^+$  287.2. Found: 287<sup>+</sup>.  $^1H$ -NMR (400 MHz, DMSO- $d_6$ )  $\delta$  10.40 (s, 1H), 7.40 (d,  $J$ =8.1 Hz, 1H), 7.21-6.95 (m, 2H), 6.08 (d,  $J$ =8.4 Hz, 1H), 4.87 (d,  $J$ =7.9 Hz, 1H), 3.89 -3.76 (m, 1H), 3.46 (br. s., 1H), 3.00-2.85 (m, 2H), 2.67-2.54 (m, 2H), 2.37 (s, 3H), 2.26 (s, 3H), 1.94 (d,  $J$ =9.5 Hz, 2H), and 1.36 (d,  $J$ =9.0 Hz, 2H).

To a solution of 2,3-dimethyl-4-(piperidin-4-ylamino)-1H-indole-7-carboxamide (50 mg, 0.122 mmol) and Hunig's base (0.085 mL, 0.489 mmol) in tetrahydrofuran (3 mL), cooled at 0 °C, was slowly

added a solution of acryloyl chloride (9  $\mu$ L, 0.110 mmol) (0.09 mL of a solution of 0.09 mL acryloyl chloride in 0.9 mL tetrahydrofuran). The reaction mixture was stirred at 0°C for 1 h. The mixture was concentrated under reduced pressure, and the residue was purified by reverse-phase, preparative HPLC to give **4n** (0.007 g, 0.020 mmol, 16% yield). HPLC purity: 96% ( $t_r$  = 1.18 min. – Method C;  $t_r$  = 1.09 min. – Method D); LCMS (ESI)  $m/z$  Calcd for  $C_{19}H_{24}N_4O_2$   $[M + H]^+$  341.2. Found: 341.2.  $^1H$ -NMR (500 MHz, DMSO- $d_6$ )  $\delta$  10.40 (s, 1H), 7.59 (br. s., 1H), 7.42 (d,  $J$ =7.9 Hz, 1H), 6.83 (dd,  $J$ =16.5, 10.4 Hz, 2H), 6.16 (d,  $J$ =8.5 Hz, 1H), 6.10 (d,  $J$ =16.5 Hz, 1H), 5.67 (d,  $J$ =10.4 Hz, 1H), 4.95 (d,  $J$ =7.9 Hz, 1H), 4.32 (d,  $J$ =6.1 Hz, 1H), 4.02 (d,  $J$ =13.4 Hz, 1H), 3.79 - 3.65 (m, 1H), 3.31 - 3.22 (m, 1H), 3.00 - 2.90 (m, 1H), 2.35 (s, 3H), 2.25 (s, 3H), 2.08 - 1.98 (m, 2H), and 1.50 - 1.40 (m, 2H).

**2,3-Dimethyl-4-((1-propioloylpiperidin-4-yl)amino)-1H-indole-7-carboxamide (4o).**<sup>26</sup> A mixture of 2,3-dimethyl-4-(piperidin-4-ylamino)-1H-indole-7-carboxamide (35 mg, 0.122 mmol) (*see procedure for 4n*), propiolic acid (25.7 mg, 0.367 mmol), HATU (139 mg, 0.367 mmol) and Hunig's base (0.085 mL, 0.489 mmol) in dimethylformamide (1 mL) was stirred at room temperature for 1.5 h, concentrated under reduced pressure, and purified by reverse-phase, preparative HPLC to give **4o** (6.2 mg; 0.018, 15% yield). HPLC purity: 97% ( $t_r$  = 1.19 min. – Method C;  $t_r$  = 1.13 min. – Method D); LCMS (ESI)  $m/z$  Calcd for  $C_{19}H_{22}N_4O_2$   $[M + H]^+$  339.2. Found: 339.2.  $^1H$ -NMR (500 MHz, DMSO- $d_6$ )  $\delta$  10.41 (s, 1H), 7.59 (br. s., 1H), 7.42 (d,  $J$ =8.5 Hz, 1H), 6.85 (br. s., 1H), 6.16 (d,  $J$ =8.5 Hz, 1H), 4.96 (d,  $J$ =8.5 Hz, 1H), 4.53 (s, 1H), 4.26 - 4.11 (m, 2H), 3.73 (q,  $J$ =9.0 Hz, 1H), 3.48 - 3.42 (m, 1H), 2.98 (t,  $J$ =11.0 Hz, 1H), 2.35 (s, 3H), 2.25 (s, 3H), 2.08 (d,  $J$ =11.6 Hz, 1H), 2.01 (d,  $J$ =9.8 Hz, 1H), 1.61 - 1.49 (m, 1H), and 1.47 - 1.34 (m, 1H).

**(*RS*)-4-((1-Acryloylpiperidin-3-yl)amino)-2,3-dimethyl-1H-indole-7-carboxamide (4p).**<sup>26</sup>

Following the procedures used to prepare **4d** but substituting (*RS*)-benzyl 3-aminopiperidine-1-carboxylate for (*S*)-benzyl piperidin-3-ylcarbamate, 4-bromo-2,3-dimethyl-1H-indole-7-carbonitrile (**6**) was converted into (*RS*)-2,3-dimethyl-4-(piperidin-3-ylamino)-1H-indole-7-carboxamide. LCMS (ESI)  $m/z$  Calcd for  $C_{16}H_{22}N_4O$   $[M + H]^+$  287.2. Found: 287<sup>+</sup>.  $^1H$ -NMR (500 MHz, DMSO- $d_6$ )  $\delta$  10.40 (s, 1H), 7.94 (s, 1H), 7.56 (br. s., 1H), 7.41 (d,  $J$ =7.9 Hz, 1H), 6.81 (br. s., 1H), 6.08 (d,  $J$ =8.5 Hz, 1H), 5.40-5.23

(m, 1H), 3.77-3.56 (m, 2H), 3.06 (d,  $J=12.2$  Hz, 1H), 2.78 (br. s., 1H), 2.70-2.61 (m, 2H), 2.38 (s, 3H), 2.26 (s, 3H), 1.86-1.78 (m, 1H), 1.69-1.60 (m, 1H), and 1.52-1.41 (m, 1H).

To a solution of 2,3-dimethyl-4-(piperidin-3-ylamino)-1H-indole-7-carboxamide (42.7 mg, 0.149 mmol) and Hunig's base (0.078 mL, 0.447 mmol) in tetrahydrofuran (2 mL), cooled at 0°C, was slowly added a solution of acryloyl chloride (11  $\mu$ L, 0.134 mmol) (0.1 mL of a solution of 0.1 mL acryloyl chloride in 1 mL tetrahydrofuran). The reaction mixture was stirred at 0 °C for 1 h, concentrated under reduced pressure, and purified by reverse-phase, preparative HPLC to afford **4p** (3.0 mg, 0.007 mmol, 5% yield). HPLC purity: 97% ( $t_r$  = 1.36 min. – Method C;  $t_r$  = 1.01 min. - Method D); LCMS (ESI)  $m/z$  Calcd for  $C_{19}H_{24}N_4O_2$   $[M + H]^+$  341.2. Found: 341.2.  $^1H$ -NMR (500 MHz, DMSO- $d_6$ )  $\delta$  10.42 (br. s., 1H), 7.61 (br. s., 1H), 7.43 (d,  $J=7.9$  Hz, 1H), 6.85 (dd,  $J=16.5, 11.0$  Hz, 1H), 6.67 - 6.52 (m, 0.5H), 6.14 (d,  $J=17.7$  Hz, 2H), 6.08 - 5.95 (m, 0.5H), 5.75 - 5.66 (m, 0.5H), 5.62 - 5.51 (m, 0.5H), 5.04 - 4.90 (m, 1H), 4.27 - 4.17 (m, 1H), 3.88 - 3.81 (m, 1H), 3.79 - 3.72 (m, 1H), 3.70- 3.62 (m, 1H), 3.56 - 3.49 (m, 1H), 2.89 (s, 3H), 2.73 (s, 3H), 2.03 - 1.93 (m, 1H), 1.80 - 1.69 (m, 1H), 1.58 - 1.49 (m, 1H), and 1.30 - 1.20 (m, 1H).

**(*RS*)-2,3-Dimethyl-4-((1-propioloylpiperidin-3-yl)amino)-1H-indole-7-carboxamide (4q).**<sup>26</sup> A mixture of 2,3-dimethyl-4-(piperidin-3-ylamino)-1H-indole-7-carboxamide (28.4 mg, 0.099 mmol) (*see procedure for 4p*), propiolic acid (13.87 mg, 0.198 mmol), HATU (83 mg, 0.218 mmol), and Hunig's base (0.086 mL, 0.495 mmol) in dimethylformamide (1 mL) was stirred at room temperature for 1.5 h. The crude material was purified by reverse-phase, preparative HPLC to provide **4q** (6.2 mg, 0.017, 18% yield). HPLC purity: 95% ( $t_r$  = 1.36 min. – Method C;  $t_r$  = 1.36 min. - Method D); LCMS (ESI)  $m/z$  Calcd for  $C_{19}H_{22}N_4O_2$   $[M + H]^+$  339.2. Found: 339.2.  $^1H$ -NMR (500 MHz, DMSO- $d_6$ )  $\delta$  10.43 (s, 1H), 7.59 (br. s., 1H), 7.43 (dd,  $J=8.1, 4.4$  Hz, 1H), 6.85 (br. s., 1H), 6.29 - 6.08 (m, 1H), 4.98 (t,  $J=7.9$  Hz, 1H), 4.18 (d,  $J=11.4$  Hz, 1H), 3.94 (d,  $J=13.5$  Hz, 0.5H), 3.76 (d,  $J=12.5$  Hz, 0.5H), 3.64 (d,  $J=3.7$  Hz, 0.5H), 3.58 - 3.43 (m, 0.5H), 3.41 - 3.34 (m, 1H), 3.29 - 3.22 (m, 0.5H), 3.12 (dd,  $J=12.5, 8.4$  Hz, 0.5H), 2.35 (s, 3H), 2.26 (s, 3H), 1.99 - 1.90 (m, 1H), 1.83 - 1.65 (m, 2H), 1.62 - 1.48 (m, 1H), and 1.28 - 1.22 (m, 1H).

**(S)-4-(3-(But-2-ynamido)piperidin-1-yl)-5-fluoro-2,3-dimethyl-1H-indole-7-carboxamide**

**(5a).**<sup>26</sup> A mixture of (*S*)-tert-butyl piperidin-3-ylcarbamate (33.9 g, 169 mmol), 4-bromo-5-fluoro-2,3-dimethyl-1H-indole-7-carbonitrile (**9**, 41.1 g, 154 mmol), cesium carbonate (100 g, 308 mmol), and BINAP (9.59 g, 15.4 mmol) in 1,4-dioxane (1,380 mL) was degassed by bubbling nitrogen for 5 min. To the mixture was added Pd<sub>2</sub>(dba)<sub>3</sub> (7.05 g, 7.70 mmol), and the reaction mixture was stirred at reflux for 24 h. The reaction mixture was diluted with ethyl acetate (750 mL), washed with water (1000 mL), washed with brine (100 mL), and dried over anhydrous sodium sulfate. Concentration under reduced pressure afforded the crude product as a brown solid, which was passed through a pad of silica gel with ethyl acetate (900 mL) to remove any inorganics. The reddish crude product was then purified by recrystallization from acetonitrile to give two crops of (*S*)-tert-butyl (1-(7-cyano-5-fluoro-2,3-dimethyl-1H-indol-4-yl)piperidin-3-yl)carbamate (53 g, 108 mmol, 86% yield). LCMS (ESI) *m/z* Calcd for C<sub>19</sub>H<sub>22</sub>N<sub>4</sub>O<sub>2</sub> [M + H]<sup>+</sup> 387.2. Found: 387.3.

To a 100 mL 3-neck flask was added sulfuric acid (90 g). The solution was heated to 60 °C, and (*S*)-tert-butyl (1-(7-cyano-5-fluoro-2,3-dimethyl-1H-indol-4-yl)piperidin-3-yl)carbamate (21 g, 54.3 mmol) was added portion wise over a period of 1.5 h. After 1 h at 60 °C, the reaction mixture was added to ice and warmed to room temperature with stirring. The aqueous phase was extracted with dichloromethane (3x) to remove organic impurities. The pH of the aqueous phase was adjusted to 8, and the solution was extracted with ethyl acetate (2x). The combined organic layers were washed with brine (500 mL), dried over anhydrous sodium sulfate, and concentrated under reduced pressure to give (*S*)-4-(3-aminopiperidin-1-yl)-5-fluoro-2,3-dimethyl-1H-indole-7-carboxamide (13.6 g, 44.7 mmol, 82% yield) as a yellow solid. LCMS (ESI) *m/z* Calcd for C<sub>16</sub>H<sub>21</sub>FN<sub>4</sub>O [M + H]<sup>+</sup> 305.2. Found: 305.2.

To a 500 mL 3-neck flask was added (*S*)-4-(3-aminopiperidin-1-yl)-5-fluoro-2,3-dimethyl-1H-indole-7-carboxamide (33.2 g, 109 mmol) in N,N-dimethylformamide (364 mL), but-2-ynoic acid (11.9 g, 142 mmol), HATU (62.2 g, 164 mmol), and Hunig's base (38 mL, 218 mmol) (temperature rose to 35 °C). The resulting solution was stirred at room temperature for 1.5 h. The mixture was diluted with ethyl acetate (250 mL) and washed with water (500 mL). The organic phase was separated, and the aqueous

layer was extracted with ethyl acetate (2 x 250 mL) (layer separation was facilitated with a small amount of NaCl). The combined organic extracts were washed with water (with small amount of NaCl) (4 x 500 mL), washed with brine (500 mL), and dried over anhydrous sodium sulfate. Concentration under reduced pressure afforded the crude product, which was purified by recrystallization from ethyl acetate to give (*S*)-4-(3-(but-2-ynamido)piperidin-1-yl)-5-fluoro-2,3-dimethyl-1H-indole-7-carboxamide (31 g, 83 mmol, 76% yield) as a white solid.

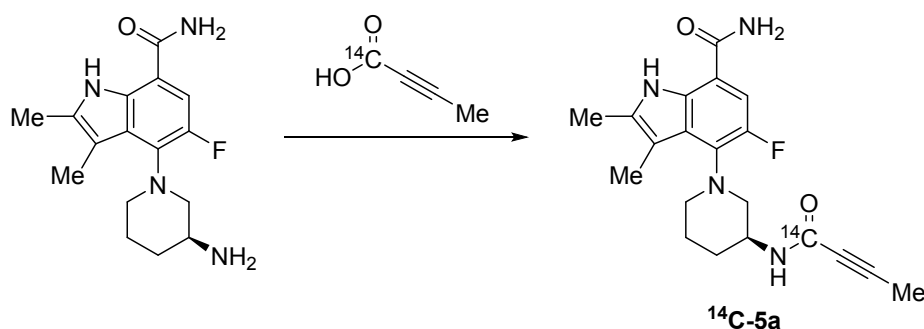
HPLC purity: >99.5%;  $t_r$  = 9.18 min. (Method A); >99.5%;  $t_r$  = 7.90 min. (Method B); 99.7%;  $t_r$  = 7.44 min. (Method F); Chiral purity: 99.8% ee; LCMS (ESI)  $m/z$  Calcd for  $C_{20}H_{23}FN_4O_2$   $[M + H]^+$  371.2. Found: 371.1. Anal. Calcd. for  $C_{20}H_{23}FN_4O_2$ , 0.36%  $H_2O$ : C 64.85, H 6.26, N 15.13; Found: C 64.95, H 6.05, N 15.15.

$^1H$ -NMR (500 MHz, DMSO- $d_6$ )  $\delta$  10.61 (s, 1H), 8.46 (br d,  $J$ =5.6 Hz, 1H), 7.91 (br s, 1H), 7.40 (d,  $J$ =14.2 Hz, 1H), 7.32 (br s, 1H), 3.99 - 3.81 (m, 1H), 3.19 - 3.07 (m, 1H), 3.06 - 2.89 (m, 1H), 3.06 - 2.89 (m, 1H), 2.80 (br s, 1H), 2.37 (s, 3H), 2.31 (s, 3H), 1.94 (s, 3H), 1.91 - 1.80 (m, 1H), 1.72 (br s, 2H), and 1.33 (br s, 1H).

$^{13}C$ -NMR (126 MHz, DMSO- $d_6$ )  $\delta$  168.7 (d,  $J$ =1.8 Hz, 1C), 153.8 (d,  $J$ =233.4 Hz, 1C), 152.4, 134.8, 133.7 (d,  $J$ =9.1 Hz, 1C), 132.6, 127.0 (dd,  $J$ =5.4, 1.0 Hz, 1C), 112.8 (d,  $J$ =7.3 Hz, 1C), 108.9 (d,  $J$ =26.3 Hz, 1C), 106.5 (d,  $J$ =5.5 Hz, 1C), 82.8, 76.2, 57.4, 52.4, 46.8, 30.2, 24.9, 11.6, 10.7, and 3.5.

**(*S*)-4-(3-(but-2-ynamido-1- $^{14}C$ )piperidin-1-yl)-5-fluoro-2,3-dimethyl-1H-indole-7-carboxamide ( $^{14}C$ -5a).**  $Ba[^{14}C]CO_3$  (105 mg, 0.497 mmol, 25 mCi, 1 equivalent) was weighed into a 100 mL 2-neck flask equipped with a septa, and the flask was attached to a vacuum line. A solution of propynyl magnesium bromide (0.5 M in tetrahydrofuran, 1.24 mL, 0.621 mmol, 1.25 equivalent) was transferred by syringe to a 50 mL round bottom flask which was then placed on the vacuum line and frozen with liquid nitrogen. The system was evacuated and isolated. Concentrated sulfuric acid (2 mL, 0.497 mmol) was added to the  $Ba[^{14}C]CO_3$  through the septa to generate  $[^{14}C]CO_2$  which was allowed to condense into the frozen flask containing propynyl magnesium bromide for 40 min. The frozen propynyl magnesium bromide containing condensed  $[^{14}C]CO_2$  was then sealed and allowed to warm to room temperature with stirring for an

additional hour. After addition of 1 N HCl (2 mL), the aqueous solution was extracted with ether (4 x 4 mL). The combined ether phases were washed with 2 mL of brine and dried over MgSO<sub>4</sub>. After filtration, the solvent was removed, and the resulting residue was redissolved in 4 mL of N,N-dimethylformamide. Scintillation counting of the solution showed that it contained 22.6 mCi (90% radiochemical yield) of [1-<sup>14</sup>C]butynoic acid. HPLC analysis of the solution with radioactivity detection (mobile phase A = 0.1% TFA in water, mobile phase B = acetonitrile, Column = Zorbax SBC18, 4.6 x 250 mm, linear gradient 5% to 50% over 20 min, RT = 6.9 min) showed radiochemical purity = 99.2%.



To a solution of (S)-4-(3-aminopiperidin-1-yl)-5-fluoro-2,3-dimethyl-1H-indole-7-carboxamide (30 mg, 0.099 mmol) dissolved in 1 mL of N,N-dimethylformamide was added a 1.2 mL portion of the above N,N-dimethylformamide solution of [1-<sup>14</sup>C]butynoic acid (6.8 mCi, 0.118 mmol). To the stirred solution was added Hunig's base (34 μL, 0.20 mmol), and the resulting solution was stirred for 5 min. HATU (45.0 mg, 0.118 mmol, 1.2 equiv.) was dissolved in approximately 200 μL of N,N-dimethylformamide and then added dropwise to the solution. The resulting mixture was stirred for 30 min at room temperature and then quenched by addition of 2.5 mL of water. This solution was subjected to semi-preparative HPLC (mobile phase A = 0.1% trifluoroacetic acid in water, mobile phase B = acetonitrile, column = Luna C18(2) 25 mm x 250 mm, linear gradient 30% to 95% B over 20 min). Fractions containing pure product were collected and combined. After removal of the majority of the acetonitrile, the solution was neutralized with aqueous bicarbonate solution and then loaded onto an Oasis 500 mg solid phase extraction cartridge. Pure amide product (3.3 mCi, 49% radiochemical yield) was eluted from the sep-pak with acetonitrile: LC/MS (Positive ion, mobile phase A: 0.1% formic acid in water, mobile phase B:

0.1% formic acid in acetonitrile, linear gradient 20%B to 90%B over 5.5 min, column: Luna C18(2), 3 $\mu$ , 50 x 100 mm, RT = 3.3 min)  $m/z$  = 371 (unlabeled) 373, 374; HPLC analysis with UV and radioactivity detection (mobile phase A = 0.1% TFA in water, mobile phase B = 0.1% formic acid in acetonitrile, Column = Luna C18(2) 3  $\mu$ , 50 x 100 mm, isocratic gradient 30% B for 2 min then linear gradient 30% B to 60% B over 14 min, RT = 12.9 min) showed radiochemical purity = 98.4% with an identical retention time to a standard of unlabeled **5a**; LC/MS analysis of labeled **5a** versus unlabeled **5a** determined specific activity = 60.1 mCi/mmol (162  $\mu$ Ci/mg).

**(S)-5-Fluoro-2,3-dimethyl-4-(3-propiolamidopiperidin-1-yl)-1H-indole-7-carboxamide (5b).**<sup>26</sup>

A mixture of (S)-4-(3-aminopiperidin-1-yl)-5-fluoro-2,3-dimethyl-1H-indole-7-carboxamide (*see procedure for 5a*, 0.255 g, 0.838 mmol), propiolic acid (0.070 g, 1.005 mmol), HATU (0.446 g, 1.173 mmol), and Hunig's base (0.512 mL, 2.93 mmol) in N,N-dimethylformamide (4 mL) was stirred at room temperature for 40 min. The mixture was diluted with ethyl acetate, washed with 10% aqueous lithium chloride (2x), and washed with brine. The organic layer was collected, and the aqueous layers were sequentially extracted with ethyl acetate (2x). The combined organic layers were dried over anhydrous sodium sulfate and concentrated. Purification by silica gel chromatography (ISCO 24 g column; 0% - 5% methanol in dichloromethane) afforded **5b** (0.136 g, 0.374 mmol, 45% yield) as a pale yellow solid. HPLC purity: 98.2%;  $t_r$  = 8.86 min. (Method A); 98.3%;  $t_r$  = 8.27 min. (Method B); LCMS (ESI)  $m/z$  Calcd for C<sub>19</sub>H<sub>21</sub>FN<sub>4</sub>O<sub>2</sub> [M + H]<sup>+</sup> 357.2. Found: 357.3. <sup>1</sup>H-NMR (400 MHz, DMSO-d<sub>6</sub>)  $\delta$  10.69 - 10.55 (m, 1H), 8.82 - 8.63 (m, 1H), 8.00 - 7.82 (m, 1H), 7.41 (d,  $J$ =14.2 Hz, 1H), 7.33 (br s, 1H), 4.00 - 3.85 (m, 1H), 3.23 - 3.10 (m, 2H), 3.07 - 2.90 (m, 2H), 2.89 - 2.75 (m, 1H), 2.43 - 2.35 (m, 3H), 2.32 (s, 3H), 1.96 - 1.84 (m, 1H), 1.81 - 1.63 (m, 2H), and 1.46 - 1.30 (m, 1H).

**4-Bromo-2,3-dimethyl-1H-indole-7-carbonitrile (6).**<sup>26</sup> A suspension of 4-bromo-2,3-dimethyl-1H-indole-7-carboxamide (**14a**) (5.65 g, 21.2 mmol) in tetrahydrofuran (151 mL) was treated slowly with phosphorus oxychloride (13.8 mL, 148 mmol). The resulting mixture was stirred at room temperature for 23 h and was then concentrated under reduced pressure. The residue was suspended in ethyl acetate, and

the precipitate was collected by filtration, and the solid was washed sequentially with water, saturated aqueous sodium bicarbonate, and water. The organic filtrate was concentrated, and the residue was suspended in water. The resulting precipitate was collected by filtration, washed sequentially with water, saturated aqueous sodium bicarbonate, and water. The combined precipitates were dried well to give 4-bromo-2,3-dimethyl-1*H*-indole-7-carbonitrile as a yellow solid (4.68 g, 89% yield). LCMS (ESI) *m/z* Calcd for C<sub>11</sub>H<sub>9</sub>BrN<sub>2</sub> [M + H]<sup>+</sup> 249.0. Found: 249<sup>+</sup> and 251<sup>+</sup>. <sup>1</sup>H-NMR (400 MHz, DMSO-*d*<sub>6</sub>) δ 11.89 (br. s., 1H), 7.35 (d, *J*=7.9 Hz, 1H), 7.26 (d, *J*=7.9 Hz, 1H), 2.39 (s, 3H), and 2.34 (s, 3H).

**4-Bromo-5-fluoro-2,3-dimethyl-1*H*-indole-7-carbonitrile (9).**<sup>26</sup> To a solution of 4-bromo-5-fluoro-2,3-dimethyl-1*H*-indole-7-carboxamide (**14b**, 40.4 g, 142 mmol) in dichloromethane (810 mL) was added pyridine (50 g, 2.5 eq) followed by phosphoryl trichloride (19.8 mL, 213 mmol) dropwise at room temperature over 2 minutes. The reaction mixture was stirred for 20 min., and the solvent was removed under reduced pressure. To the residue was added water, and the mixture was stirred for 30 min. The precipitate was collected by filtration and dried to give 4-bromo-5-fluoro-2,3-dimethyl-1*H*-indole-7-carbonitrile (35 g, 131 mmol, 92 % yield) as a tan solid. LCMS (ESI) *m/z* Calcd for C<sub>11</sub>H<sub>8</sub>BrFN<sub>2</sub> [M + H]<sup>+</sup> 266.0. Found: 266.2 and 268.2.

**4-Bromo-2,3-dimethyl-1*H*-indole-7-carboxamide (14a).**<sup>26</sup> A suspension of 4-bromo-2-hydrazinylbenzoic acid hydrochloride<sup>19b,20</sup> (**12a**, 5.87 g, 21.9 mmol) in acetic acid (73 mL) at 75 °C was treated with 2-butanone (9.8 mL, 110 mmol). The mixture was heated on an oil bath at 110 °C. After 18 h, the mixture was concentrated under vacuum to provide a dark brown solid. The residue was suspended in ethyl acetate, and the insoluble material was collected by filtration, washed with ethyl acetate, and dried. The filtrate was concentrated, and the residue was again suspended in ethyl acetate. Additional solid was collected by filtration, washed with ethyl acetate, and dried. The combined solids were dried well to provide 4-bromo-2,3-dimethyl-1*H*-indole-7-carboxylic acid as a brown solid (**13a**, 4.63 g, 79% yield). LCMS (ESI) *m/z* Calcd for C<sub>11</sub>H<sub>10</sub>BrNO<sub>2</sub> [M + H]<sup>+</sup> 268.0. Found: 268<sup>+</sup> and 270<sup>+</sup>. <sup>1</sup>H-NMR (400 MHz, DMSO-*d*<sub>6</sub>) δ 13.29-12.97 (m, 1H), 10.87 (br. s., 1H), 7.48 (d, *J*=7.9 Hz, 1H), 7.20 (d, *J*=8.1 Hz, 1H), 2.40 (s, 3H), and 2.36 (s, 3H).



A mixture of 4-bromo-2,3-dimethyl-1*H*-indole-7-carboxylic acid (**13a**, 4.63 g, 17.3 mmol), EDC (4.97 g, 25.9 mmol) and HOBT (3.44 g, 22.5 mmol) in a mixture of tetrahydrofuran (276 mL) and dichloromethane (69 mL) was stirred at room temperature for 1 h, then treated with 28% aqueous ammonium hydroxide (5.38 mL, 138 mmol). The resulting suspension was stirred at room temperature for 4 days. The mixture was concentrated under reduced pressure, and the residue was partitioned between water and ethyl acetate. The organic layer was collected, and the aqueous phase was extracted with ethyl acetate. The combined organic layers were washed with brine, dried over anhydrous sodium sulfate, and concentrated to provide 4-bromo-2,3-dimethyl-1*H*-indole-7-carboxamide as a yellow solid (**14a**, 3.34 g, 72% yield). LCMS (ESI)  $m/z$  Calcd for  $C_{11}H_{11}BrN_2O$   $[M + H]^+$  267.0. Found: 267<sup>+</sup> and 269<sup>+</sup>. <sup>1</sup>H-NMR (400 MHz, DMSO- $d_6$ )  $\delta$  10.92 (s, 1H), 8.01 (br. s., 1H), 7.48-7.31 (m, 2H), 7.14 (d,  $J=7.9$  Hz, 1H), 2.39 (d,  $J=0.4$  Hz, 3H), and 2.34 (s, 3H).

**4-Bromo-5-fluoro-2,3-dimethyl-1*H*-indole-7-carboxamide (**14b**).**<sup>26</sup> A stirred suspension of 4-bromo-5-fluoro-2-hydrazinylbenzoic acid hydrochloride (**12b**, 1.00 g, 3.50 mmol)<sup>15c,20,24</sup> in acetic acid (11.7 mL) was treated with 2-butanone (1.26 mL, 14.0 mmol) at room temperature. The mixture was heated at 75 °C for 30 min, forming a brown solution, and then at 110 °C for 16 h. The reaction mixture was concentrated, and the residue was suspended in ethyl acetate. The precipitate was collected by filtration, washed with ethyl acetate, and dried. The filtrates were concentrated, and the residue was suspended in ethyl acetate, forming additional precipitate which was collected by filtration, washed with ethyl acetate, and air dried. The combined solids were dried well to provide 4-bromo-5-fluoro-2,3-dimethyl-1*H*-indole-7-carboxylic acid as a brown solid (**13b**, 0.515 g, 51% yield). LCMS (ESI)  $m/z$  Calcd for  $C_{11}H_9BrFNO_2$   $[M + H]^+$  286.0. Found: 286<sup>+</sup> and 288<sup>+</sup>. <sup>1</sup>H-NMR (400 MHz, DMSO- $d_6$ )  $\delta$  13.84-12.75 (m, 1H), 10.96 (s, 1H), 7.45 (d,  $J=9.7$  Hz, 1H), 2.40 (s, 3H), and 2.37 (s, 3H).

Following the procedure used in the final step of the preparation of **14a**, 4-bromo-5-fluoro-2,3-dimethyl-1*H*-indole-7-carboxylic acid (**13b**) was converted into 4-bromo-5-fluoro-2,3-dimethyl-1*H*-indole-7-carboxamide in 75% yield. LCMS (ESI)  $m/z$  Calcd for  $C_{11}H_{10}BrFN_2O$   $[M + H]^+$  285.0. Found:

285<sup>+</sup> and 287<sup>+</sup>. <sup>1</sup>H-NMR (400 MHz, DMSO-d<sub>6</sub>) δ 10.98 (s, 1H), 8.08 (br. s., 1H), 7.62-7.44 (m, 2H), 2.39 (s, 3H), and 2.35 (s, 3H).

**Human recombinant BTK enzyme assay:** To V-bottom 384-well plates were added test compounds, human recombinant BTK (1 nM, Invitrogen Corporation), fluoresceinated peptide (1.5 μM), ATP (20 μM), and assay buffer (20 mM HEPES pH 7.4, 10 mM MgCl<sub>2</sub>, 0.015% Brij 35 surfactant and 4 mM DTT in 1.6% DMSO), with a final volume of 30 μL. After incubating at room temperature for 60 min, the reaction was terminated by adding 45 μL of 35 mM EDTA to each sample. The reaction mixture was analyzed on the Caliper LabChip 3000 (Caliper, Hopkinton, MA) by electrophoretic separation of the fluorescent substrate and phosphorylated product. Inhibition data were calculated by comparison to control reactions with no enzyme (for 100% inhibition) and controls with no inhibitor (for 0% inhibition). Dose response curves were generated to determine the concentration required for inhibiting 50% of BTK activity (IC<sub>50</sub>). Compounds were dissolved at 10 mM in DMSO and evaluated at eleven concentrations.

**BCR-Stimulated calcium flux in Ramos B cells:** Human Ramos (RA1) B cells (ATCC CRL-1596) at a density of 2 x 10<sup>6</sup> cells/mL in RPMI minus phenol red (Invitrogen 11835-030) and 50 mM HEPES (Invitrogen 15630-130) containing 0.1% BSA (Sigma A8577) were added to one half volume of calcium loading buffer (BD bulk kit for probenecid sensitive assays, # 640177) and incubated at room temperature in the dark for 1 hour. Dye-loaded cells were pelleted (Beckmann GS-CKR, 1200 rpm, room temperature, 5 min) and resuspended at room temperature in RPMI minus phenol red with 50 mM HEPES and 10% FBS to a density of 1 x 10<sup>6</sup> cells/mL. 150 μL aliquots (150,000 cells/well) were plated into 96 well poly-D-lysine coated assay plates (BD 35 4640) and briefly centrifuged (Beckmann GS-CKR 800 rpm, 5 min, without brake). Next, 50 μL compound dilutions in 0.4% DMSO/RPMI minus phenol red + 50 mM HEPES + 10% FBS were added to the wells and the plate was incubated at room temperature in the dark for 1 hour. The assay plate was briefly centrifuged as above prior to measuring calcium levels. Using the FLIPR1 (Molecular Devices), cells were stimulated by adding goat anti-human IgM (Invitrogen AHI0601) to 2.5 μg/mL. Changes in intracellular calcium concentrations were measured for 180 seconds

and percent inhibition was determined relative to peak calcium levels seen in the presence of stimulation only.

**BTK inactivation determination in human whole blood:** The rate of inactivation of BTK in human whole blood was measured by adding the compound at various concentrations to blood and incubated at 37°C. At various time points, aliquots were removed and lysed with lysis buffer (Cell Signaling, 9803) containing protease inhibitor (Calbiochem, 539134) and 120 nM of a biotinylated inactivator of BTK. After agitation for 1 hour at room temperature, the lysate was transferred to a streptavidin-coated plate and incubated for 1 hour at room temperature. After washing 3-times with PBS containing 0.05% Tween20) 100  $\mu$ L of anti-BTK antibody (Cell Signaling, cat# 8547) in PBS containing 0.05% Tween20 and 0.5% BSA was added and incubated with continuous agitation for 1 hour at room temperature. After washing 3-times, goat anti-rabbit horseradish peroxidase secondary antibody was added, incubated for 1 hour at room temperature, then washed 3-times as above. The ELISA was developed with the addition of 100  $\mu$ L tetramethyl benzidine (Sigma, T0440) and allowed to develop for 20 minutes before quenching with the addition of 100  $\mu$ L 2 N sulfuric acid. The absorbance 450nm was measured and the relative percentage of free active sites calculated from a standard curve of samples containing different ratios of lysates from normal blood mixed with lysates from blood pretreated with 2  $\mu$ M of a rapid inactivator. A global fit of the data to an integrated rate equation defining second order kinetics (enzyme and compound being the two reactants) was used to determine a second order rate constant of the inactivation in whole blood.

**Determining  $k_{inact}/K_i$  for irreversible inhibitors using Time Resolved Fluorescence (HTRF):** His tagged kinase (1 nM) was preincubated with anti-6xHis-terbium labelled antibody (0.2 nM; Cis-bio) and an ATP competitive fluorescent probe at  $K_d$  for 1.5 hours to perform the kinase-antibody- probe FRET complex. Test compound was 3x serially diluted in DMSO for 11 concentrations, and an assay plate was prepared with 1000x inhibitor. Reactions were initiated by adding kinase-antibody-probe FRET complex to wells of the assay plate, and fluorescence decrease monitored kinetically over time. Assays were performed in black, flat-bottom, 384-well plates, and the final reaction volume was 20  $\mu$ L in assay buffer

consisting of 20 mM Hepes pH 7.5, 150 mM NaCl, 10 mM MgCl<sub>2</sub>, 2 mM DTT, 50 µg/ml BSA, 0.015% Brij 35. The HTRF signal, a ratio of fluorescence intensities at emission wavelengths for fluorescein acceptor (520 nm) and terbium donor (495 nm), generated by the reaction was measured on the Envision Plate Reader. Progress curve data was fit to a single exponential decay function to determine  $k_{\text{obs}}$ , and  $k_{\text{inact}}$  and  $K_I$  were determined by plotting  $k_{\text{obs}}$  versus inhibitor concentration and fitting to the following equation using Graph Pad Prism software:  $k_{\text{obs}} = k_{\text{inact}} / (1 + K_I/[I])$ .

**Collagen-induced arthritis in mice:** DBA/1 male mice (8-10wk of age; Harlan) were immunized subcutaneously at the base of the tail on Day 0 and again on Day 21 with 200 µg bovine type II collagen admixed with reconstituted Sigma Adjuvant System (SAS; Sigma-Aldrich). For “preventative” dosing, mice were dosed daily (beginning on Day 0) by oral gavage with vehicle (EtOH:TPGS:PEG300; 5:5:90) or compound **5a**. For “pseudo-established” dosing, the start of dosing was delayed until the Day 21 booster immunization. Following the booster immunization, mice were monitored 3 times per week for the development and severity of paw inflammation. Each paw was visually scored by the following scheme: +0 = normal. +1 = one (or more) joints inflamed on digits. +2 = mild-moderate inflammation of plantar surface of paw and paw thickness modestly increased. +3 = moderate-severe inflammation of plantar surface of paw and paw thickness significantly increased. +4 = ankylosis of ankle joint (significantly reduced hock joint motion on flexion/extension). Unblinded clinical paw scores for all four paws were summed for each mouse, and mean ± SEM was calculated for each treatment group.

For histological evaluation, rear paws were fixed, decalcified and embedded in paraffin. Sections were cut in the sagittal plane, stained in H & E and evaluated microscopically without knowledge of treatment group. Lesions were scored on a severity scale of 0 (normal) to 4 in two separate categories, inflammation (cellular infiltration and pannus formation) and bone resorption. Bone morphology and bone mineral density of hind paws excised postmortem was analyzed by micro-computed tomography (micro-CT) after fixation in 10% Neutral Buffered Formalin. Age-matched naïve (disease-free) paws were used as a control for comparative micro-CT analysis. The analysis was conducted in a blinded format.

**Micro-computed tomography imaging and histopathology:** Bone morphology was evaluated by micro-CT using the Scanco VivaCT40 (Scanco Medical AG, Zurich, Switzerland). Imaging parameters included approximately 500 slices (21- $\mu$ m thick) acquired with 250 projections, 500-ms integration time, 55 kVp photon energy, and 145  $\mu$ A of current. Region of interest focused on the hind/mid foot sections (talus to proximal end of the first metatarsal bone). Threshold settings were optimized using histomorphometric methods. Bone mineral density and bone surface area were evaluated using a hydroxylapatite calibration phantom and Scanco proprietary software. The analysis was conducted in a blinded format.

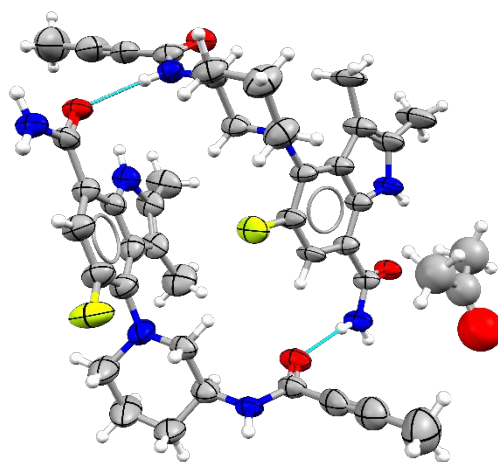
**NZB/W Lupus-Prone Mice:** Baseline body weight, proteinuria, and serum dsDNA titers were determined for female NZB/WF1 mice (Jackson Laboratories) at 24 weeks of age prior to their randomization into treatment groups, each with n=12. Mice were dosed by oral gavage, QD, for 16 weeks and included the following treatment groups: **5a** at 30 mg/kg in vehicle (80:20 PEG400:water) and prednisolone (Sigma P6004) at 10 mg/kg. Mice were routinely monitored for overall health, and body weight, proteinuria, and dsDNA titers were measured every 3 weeks. Proteinuria was measured using a colorimetric assay for albumin (Siemens Albustix Reagent Strips for Urinalysis). Anti-dsDNA antibody titers were measured by applying serial dilutions of serum samples to DNA-coated ELISA plates. Bound antibody was detected with HRP-conjugated polyclonal goat-anti-mouse IgG. The individual titers were expressed as relative to that of a pooled serum standard. At the end of the study, final body weight and proteinuria were measured. Terminal blood samples were drawn for PK and anti-dsDNA titers. The amount of BTK inactivation in blood from these mice, 24 h after their last dose, was determined as described above. At the end of the study, kidneys (n = 5-6 per group) were collected in 10% Neutral Buffered Formalin for histological evaluation. Fixed kidney tissues were routinely processed and paraffin embedded. Kidney sections were stained with periodic acid Schiff and hematoxylin and eosin for the evaluation of nephritis severity. Blinded to treatment group, severity of nephritis was evaluated using the following criteria. For glomerular damage: 1-Mesangial matrix thickening and/or mesangial cell proliferation; 2 - Crescent formation-Cellular deposits/casts in Bowman's space; 3 -

Cellular infiltration- composed of mononuclear cells in glomerular tufts; 4 - Fibrosis of Bowman's capsule. For tubular damage: 1 - Infiltration of mononuclear cells; 2 - Severity of tubular epithelial cell damage; 3-Protein casts. For tubule-interstitial damage: 1 - Fibrosis; 2 - Infiltration of mononuclear cells. Each subcategory was assigned a score from 0 to 4. The total score for each mouse was the sum of the above nine subcategories with the highest possible score of 36. To evaluate IC deposition in the glomeruli, immunohistochemistry was performed using biotinylated goat anti-mouse IgG, (Vector Laboratories, Burlingame, CA) with 45  $\mu\text{g/ml}$  normal goat serum (Jackson ImmunoResearch Laboratories, Inc.) as the negative control. Sections were conjugated to horse radish peroxidase using Vectastain ABC ELITE reagent (Vector Laboratories) and developed with Deep Space Black chromogen (Biocare Medical) for visualization of IgG. IC deposition was evaluated under 100x magnification by dividing the kidney into three sections, and randomly selecting 10 glomeruli from each section. Each glomerulus was subdivided into four quadrants, and each quadrant was assigned a score from 0 to 4 based on severity of IgG deposition, defined as: 0 - Unremarkable; 1 - Minimal linear deposition and/or focal lesion; 2 - Mild linear deposition or multi-focal lesions; 3 - Moderate/segmental lesions; 4 - Marked/global or diffuse deposition. The total score of each glomerulus was calculated, as was the total score of each kidney, and the group average score was determined. Statistical analysis was performed using a one-way ANOVA model after a square root transformation of the data to establish significant overall difference in the mean score of treatment groups with  $P < 0.0001$ . One-sided Dunnett's test was used to determine significance of inhibition of each treatment group compared to the vehicle control group.

**Single Crystal X-ray Diffraction Data for 5a.** Compound **5a** acetone solvate crystals were obtained from an acetone/n-heptane ( $v/v = 1/1$ ) solution after one day of slow evaporation of the mother liquor at room temperature. A colorless plate shaped single crystal of dimensions  $0.32 \times 0.20 \times 0.01$  mm was used to collect single crystal X-ray diffraction (XRD) data. The XRD data collection was carried out using a Bruker-AXS Microstar rotating anode equipped with  $\text{CuK}\alpha$  radiation ( $\lambda = 1.54178 \text{ \AA}$ ), a Kappa2000 diffractometer and APEX II detector. The crystal was kept at  $-70^\circ\text{C}$  (203 K) and the XRD data acquired using sets of Omega and Phi scans; each at a frame width of  $1.2^\circ$ . Indexing and processing of the measured

intensity data was performed using the BrukerSAINT-APEX2 software package/program suite [Bruker (2012); BrukerSAINT-APEX2; Bruker AXS Inc., Madison, Wisconsin, USA]. A direct methods solution was calculated using SHELXS-97 [Sheldrick, G.M. (1997) SHELXS97 and SHELXL97; Program for Crystal Structure Solution and Refinement; University of Göttingen, Göttingen], which provided the atomic positions from the E-map. Full-matrix least squares refinement and difference Fourier cycles were performed using SHELXL-2014/6 [Sheldrick, G.M. (2008) SHELX Version 2014/6; Acta Crystallographica, A64, 112-122]. The non-hydrogen atoms for compound **5a** were refined with anisotropic displacement parameters. Due to partial desolvation, the non-hydrogen atoms for the acetone molecule were refined isotropically and with geometric constraints. Hydrogen atoms were placed in ideal positions and refined as riding atoms with relative isotropic displacement parameters.

Single crystal X-ray data for compound **5a**. Crystal data (CCDC 1901788):  $C_{13}H_9N_3OS_2$ , FW = 287.36, orthorhombic  $P2_12_12_1$ ,  $a = 9.5112(4)$  Å,  $b = 20.9712(7)$  Å,  $c = 26.3443(12)$  Å,  $V = 5254.7(4)$  Å<sup>3</sup>,  $T = 203$  K, Cu K $\alpha$ , 88907 reflections, 6619 unique ( $R_{int} = 0.0818$ ),  $R1 = 0.0953$ ,  $wR2 = 0.2817$  (for 5730 observed reflections with  $I > 2\sigma(I)$  and 513 parameters), Flack(x) = 0.00(9), Hooft (y) = -0.06(8), P3True = 1.000.



**X-ray crystallography of 5a bound to the kinase domain of BTK.** Purification, crystallization, X-ray data collection and first maps were performed by Proteros Biostructures GmbH. The final refinement was carried out with BUSTER/TNT (Blanc, E., Roversi, P., Vonnrhein, C., Flensburg, C., Lea, S. M. & Bricogne, G. (2004). Acta Cryst. D60, 2210-2221) (GlobalPhasing, Ltd., Cambridge, UK), GRADE

(GlobalPhasing, Ltd., Cambridge, UK) for restraint dictionary generation, and COOT (Emsley, P., Lohkamp, B., Scott, W. G. & Cowtan, K. (2010). *Acta Cryst. D* 66, 486-501) for modeling building into electron density. The structure of hBTK + Compound **5a** has been deposited to RCSB with PDB ID: 608I.

## Supporting Information

Molecular formula strings (CSV)

## Author Information

\* Corresponding Author: Phone: 609-252-6778; E-mail: [scott.watterson@bms.com](mailto:scott.watterson@bms.com).

**Note:** The authors declare no competing financial interest.

PDB ID code for **5a**: 608I (*Authors will release the atomic coordinates upon article publication.*)

## Acknowledgements

Proteros Biostructures GmbH is acknowledged for the purification, crystallization, X-ray data collection and first maps of the X-ray co-crystal structure of **5a** bound to the active site of BTK.

## Abbreviations Used

BTK, Bruton's tyrosine kinase; PK, pharmacokinetic; SAR, structure-activity relationship; hERG, human ether-a-go-go-related gene.

## References

- (1) (a) Jansson, L.; Holmdahl, R. Genes on the X chromosome affect development of collagen-induced arthritis in mice. *Clin. Exp. Immunol.* **1993**, *94*, 459-465. (b) Steinberg, B. J.; Smathers, P. A.; Frederiksen, K.; Steinberg, A. D. Ability of the *xid* gene to prevent autoimmunity in (NZBXNZW)F1 mice during the course of their natural history, after polyclonal stimulation, or following immunization with DNA. *J. Clin. Invest.* **1982**, *70*, 587-597.
- (2) (a) Xu, D.; Kim, Y.; Postelnek, J.; Vu, M. D; Hu, D.-Q.; Liao, C.; Bradshaw, M.; Hsu, J.; Zhang, J.; Pashine, A.; Srinivassan, D.; Woods, J.; Levin, A.; O'Mahony, A.; Owens, T. D.; Lou, Y.; Hill, R. J.; Narula, S.; DeMartino, J.; Fine, J. S. RN486, a selective Bruton's tyrosine kinase inhibitor, abrogates immune hypersensitivity responses and arthritis in rodents. *J. Pharmacol. Exp. Ther.*



- 2012**, *341*, 90-103. (b) Di Paolo, J. A.; Huang, T.; Balazs, M.; Barbosa, J.; Barck, K. H.; Bravo, B. J.; Carano, R. A. D.; Darrow, J.; Davies, D. R.; DeForge, L. E.; Diehl, L.; Ferrando, R.; Gallion, S. L.; Giannetti, A. M.; Gribbling, P. P.; Hurez, V.; Hymowitz, S. G.; Jones, R.; Kropf, J. E.; Lee, W. P.; Maciejewski, P. M.; Mitchell, S. A.; Rong, H.; Staker, B. L.; Whitney, J. A.; Yeh, S.; Young, W. B.; Yu, C.; Zhang, J.; Reif, K.; Currie, K. S. Specific Btk inhibition suppresses B cell and myeloid cell-mediated arthritis. *Nat. Chem. Bio.* **2011**, *7*, 41-50. (c) Rankin, A. L.; Seth, N.; Keegan, S.; Andreyeva, T.; Cook, T. A.; Edmonds, J.; Mathialagan, N.; Benson, M. J.; Syed, J.; Zhan, Y.; Benoit, S. E.; Miyashiro, J. S.; Wood, N.; Mohan, S.; Peeva, E.; Ramaiah, S. K.; Messing, D.; Homer, B. L.; Dunussi-Joannopoulos, K.; Nickerson-Nutter, C. L.; Schnute, M. E.; Douhan, J., III. Selective inhibition of BTK prevents murine lupus and antibody-mediated glomerulonephritis. *J. Immunol.* **2013**, *193*, 4540-4550.
- (3) Mease, P. J. B cell-targeted therapy in autoimmune disease: rationale, mechanisms, and clinical application. *J. Rheumatol.* **2008**, *35*, 1245-1255.
- (4) (a) Mohamed, A. J.; Yu, L.; Bäckesjö, C.-M.; Vargas, L.; Faryal, R.; Aints, A.; Christensson, B.; Berglöf, A.; Vihinen, M.; Nore, B. F.; Smith, C. I. E. Bruton's tyrosine kinase (Btk): function, regulation, and transformation with special emphasis on the PH domain. *Immunol. Rev.* **2009**, *228*, 58-73; (b) Mohamed, A. J.; Nore, B. F.; Christensson, B.; Smith, C. I. E. Signaling of Bruton's tyrosine kinase, Btk. *Scand. J. Immunol.* **1999**, *49*, 113-118. (c) Takata, M.; Kurosaki, T. A role for Bruton's tyrosine kinase in B cell antigen receptor-mediated activation of phospholipase C- $\gamma$ 2. *J. Exp. Med.* **1996**, *184*, 31-40.
- (5) (a) Jongstra-Bilen, J.; Puig Cano, A.; Hasija, M.; Xiao, H.; Smith, C. I.; Cybulsky, M. I. Dual functions of Bruton's tyrosine kinase and Tec kinase during Fc $\gamma$  receptor-induced signaling and phagocytosis. *J. Immunol.* **2008**, *181*, 288-298. (b) Kuehn, H. S.; Rader, M.; Brown, J. M.; Ali, K.; Vanhaesebroeck, B.; Beaven, M. A.; Metcalfe, D. D.; Gilfillan, A. M. Btk-dependent Rac activation and actin rearrangement following Fc $\epsilon$ RI aggregation promotes enhanced chemotactic

- responses of mast cells. *J. Cell Sci.* **2010**, *123*, 2576-2585. (c) Tsukada, S.; Rawlings, D. J.; Witte, O. N. Role of Bruton's tyrosine kinase in immunodeficiency. *Curr. Opin. Immunol.* **1994**, *6*, 623-630.
- (6) Lee, S. H.; Kim, T.; Jeong, D.; Kim, N.; Choi, Y. The Tec family tyrosine kinase Btk regulates RANKL-induced osteoclast maturation. *J. Biol. Chem.* **2008**, *283*, 11526-11534.
- (7) (a) Middendorp, S.; Dingjan, G. M.; Maas, A.; Dahlenborg, K.; Hendriks, R. W. Function of Bruton's tyrosine kinase during B cell development is partially independent of its catalytic activity. *J. Immunol.* **2003**, *171*, 5988-5996. (b) Petro, J. B.; Rahman, S. M. J.; Ballard, D. W.; Khan, W. N. Bruton's tyrosine kinase is required for activation of I $\kappa$ B kinase and nuclear factor  $\kappa$ B in response to B cell receptor engagement. *J. Exp. Med.* **2000**, *191*, 1745-1753.
- (8) Whyburn, L. R.; Halcomb, K. E.; Contreras, C. M.; Pappu, R.; Witte, O. N.; Chan, A. C.; Satterthwaite, A. B. Haploinsufficiency of B cell linker protein enhanced B cell signaling defects in mice expressing a limiting dosage of Bruton's tyrosine kinase. *Int. Immunol.* **2003**, *15*, 383-392.
- (9) (a) Cohen, M. S.; Zhang, C.; Shokat, K. M.; Taunton, J. Structural bioinformatics-based design of selective, irreversible kinase inhibitors. *Science* **2005**, *308*, 1318-1321. (b) Leproult, E.; Barluenga, S.; Moras, D.; Wurtz, J.-M.; Winssinger, N. Cysteine mapping in conformationally distinct kinase nucleotide binding sites: application to the design of selective covalent inhibitors. *J. Med. Chem.* **2011**, *54*, 1347-1355.
- (10) (a) Byrd, J. C.; Brown, J. R.; O'Brien, S.; Barrientos, J. C.; Kay, N. E.; Reddy, N. M.; Coutre, S.; Tam, C. S.; Mulligan, S. P.; Jaeger, U.; Devereux, S.; Barr, P. M.; Furman, R. R.; Kipps, T. J.; Cymbalista, F.; Pocock, C.; Thornton, P.; Caligaris-Cappio, F.; Robak, T.; Delgado, J.; Schuster, S. J.; Montillo, M.; Schuh, A.; de Vos, S.; Gill, D.; Bloor, A.; Dearden, C.; Moreno, C.; Jones, J. J.; Chu, A. D.; Fardis, M.; McGreivy, J.; Clow, F.; James, D. F.; Hillmen, P. Ibrutinib versus ofatumumab in previously treated chronic lymphoid leukemia. *N. Eng. J. Med.* **2014**, *371*, 213-223. (b) Wang, M. L.; Rule, S.; Martin, P.; Goy, A.; Auer, R.; Kahl, B. S.; Jurczak, W.; Advani,

- R. H.; Romaguera, J. E.; Williams, M. E.; Barrientos, J. C.; Chmielewska, E.; Radford, J.; Stilgenbauer, S.; Dreyling, M.; Jedrzejczak, W. Wiktor; Johnson, P.; Spurgeon, S. E.; Li, L.; Zhang, L.; Newberry, K.; Ou, Z.; Cheng, N.; Fang, B.; McGreivy, J.; Clow, F.; Buggy, J. J.; Chang, B. Y.; Beaupre, D. M.; Kunkel, L. A.; Blum, K. A. Targeting BTK with ibrutinib in relapsed or refractory mantle-cell lymphoma. *N. Eng. J. Med.* **2013**, *369*, 507-516. (c) Treon, S. P.; Tripsas, C. K.; Meid, K.; Warren, D.; Varma, G.; Green, R.; Argyropoulos, K. V.; Yang, G.; Cao, .; Xu, L.; Patterson, C. J.; Rodig, S.; Zehnder, J. L.; Aster, J. C.; Harris, N. L.; Kanan, S.; Ghobrial, I.; Castillo, J. J.; Laubach, J. P.; Hunter, Z. R.; Salman, Z.; Li, J.; Cheng, M.; Clow, F.; Graef, T.; Palomba, M. L.; Advani, R. H. Ibrutinib in previously treated waldenstrom's macroglobulinemia. *N. Eng. J. Med.* **2015**, *372*, 1430-1440.
- (11) Mauro, F. R.; Caputo, M. D.; Rosati, S.; Pepe, S.; De Benedittis, D.; De Luca, M. L.; Foa, R. Balancing efficacy and toxicity of targeted agents currently used for the treatment of patients with chronic lymphocytic leukemia. *Exp. Rev. Hematol.* **2018**, *11*, 601-611.
- (12) (a) Norman, P. Investigational Bruton's tyrosine kinase inhibitors for the treatment of rheumatoid arthritis. *Expt. Opin. Invest. Drugs* **2016**, *25*, 891-899. (b) Thompson, P. A.; Burger, J. A. Bruton's tyrosine kinase inhibitors: first and second generation agents for patients with chronic lymphocytic leukemia (CLL). *Expt. Opin. Invest. Drugs* **2018**, *27*, 31-42. (c) Smith, P. F.; Krishnarajah, J.; Nunn, P. A.; Hill, R. J.; Karr, D.; Tam, D.; Masjedizadeh, M.; Funk, J. O., Gourlay, S. G. A phase I trial of PRN1008, a novel reversible covalent inhibitor of Bruton's tyrosine kinase in healthy volunteers. *Br. J. Clin. Pharmacol.* **2017**, *83*, 2367-2376. (d) Brown, J. R.; Harb, W. A.; Hill, B. T.; Gabrilove, J.; Sharman, J. P.; Schreeder, M. T.; Barr, P. M.; Foran, J. M.; Miller, T. P.; Burger, J. A.; Kelly, K. R.; Mahadevan, D.; Ma, S.; Li, Y.; Pierce, D. W.; Barnett, E.; Marine, J.; Miranda, M.; Azaryan, A.; Yu, X.; Nava-Parada, P.; Mei, J.; Kipps, T. J. Phase I study of single-agent CC-292, a highly selective Bruton's tyrosine kinase inhibitor, in relapsed/refractory chronic lymphocytic leukemia. *Haematologica* **2016**, *101*, e295-e298. (e) Kivitz, A. J.; Gupta, R.; Valenzuela, G.; Smith, E.; Rehman, Q.; El Kadi, H.; Bretton, E.; Aelion,

J. A.; Chadha, A.; Tesser, J.; Hough, D.; Korish, S.; Schafer, P. H.; Ringheim, G.; Sutherland, D.; Li, L. A phase 2a, 4-week double-blind, proof of concept efficacy and safety study of CC-292 versus placebo as co-therapy with methotrexate in active rheumatoid arthritis (RA). *Arthritis Rheumatol.* **2016**, *68*, (suppl 10).

- (13) (a) Rule, S.; Chen, R. W. New and emerging Bruton tyrosine kinase inhibitors for treating mantle cell lymphoma – where do they fit in? *Exp. Rev. Hematol.* **2018**, *11*, 749-756. (b) Wang, M.; Rule, S.; Zinzani, P. L.; Goy, A.; Casasnovas, O.; Smith, S. D.; Damaj, G.; Doorduijn, J.; Lamy, T.; Morschhauser, F.; Panizo, C.; Shah, B.; Davies, A.; Eek, R.; Dupuis, J.; Jacobsen, E.; Kater, A. P.; Le Gouill, S.; Oberic, L.; Robak, T.; Covey, T.; Dua, R.; Hamdy, A.; Huang, X.; Izumi, R.; Patel, P.; Rothbaum, W.; Slatter, J. G.; Jurczak, W. Acalabrutinib in relapsed or refractory mantle cell lymphoma (ACE-LY-004): a single-arm, multicentre, phase 2 trial. *Lancet* **2018**, *391*, 659-667. (c) Barf, T.; Covey, T.; Izumi, R.; van de Kar, B.; Gulrajani, M.; van Lith, B.; van Hoek, M.; de Zwart, E.; Mittag, D.; Demont, D.; Verkaik, S.; Krantz, F.; Pearson, P. G.; Ulrich, R.; Kaptein, A. Acalabrutinib (ACP-196): a covalent Bruton tyrosine kinase inhibitor with a differentiated selectivity and in vivo potency profile. *J. Pharmacol. Exp. Ther.* **2017**, *363*, 240-252.
- (14) Crawford, J. J.; Johnson, A. R.; Misner, D. L.; Belmont, L. D.; Castanedo, G.; Choy, R.; Coraggio, M.; Dong, L.; Eigenbrot, C.; Erickson, R.; Ghilardi, N.; Hau, J.; Katewa, A.; Kohli, P. B.; Lee, W.; Lubach, J. W.; McKenzie, B. S.; Ortwine, D. F.; Schutt, L.; Tay, S.; Wei, BinQing; R., Karin; Liu, L.; Wong, H.; Young, W. B. Discovery of GDC-0853: A potent, selective, and noncovalent Bruton's tyrosine kinase inhibitor in early clinical development. *J. Med. Chem.* **2018**, *61*, 2227-2245.
- (15) (a) ClinicalTrials.gov Identifiers: Phase II NCT02638948; Phase I NCT02257151, NCT02880670, NCT02762123, NCT02456844, NCT02832180. (b) Lee, S. K.; Xing, J.; Catlett, I. M.; Adamczyk, R.; Griffies, A.; Liu, A.; Murthy, B.; Nowak, M. Safety, pharmacokinetics, and pharmacodynamics of BMS-986142, a novel reversible BTK inhibitor, in healthy participants.

- Eur. J. Clin. Pharmacol.* **2017**, *73*, 689-698. (c) Gillooly, K. M.; Pulicchio, C.; Pattoli, M. A.; Cheng, L.; Heimrich, E. M.; McIntyre, K. W.; Taylor, T. L.; Kukral, D. W.; Dudhgaonkar, S.; Nagar, J.; Watterson, S. H.; Tino, J. A.; Fura, A.; Burke, J. R. Bruton's Tyrosine Kinase Inhibitor BMS-986142 in experimental models of rheumatoid arthritis enhances efficacy of agents representing clinical standard-of-care. *PLOS One* **2017**, e0181782. (d) Watterson, S. H.\*; De Lucca, G. V.; Shi, Q.; Langevine, C. M.; Liu, Q.; Batt, D. G.; Beaudoin Bertrand, M.; Gong, H.; Dai, J.; Yip, S.; Li, P.; Sun, D.; Wu, D.-R.; Wang, C.; Zhang, Y.; Traeger, S. C.; Pattoli, M. A.; Skala, S.; Cheng, L.; Obermeier, M. T.; Vickery, R.; Discenza, L.; D'Arienzo, C.; Gillooly, K.; Taylor, T. L.; Pulicchio, C.; McIntyre, K. W.; Tebben, A. J.; Muckelbauer, J. K.; Chang, C. Y.; Rampulla, R.; Mathur, A.; Salter-Cid, L.; Barrish, J. C.; Carter, P. H.; Fura, A.; Burke, J. R.; Tino, J. A. Discovery of 6-fluoro-5-(*R*)-(3-(*S*)-(8-fluoro-1-methyl-2,4-dioxo-1,2-dihydroquinazolin-3(4*H*)-yl)-2-methylphenyl)-2-(*S*)-(2-hydroxypropan-2-yl)-2,3,4,9-tetrahydro-1*H*-carbazole-8-carboxamide (BMS-986142): A reversible inhibitor of bruton's tyrosine kinase conformationally constrained by two locked atropisomers. *J. Med. Chem.* **2016**, *59*, 9173-9200.
- (16) (a) Lonsdale, R.; Ward, R. S. Structure-based design of targeted covalent inhibitors. *Chem. Soc. Rev.* **2018**, *47*, 3816-3830. (b) Conzalez-Bello, C. Designing irreversible inhibitors – Worth the effort? *ChemMedChem* **2016**, *11*, 22 – 30.
- (17) (a) Johnson, D. S.; Weerapana, E; Cravatt, B. F. Strategies for discovering and derisking covalent, irreversible enzyme inhibitors. *Future Med. Chem.* **2010**, *2*, 949-964. (b) Uetrecht, J. P. New concepts in immunology relevant to idiosyncratic drug reactions: The “danger hypothesis” and innate immune system. *Chem. Res. Toxicol.* **1999**, *12*, 387-395. (c) Nakayama, S.; Atsumi, R.; Takakusa, H.; Kobayashi, Y.; Kurihara, A.; Nagai, Y.; Nakai, D.; Okazaki, O. A zone classification system for risk assessment of idiosyncratic drug toxicity using daily dose and covalent binding. *Drug Met. Distrib.* **2009**, 1970-1977.
- (18) Shi, Q.; Tebben, A.; Dyckman, A. J.; Li, H.; Liu, C.; Lin, J.; Spergel, S.; Burke, J. R.; McIntyre, K. W.; Olini, G. C.; Strnad, J.; Surti, N.; Muckelbauer, J. K.; Chang, C.; An, Y.; Lin, C.; Ruan,

- Q.; Leftheris, K.; Carter, P. H.; Tino, J. A.; De Lucca, G. V. Purine derivatives as potent Bruton's tyrosine kinase (BTK) inhibitors for autoimmune diseases. *Bioorg. Med. Chem. Lett.* **2014**, *24*, 2206-2211.
- (19) (a) Liu, Q.; Batt, D. G.; Lippy, J. S.; Surti, N.; Tebben, A. J.; Muckelbauer, J. K.; Chen, L.; An, Y.; Chang, C.; Pokross, M.; Yang, Z.; Wang, H.; Burke, J. R.; Carter, P. H.; Tino, J. A. Design and synthesis of carbazole carboxamides as promising inhibitors of Bruton's tyrosine kinase (BTK) and Janus kinase 2 (JAK2). *Bioorg. Med. Chem. Lett.* **2015**, *25*, 4265-4269. (b) De Lucca, G. B.; Shi, Q.; Liu, Q.; Batt, D. G.; Bertrand, M. B.; Rampulla, R.; Mathur, A.; Discenza, L.; D'Arienzo, C.; Dai, J.; Obermeier, M. T.; Vickery, R.; Zhang, Y.; Yang, Z.; Marathe, P. H.; Tebben, A. J.; Muckelbauer, J. K.; Chang, C. Y.; Zhang, H.; Gillooly, K.; Taylor, T. L.; Pattoli, M. A.; Skala, S.; Kukral, D. W.; McIntyre, K. W.; Salter-Cid, L.; Fura, A.; Burke, J. R.; Barrish, J. C.; Carter, P. H.; Tino, J. A. Small molecule reversible inhibitors of Bruton's tyrosine kinase (BTK): Structure-activity relationships leading to the identification of 7-(2-hydroxypropan-2-yl)-4-[2-methyl-3-(4-oxo-3,4-dihydroquinazolin-3-yl)phenyl]-9H-carbazole-1-carboxamide (BMS-935177). *J. Med. Chem.* **2016**, *59*, 7915-7935.
- (20) (a) Batt, D. G.; Bertrand, M. B.; Delucca, G. V.; Galella, M. A.; Ko, S. S.; Langevine, C. M.; Liu, Qingjie; S., Qing; Srivastava, A. S.; Tino, J. A.; Watterson, S. H. Substituted Carbazolecarboxamide Derivatives as BTK Inhibitors and Their Preparation and Use for the Treatment of Diseases. WO 2014210085; *Chem. Abstr.* **2014**, *162*, 161072. (b) Ko, S. S.; Batt, D. A.; Bertrand, M. B.; Delucca, G. V.; Langevine, C. M.; Liu, Q.; Srivastava, A. S.; Watterson, S. H. Preparation of 4-Phenylcarbazole-1-carboxamide Compounds Useful as Bruton's Tyrosine Kinase (BTK) Inhibitors. WO 2014210087; *Chem. Abstr.* **2014**, *162*, 150740.
- (21) Liu, Q.; Batt, D. G.; Chaudhry, C.; Lippy, J. S.; Pattoli, M. A.; Surti, N.; Xu, S.; Carter, P. H.; Burke, J. R.; Tino, J. A. Conversion of carbazole carboxamide based reversible inhibitors of Bruton's tyrosine kinase (BTK) into potent, selective irreversible inhibitors in the carbazole,

- 1 tetrahydrocarbazole, and a new 2,3-dimethylindole series *Bioorg. Med. Chem. Lett.* **2018**,  
2 28, 3080-3084.  
3  
4  
5 (22) Ahmad, S.; Batt, D. G.; Liu, Q.; Macor, J. E.; Tino, J. A.; Watterson, S. H. Carbazole Inhibitors  
6 WO 2016065236; *Chem. Abstr.* **2016**, 164, 556167 (Example 88).  
7  
8  
9 (23) Burke, J. R.; Pattoli, M. A.; Cheng, L.; Skala, S.; Heimrich, E. M.; Taylor, T. L.; Pulicicchio, C.;  
10 Kukral, D. W.; Petrone, T.; Catlett, I. M.; Zheng, N.; Li, W.; Watterson, S. H.; Tino, J. A. BMS-  
11 986195 is a highly selective and rapidly acting covalent inhibitor of bruton's tyrosine kinsase with  
12 robust efficacy at low doses in preclinical models of RA and lupus nephritis. *Arthritis Rheumatol.*  
13 **2017**, 69 (suppl 10).  
14  
15  
16 (24) Dahal, U. P.; Obach, R. S.; Gilbert, A. M. Benchmarking in vitro covalent binding burden as a  
17 tool to assess potential toxicity caused by nonspecific covalent binding of covalent drugs. *Chem.*  
18 *Res. Toxicol.* **2013**, 26, 1739-1745.  
19  
20  
21 (25) (a) Catlett, I., Wei, L., Zheng, N., Liu, A., He, B., Girgis, I., Nowak, M. BMS-986195, a novel,  
22 rapidly acting, covalent inhibitor of Bruton's tyrosine kinase: safety, pharmacokinetic and  
23 pharmacodynamic profiles in healthy participants. *Arthritis Rheumatol.* **2017**; 69 (suppl 10). (b)  
24 ClinicalTrials.gov Identifiers: NCT02705989, NCT03245515, NCT03262740, NCT03131973.  
25  
26  
27 (26) (a) Liu, Q.; Watterson, S. H.; Ahmad, S. Indole Carboxamide Compounds US 9,688,629 **2017**.  
28 (b) Liu, Q.; Watterson, S. H.; Batt, D. G.; Ahmad, S.; Beaudoin Bertrand, M.; Gong, H.; Guo, W.;  
29 Macor, J. E.; Ngu, K. ; Tebben, A.; Tino, J. A. Indole Carboxamide Compounds US  
30 2016/0115126; *Chem. Abstr.* **2016**, 164, 556179.  
31  
32  
33 (27) Ruiz-Castillo, P.; Buchwald, S. L. Applications of palladium-catalyzed C–N cross-coupling  
34 reactions. *Chem. Rev.* **2016**, 116, 12564-12649.  
35  
36  
37  
38  
39  
40  
41  
42  
43  
44  
45  
46  
47  
48  
49  
50  
51  
52  
53  
54  
55  
56  
57  
58  
59  
60

**Figure 1.** Approved covalent, irreversible inhibitors of BTK.

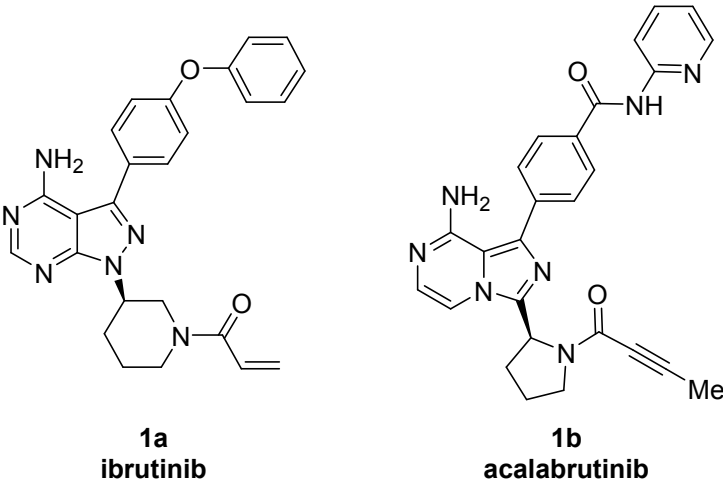


**Figure 2.** Compound **2** is a potent reversible BTK inhibitor.

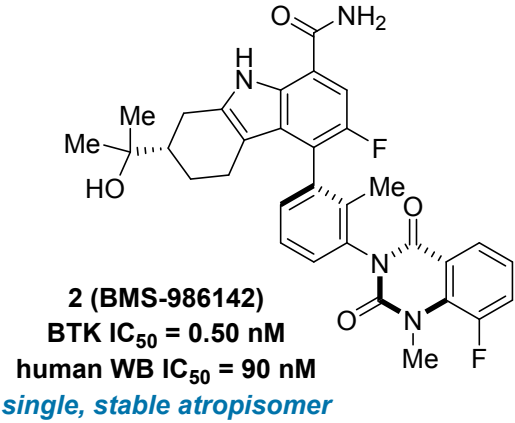
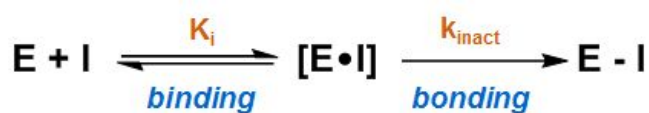
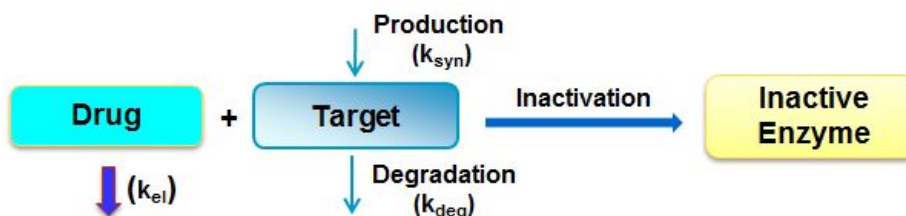




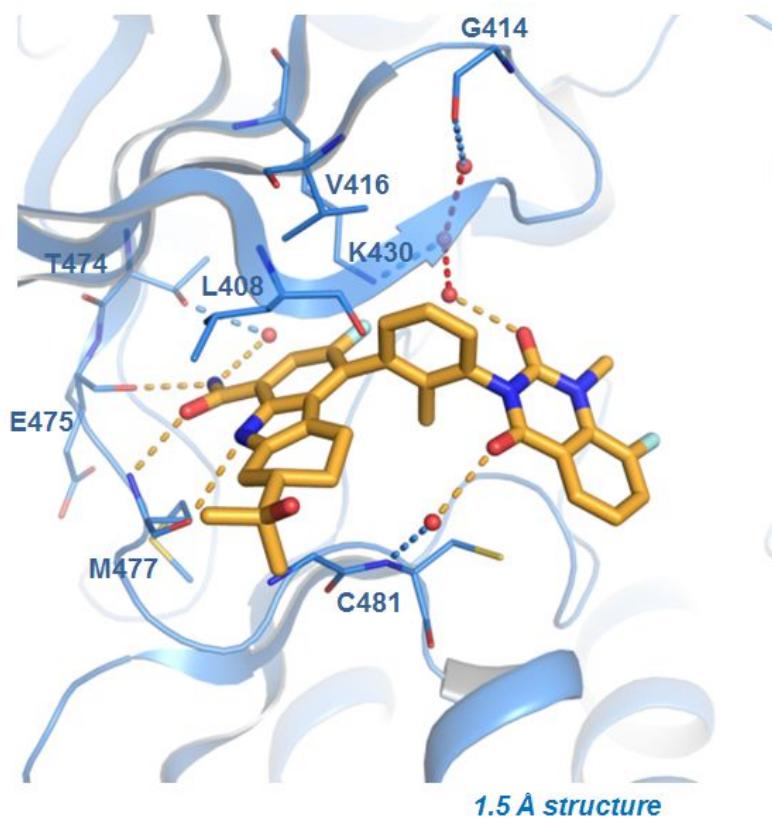
Figure 3.



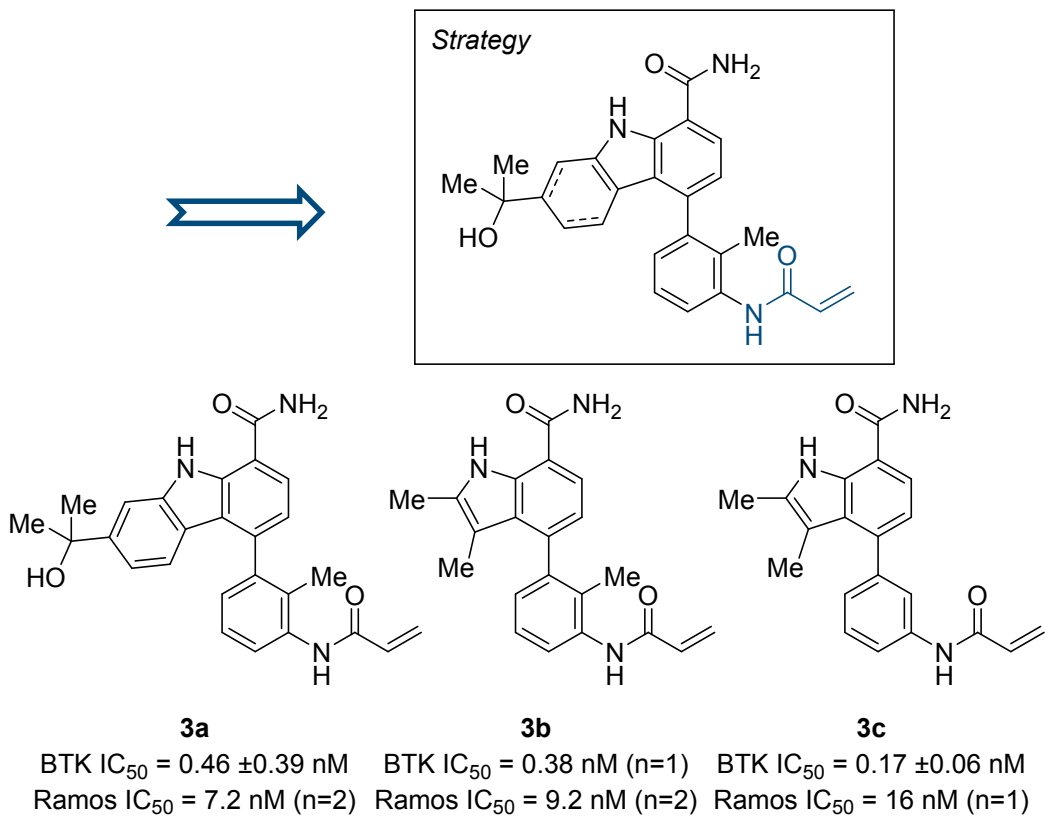
**Figure 4.** Desired PK properties – rate of inactivation must be faster than the rate of elimination.



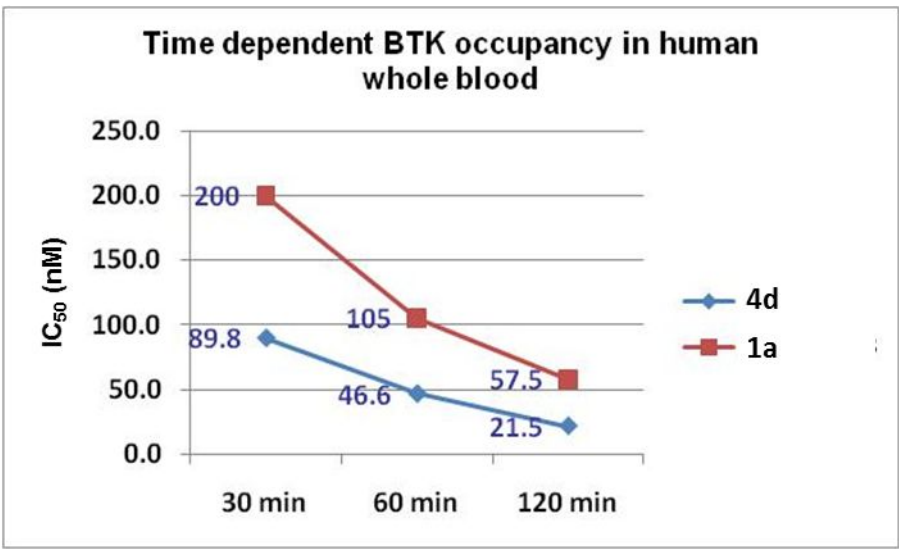
**Figure 5.** X-ray crystal structure of **2** bound to the kinase domain of BTK (1.5 Å structure) (PDB ID code: 5T18).<sup>15d</sup>

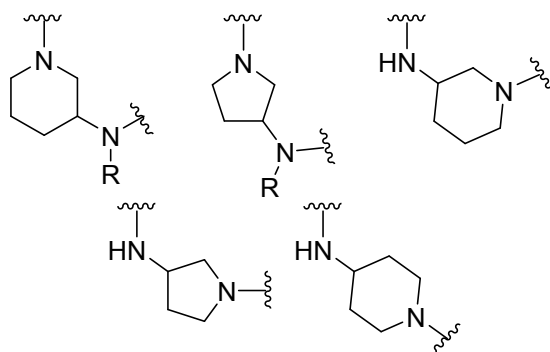
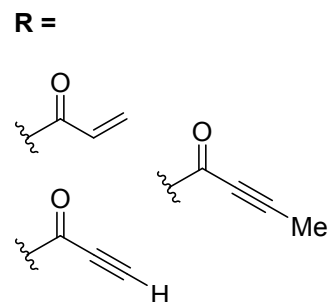
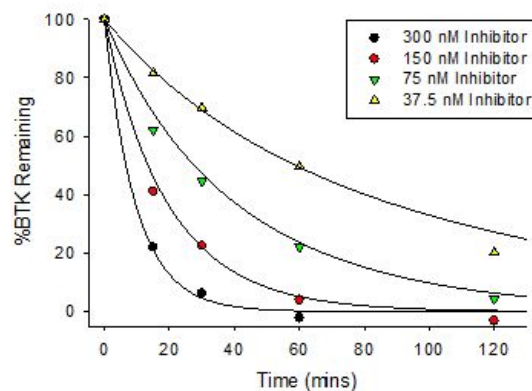
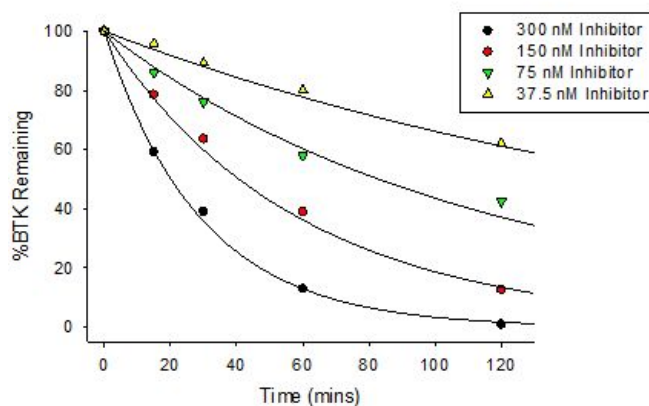


**Figure 6.** Initial design strategy for covalent, irreversible inhibition.



**Figure 7.** BTK inactivation rate comparison between **4d** and **1a**.



**Figure 8.** Optimizing linker and acceptor geometry to improve intrinsic covalent potency.**Linkers****Acceptors****Figure 9.** Time- and dose-dependent inactivation of BTK with **5a** (A) vs. **1a** (B). Either **5a** or **1a** at various concentrations was added to human whole blood, and the kinetics of BTK inactivation were measured. The solid line represents the fit of the data to a second order rate constant of  $3.5 \times 10^{-4} \text{ nM}^{-1} \cdot \text{min}^{-1}$  (**5a**) vs.  $1.2 \times 10^{-4} \text{ nM}^{-1} \cdot \text{min}^{-1}$  (**1a**).**A. Compound 5a****B. Compound 1a**

**Figure 10.** Compound **5a** is highly selective for BTK.  
(Illustration reproduced courtesy of Cell Signaling Technology, Inc.)

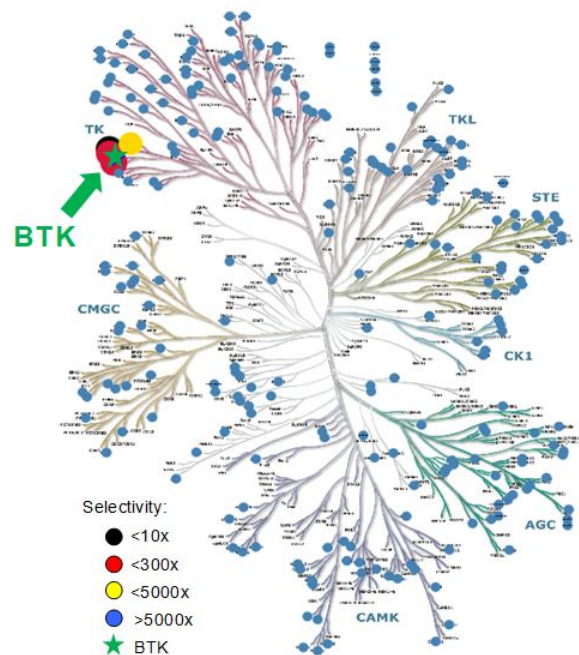


**Figure 11.** X-ray crystal structure of **5a** covalently bound to the kinase domain of BTK (PDB ID code:608I).

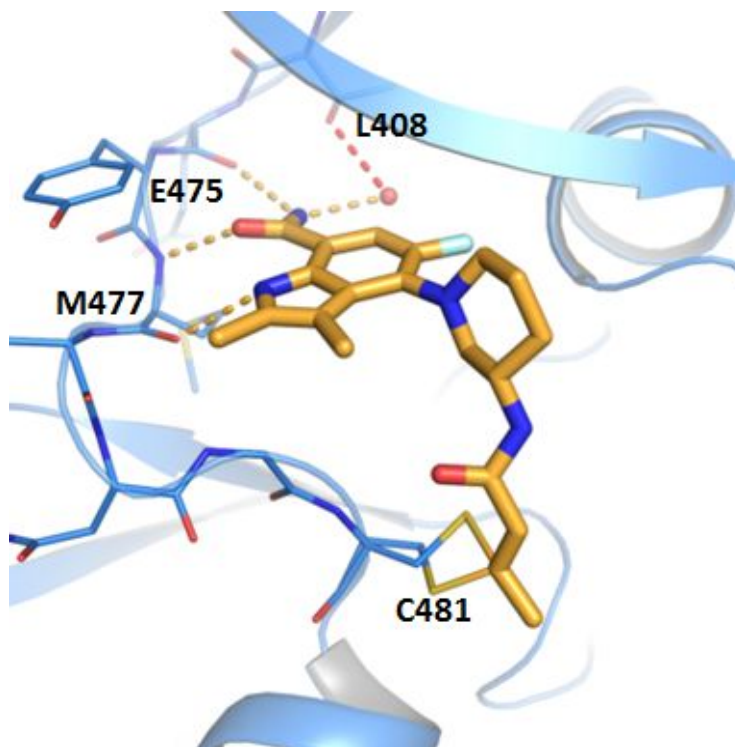


**Figure 12.** Overlay of the single crystal X-ray structure (pink) with the X-ray crystal structure of **5a** bound to the active site of BTK (gold).

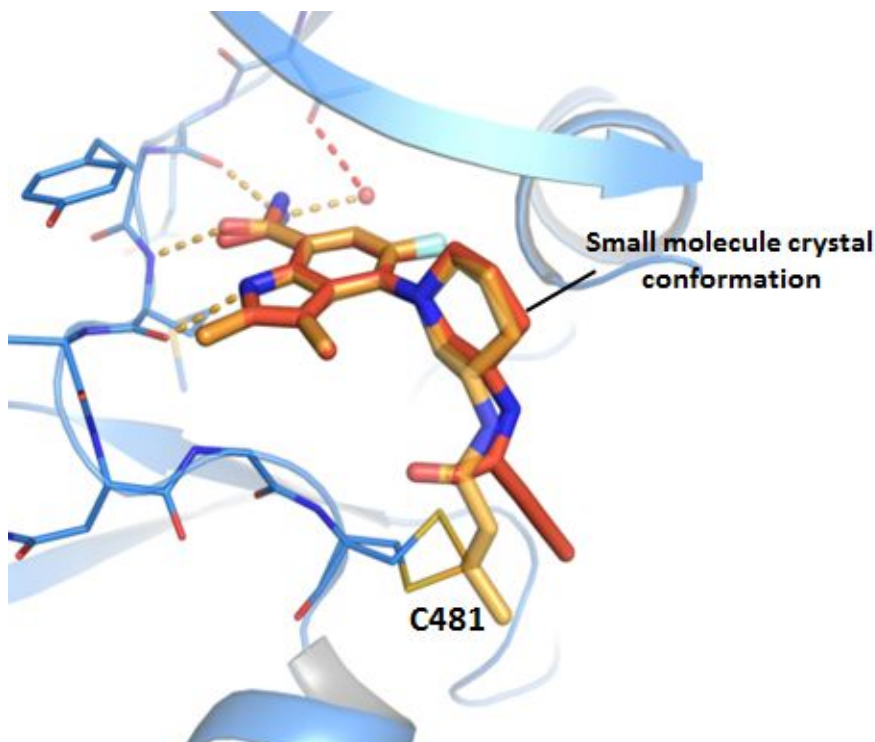
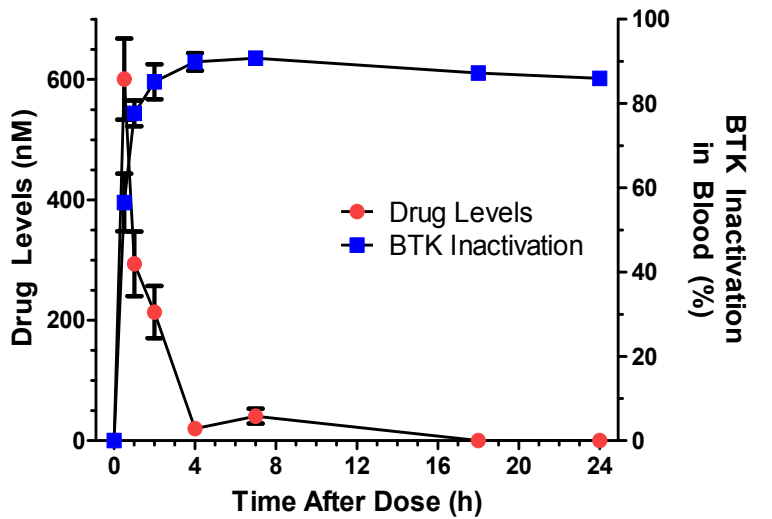
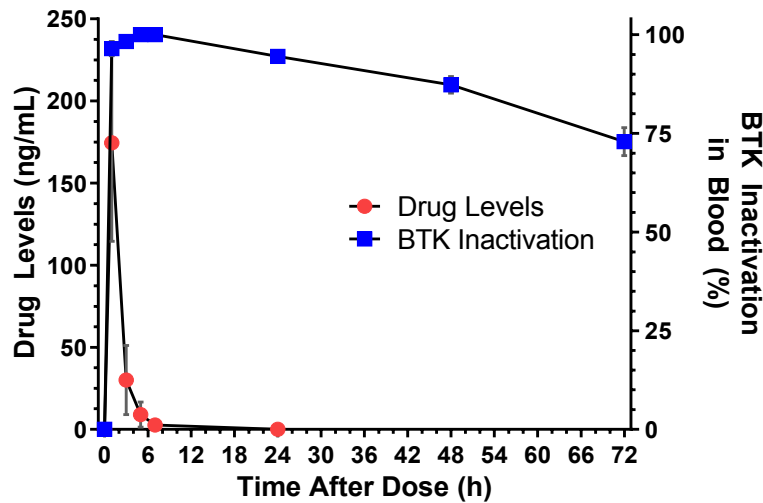


**Figure 13.** A single, low dose of **5a** (0.5 mg/kg orally, once daily) resulted in >90% BTK inactivation in mice (A) and 100% inactivation in cynomolgus monkey (B). (c) Compound **5a** inactivated BTK in mice significantly faster than **1a**.

**A. Mice**



**B. Cynomolgus monkeys**



**C. 5a vs. 1a in mice**

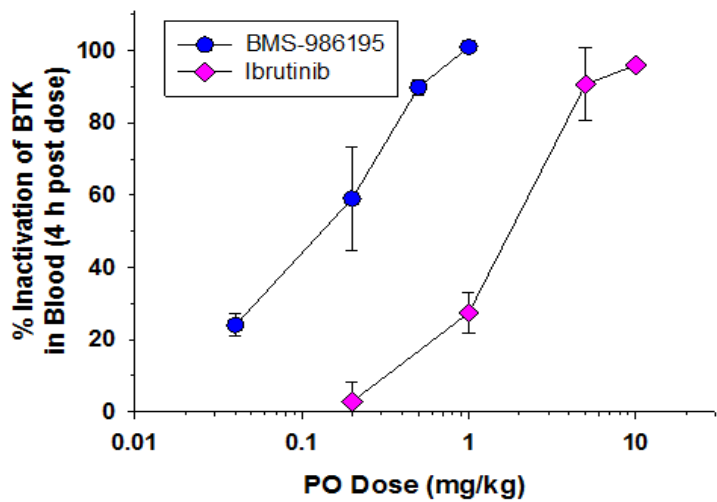
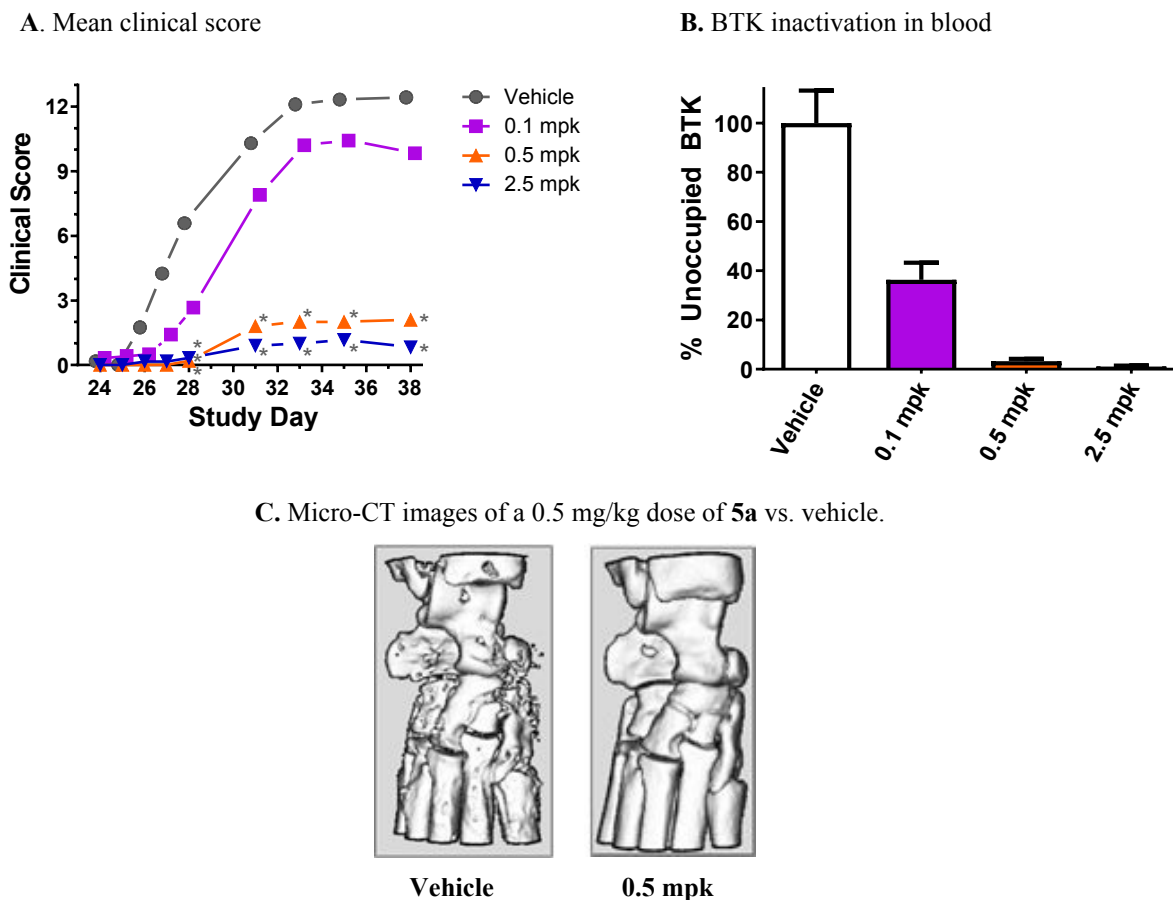


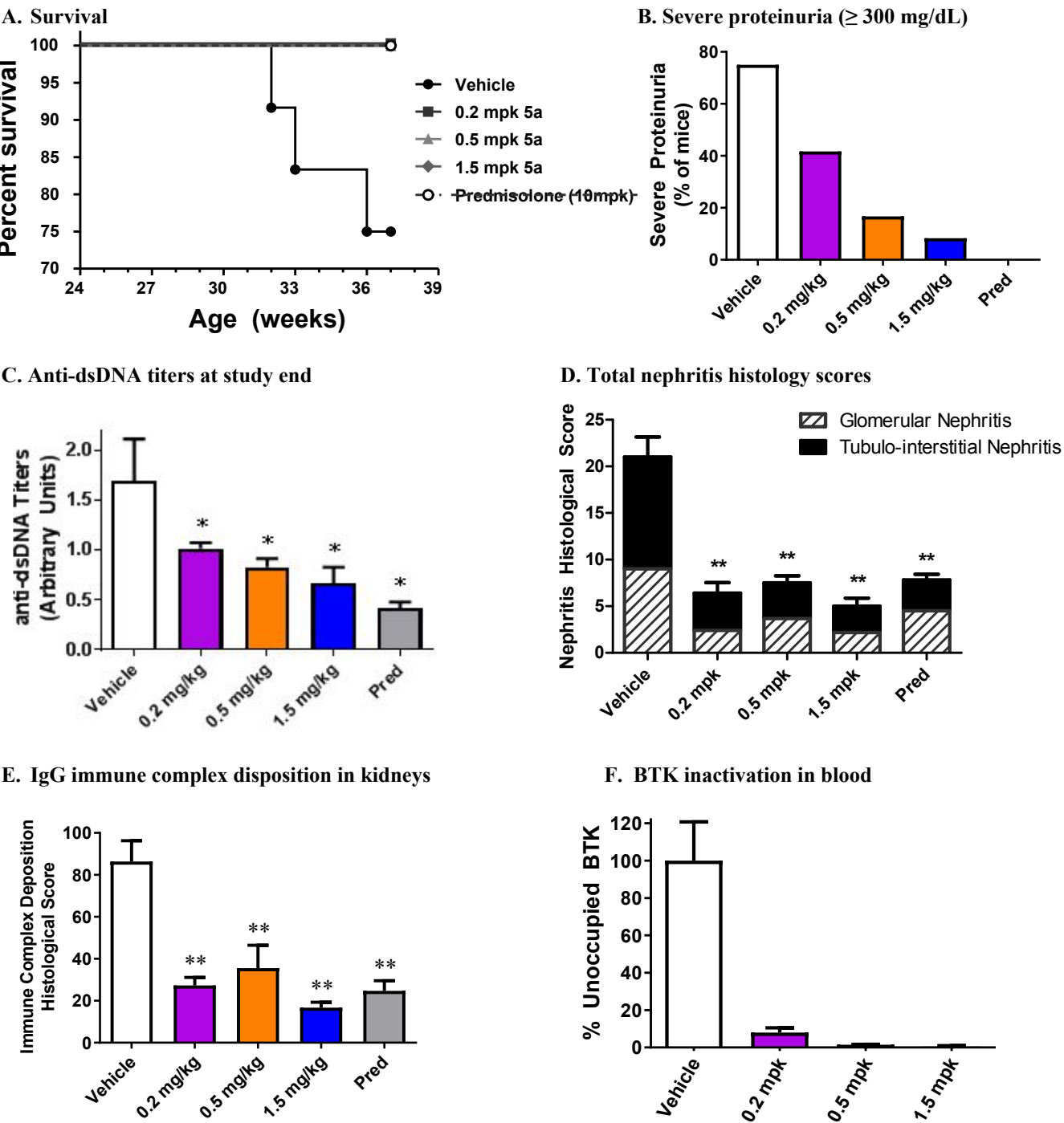
**Figure 14.** Potent and robust activity against collagen-induced arthritis in vivo was observed with **5a** (fully preventative dosing).<sup>a</sup>



<sup>a</sup> Error bars represent the mean  $\pm$  SEM. \* $P < 0.05$ , \*\* $P < 0.01$  versus vehicle control group.

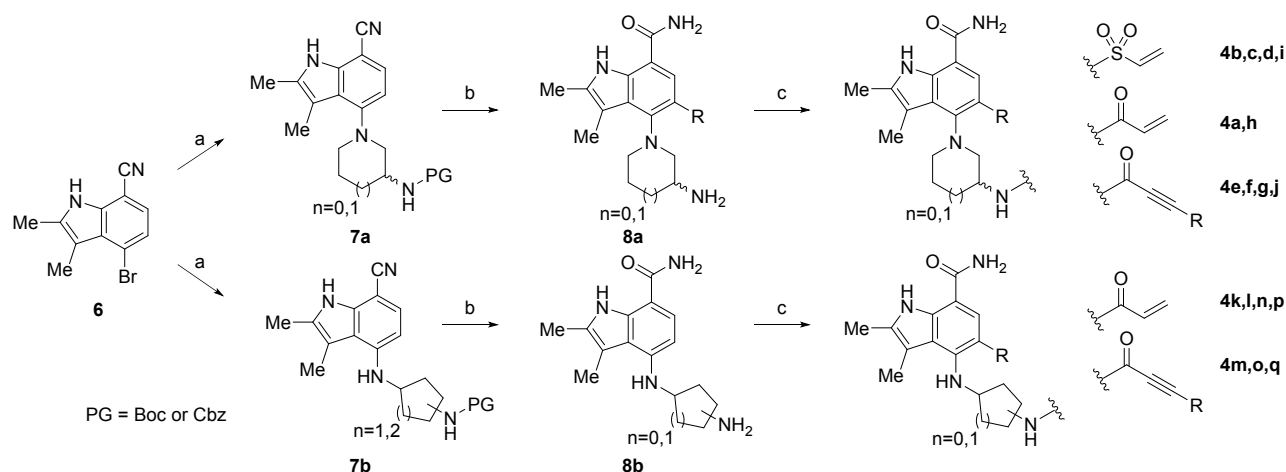


**Figure 15.** Protection Against Lupus Nephritis by **5a** in NZB/W mice vs. vehicle and prednisolone.<sup>a</sup>

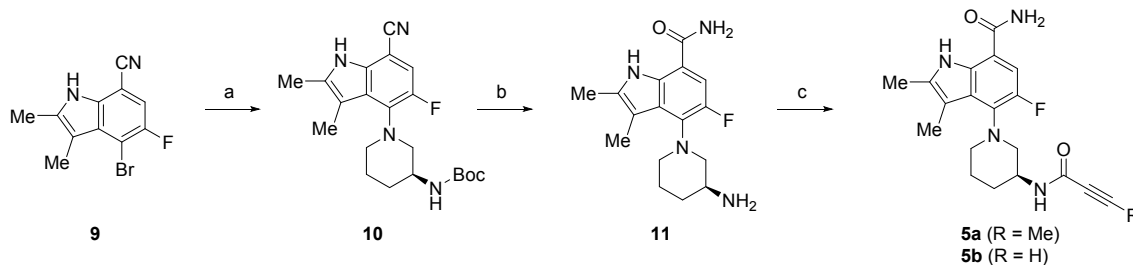


<sup>a</sup> Error bars represent the mean  $\pm$ SEM. \* $P < 0.05$ , \*\* $P < 0.01$  versus vehicle control group; ds-DNA = double-stranded DNA; Ig = I mmunoglobulin; Pred = prednisolone.

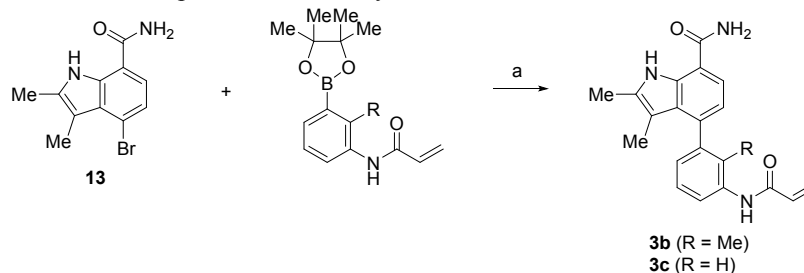


**Scheme 1.<sup>a</sup>** Preparation of dimethylindoles **4**.

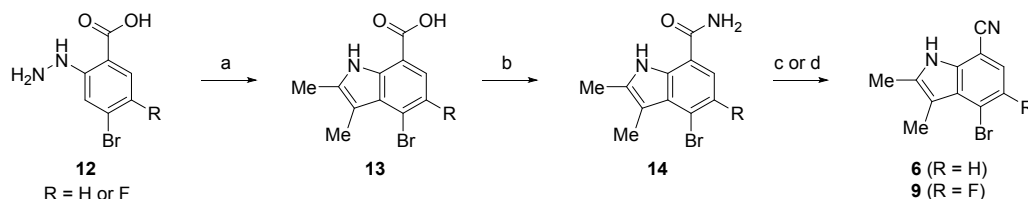
<sup>a</sup> Reagents and conditions: (a)  $R^1R^2NH$ ,  $Pd_2(dba)_3$ , BINAP,  $Cs_2CO_3$ ; (b)  $H_2SO_4$ , 60 °C; (c) chloroethanesulfonyl chloride, THF/ $CH_2Cl_2$ ; (d) acryloyl chloride, Hunig's base, THF/ $CH_2Cl_2$ ; (e) propionic acid or but-2-ynoic acid, HATU, Hunig's base.

**Scheme 2.<sup>a</sup>** Preparation of dimethylindoles **5a** and **5b**.

<sup>a</sup> Reagents and conditions: (a) (*S*)-tert-butyl piperidin-3-ylcarbamate,  $Pd_2(dba)_3$ , BINAP,  $Cs_2CO_3$ , 86%; (b)  $H_2SO_4$ , 60 °C, 82-95%; (c) but-2-ynoic acid, HATU, Hunig's base, 75-85%; (d) propionic acid, HATU, Hunig's base, 45%.

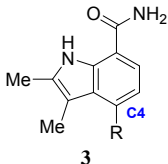
**Scheme 3.<sup>a</sup>** Preparation of dimethylindoles **3b** and **3c**.

<sup>a</sup> Reagents and conditions: (a)  $(Ph_3P)_4Pd$ , 2M  $Na_2CO_3$ , toluene/EtOH, 90 °C, 16 h.

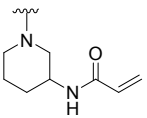
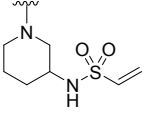
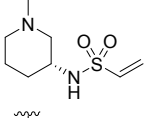
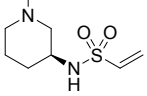
**Scheme 4.<sup>a</sup>** Preparation of intermediates **6** and **9**.

<sup>a</sup> Reagents and conditions: (a) 2-butanone, AcOH, toluene, 50-90%; (b)  $NH_4OH$ , EDC, HOBt, THF,  $CH_2Cl_2$ , 75-90%; (c)  $POCl_3$ , THF, 89%; (d)  $POCl_3$ , pyridine,  $CH_2Cl_2$ , 92%.

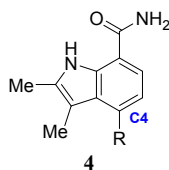
**Table 1.** In vitro potency of dimethylindole analogues **4**.



**3**

Cmpd	R <sup>1</sup>	In vitro Activity		Metabolism <sup>b</sup>	
		BTK IC <sub>50</sub> (nM) <sup>a</sup>	Ramos IC <sub>50</sub> (nM) <sup>a</sup>	HLM (% rem.)	HLM t <sub>1/2</sub> (min.)
<b>1a</b>	<i>NA</i>	0.08 ± 0.02	14 ± 8.4	1	1.5
<b>4a</b>		3.3 (n=1)	100 (n=2)		
<b>4b</b>		1.4 ± 0.4	30 (n=2)		
<b>4c</b>		1.2 (n=1)	28 (n=1)	84	
<b>4d</b>		0.60 ± 0.22	15 ± 5	90	50

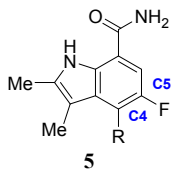
<sup>a</sup> IC<sub>50</sub> values are shown as mean values of at least three determinations unless specified otherwise; <sup>b</sup> HLM = human liver microsomes; Human liver microsomal stability (% remaining) – 0.5 μM substrate, 1 mg/mL protein, 10 min. at 37 °C; Human liver microsomal t<sub>1/2</sub> (min.) – 0.5 μM substrate, 1 mg/mL protein, 1 mM NADPH, 37 °C.

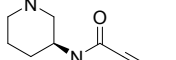
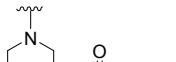
**Table 2.** In vitro potency of dimethylindole analogues **4**.

Cmpd	R <sup>1</sup>	BTK IC <sub>50</sub> (nM) <sup>a</sup>	Ramos IC <sub>50</sub> (nM) <sup>a</sup>	Cmpd	R <sup>1</sup>	BTK IC <sub>50</sub> (nM) <sup>a</sup>	Ramos IC <sub>50</sub> (nM) <sup>a</sup>
<b>4d</b>		0.60 ± 0.22	15 ± 5	<b>4k</b>		1.6 ± 1.2	6.9 ± 2.9
<b>4e</b>		1.4 (n=2)	26 ± 0.6	<b>4l</b>		8.4 (n=2)	>300
<b>4f</b>		0.14 ± 0.01	1.8 ± 0.5	<b>4m</b>		2.4 (n=2)	9.4 (n=1)
<b>4g</b>		0.52 ± 0.29	40 (n=1)	<b>4n</b>		3.3 (n=1)	43 (n=1)
<b>4h</b>		4.2 (n=1)	270 (n=1)	<b>4o</b>		0.85 (n=1)	16 (n=1)
<b>4i</b>		3.5 ± 1.2	170 (n=1)	<b>4p</b>		59 (n=1)	>300
<b>4j</b>		6.5 (n=1)	7.2 (n=1)	<b>4q</b>		29 (n=1)	>300

<sup>a</sup> IC<sub>50</sub> values are shown as mean values of at least three determinations unless specified otherwise.

**Table 3.** In vitro potency of C5-F-dimethylindole analogues **5**.

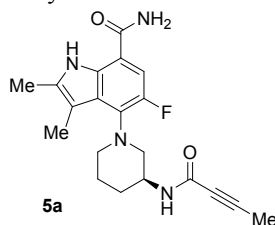


In vitro Activity			
Cmpd	R <sup>1</sup>	BTK IC <sub>50</sub> (nM) <sup>a</sup>	Ramos IC <sub>50</sub> (nM) <sup>a</sup>
5a		0.10 ±0.05	7.2 ±2.3
5b		0.07 (n=1)	1.6 (n=1)

<sup>a</sup> IC<sub>50</sub> values are shown as mean values of at least three determinations unless specified otherwise.

**Table 4.** Biochemical kinetic evaluation of the rate of inactivation of **5a** vs. **1a** ( $k_{inact}/K_{i,app}$ ).

Compound	5a	1a
$K_{i,app}$ (nM)	116	425
$K_{inact}$ (1/s)	0.11	0.09
$k_{inact}/K_{i,app}$ (1/mM·s)	0.97	0.23

**Table 5.** Partial *in vitro* cell activity data and whole blood data for **5a**.

Assay	Receptor/Stimulation	<b>5a</b> IC <sub>50</sub> (nM) <sup>a</sup>
<b>Cellular Assays</b>		
Calcium Flux in Ramos B Cells	BCR/Anti-IgM	7.2 ±2.3
Proliferation of human peripheral B Cells	BCR/Anti-IgM/IgG	0.04 ±0.01
CD86 surface expression in peripheral B Cells	BCR/Anti-IgM/IgG	0.3 <sup>b</sup>
CD86 surface expression in memory B cells (peripheral blood)	IL-6	0.9 <sup>b</sup>
CD69 surface expression in peripheral B Cells	CD40/CD40L	>300 <sup>b</sup>
TNFα from human PBMC Cells	FCγR/Immune Complex	0.3 <sup>b</sup>
<b>Human Whole Blood Assays</b>		
Human whole blood CD69 surface expression in peripheral B Cells	BCR/Anti-IgM	11 ±8
BTK Inactivation	Second order rate of Inactivation	3.5 x 10 <sup>-4</sup> nM <sup>-1</sup> .min <sup>-1</sup>

<sup>a</sup> IC<sub>50</sub> values are shown as mean values of at least three determinations unless specified otherwise; <sup>b</sup> IC<sub>50</sub> values as single determinations; PBMC = peripheral blood mononuclear cells.

**Table 6.** Partial *in vitro* selectivity data for **5a**.

Kinase	Biochemical IC <sub>50</sub> (nM)	Kinase/BTK fold selectivity
BTK (Tec family)	0.10	--
TEC (Tec family)	0.90	9x
BMX (Tec family)	1.5	15x
TXK (Tec family)	5.0	50x
ITK (Tec family)	100	1,000x
HER1 & 4 (EGFR family)	2,000/1,040	>10,000x

**Table 7.** Partial *in vitro* profiling data for **5a**.

Parameter	Result
Protein Binding (bound)	98.8% human 99.6% mouse 99.8% rat 99.8% dog 99.6% monkey
Mutagenicity	Ames negative
Invitro micronucleus assay	Negative
hERG (Patch Clamp)	IC <sub>50</sub> = 11 μM
Na <sup>+</sup> (Patch Clamp)	3.1% @ 10 μM (1 and 4 Hz)
Ca <sup>+</sup> (Patch Clamp)	23% @ 10 μM
PAMPA permeability	859/978nm/s (pH 5.5/7.4)
Caco2 Permeability:	177 – 422 nm/s (A to B)
(2.1 – 35 μM conc.)	127 to 250 nm/s (B to A)
Aqueous solubility	0.002 – 0.003 mg/mL (pH 1-7.4)
FaSSIF <sup>a</sup> solubility	0.009 mg/mL
FeSSIF <sup>b</sup> solubility	0.145 mg/mL
Log D at pH 7.0 (HPLC)	3.18

<sup>a</sup> FaSSIF = Fasted State Simulated Intestinal Fluid; <sup>b</sup> FeSSIF = Fed State Simulated Intestinal Fluid.

**Table 8.** Pharmacokinetic parameters for **5a**.

Parameter	Mouse <sup>c</sup>	Rat <sup>a</sup>	Monkey <sup>a,b</sup>	Dog <sup>a</sup>
po dose (mg/kg)	4	5	2	2
iv dose (mg/kg)	2	5	1	1
C <sub>max</sub> (μM), PO	7.7	9.6 ±1.0	2.3 ±1.5	19 ±2.5
T <sub>max</sub> (μM), PO	1.0	0.58 ±0.4	1.0 ±0.3	0.67 ±0.3
AUC (μM*h), PO	14	18 ±0.8	4.9 ±3.1	78 ±3
T <sub>1/2</sub> (h), iv	0.46	4.3 ±0.5	3.2 ±2.5	3.0 ±0.3
MRT (h), iv	0.57	0.80 ±0.20	1.0 ±0.4	4.1 ±0.7
CL (mL/min/kg),iv	14	8.7 ±0.4	9.4 ±3.7	0.94 ±0.25
V <sub>ss</sub> (L/kg), iv	0.48	0.40 ±0.10	0.45 ±0.1	0.24 ±0.11
F <sub>po</sub> (%)	106	74 ±3	46 ±18	81 ±18

<sup>a</sup> Average of three animals; <sup>b</sup> cynomolgus monkey; <sup>c</sup> average of two animals; Vehicle: PEG400/water (80/20).

## TOC Graphic

